Materials & Design 231 (2023) 112064

Contents lists available at ScienceDirect

Materials & Design

journal homepage: www.elsevier.com/locate/matdes

Ceramic materials for 3D printing of biomimetic bone scaffolds – Current state-of-the-art & future perspectives

Harshavardhan Budharaju [a,1], Shruthy Suresh [a,1], Muthu Parkkavi Sekar [a], Brigita De Vega [b], Swaminathan Sethuraman [a], Dhakshinamoorthy Sundaramurthi [a,*], Deepak M. Kalaskar [b,*]

[a] Tissue Engineering & Additive Manufacturing (TEAM) Lab, ABCDE Innovation Centre, Centre for Nanotechnology & Advanced Biomaterials, School of Chemical & Biotechnology, SASTRA Deemed University, Thanjavur 613 401, Tamil Nadu, India
[b] UCL Institute of Orthopaedics and Musculoskeletal Sciences, Division of Surgery and Interventional Science, Royal National Orthopaedic Hospital, Brockley Hill HA7 4LP, United Kingdom

HIGHLIGHTS

- Ceramic-based bone substitutes fabricated using 3D printing were reviewed.
- Clinical applications of 3D-printed ceramic scaffolds were highlighted.
- Market opportunities for 3D printed & customized ceramic implants were outlined.
- Challenges and future perspectives on 3D printed ceramic implants were discussed.

GRAPHICAL ABSTRACT

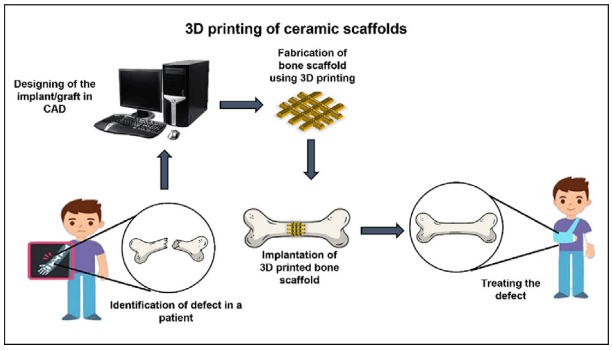

ARTICLE INFO

Article history:
Received 9 February 2023
Revised 29 April 2023
Accepted 2 June 2023
Available online 7 June 2023

Keywords:
Ceramics
Bone grafts
3D printing
Bone tissue engineering
Synthetic bone scaffolds
Hydroxyapatite

ABSTRACT

Ceramic bone implants have potential properties ideal for long-term implantation applications. On comparison with other materials, ceramic biomaterials have advantages such as biocompatibility, low cost, osteoconductivity, osteoinductivity, corrosion resistance, and can be made into various shapes with desired surface properties. Among transplantation surgeries, bone transplantation is the second largest in the globe after blood transfusion which is an indication for rising hope on the potential treatment options for bone. 3D printing is one of the most advanced fabrication techniques to create customized bone implants using materials such as ceramics and their composites. Developing bone scaffolds that precisely recapitulate the mechanical properties and other biological functions of bone remains a major challenge. However, extensive research on ceramic biomaterials have resulted in the successful 3D printing of complex bony designs with >50% porosity with cortical bone mechanical properties. This review critically analyses the use of various 3D printing techniques to fabricate ceramic bone scaffolds. Further, various natural and synthetic ceramic materials for producing customized ceramic implants are discussed along with potential clinical applications. Finally, a list of companies that offer customized 3D printed implants and the future on clinical translation of 3D printed ceramic bone implants are outlined.

* Corresponding authors.
E-mail addresses: dhakshinamoorthy@scbt.sastra.edu (D. Sundaramurthi), d.kalaskar@ucl.ac.uk (D.M. Kalaskar).
[1] These authors contributed equally to this work.

https://doi.org/10.1016/j.matdes.2023.112064
0264-1275/

1. Introduction

Over the last several years, injuries to bone have increased due to various reasons such as falls, accidents, sports injuries, and others [1,2]. As a therapeutic option, bone grafts are used to treat critical sized bone defects to promote bone repair and regeneration [3]. Tissue engineering-based strategies are employed to effectively repair bone since patient-derived cells/tissues in the scaffolds may promote the healing process [4,5]. The scaffold manufacturing techniques and materials utilized to fabricate scaffolds are critical for tissue regeneration [6]. Various tissue engineering strategies, such as electrospinning, gas foaming, particulate leaching, freeze-drying and additive manufacturing (AM) or 3D printing, are currently utilized to produce highly customizable, patient-specific functional bone scaffolds/implants for specialized clinical needs [5,7]. Biomaterials used to prepare scaffolds are critical for tissue engineering, and the use of each biomaterial differs based on the application [8,9]. An ideal biomaterial for bone tissue engineering and regeneration should be biocompatible, biodegradable, bioactive, and osteoconductive. Various natural and synthetic biomaterials are used for bone tissue engineering. Interestingly, archaeological findings have revealed that the missing bones and teeth were replaced using wood, shells, corals, human or animal teeth, and several other metals like gold, silver, amalgam, etc. [10].

Over the last few decades, various scaffolds have been fabricated using biometallics, bioceramics, biopolymers, and biocomposites for bone tissue engineering. Still, it remains challenging to design scaffolds that mimic the native microenvironment & functions of bone. Stainless steel, titanium-based alloys, cobalt-based alloys, nickel & titanium alloys, magnesium-based alloys, and bulk metallic glass (BMG) are the commonly used metals for the fabrication of bone implants. However, different reasons may contribute to the failure of metallic implants, such as releasing ions from the metallic surface, high stiffness, reactivity of metal surface with enzymes, high corrosion rate, toxicity, loosening or instability, and infection [11]. Polymers consist of repeating monomer units arranged in long chains, connected by branches or crosslinks. Natural polymers used for bone scaffold preparation include protein-based natural biomaterials like silk, fibrin, and collagen; polysaccharide-based materials like agarose, hyaluronan, alginate, and chitosan. Although natural polymers promote cell adhesion and proliferation owing to their biocompatibility, biodegradability, biomimetic, and immunomodulatory properties, they have several drawbacks, such as poor mechanical strength, difficulties in preserving their integrity and rapid degradation due to enzymatic reactions [12]. Hence, researchers are developing synthetic polymers to overcome the limitations of natural biomaterials in developing bone scaffolds. Synthetic polymers which are biocompatible and biodegradable are widely used in the preparation of scaffolds to treat damaged tissues and organs [13]. The most commonly used synthetic polymers for bone tissue engineering include polyanhydrides, polypropylene fumarate, polycaprolactones, polyphosphazenes, polylactide, polyglycolide, etc. Tunable mechanical properties, porosity, controllable degradation, ease of fabrication, and potential for offering structural support have made synthetic polymers highly attractive as materials for bone regeneration. However, synthetic polymers have various disadvantages for bone applications, including lack of bioactivity, poor osteoconductivity, toxicity, and poor integration with host tissues. Recent studies have shown that ceramics are more durable and fracture resistant than metals and polymers in *in vivo* conditions & demonstrate high wear resistance and hardness similar to natural bone. Several synthetic ceramic biomaterials such as tricalcium phosphate, zirconium oxide, barium titanate, silicon carbide, and hydroxyapatite, are commonly used for bone tissue engineering, due to their superior biocompatibility, mechanical strength, and chemical inertness [14]. Moreover, the wear debris produced by ceramic implants are practically negligible when compared with metals and polymer-based implants. Although the main drawback of ceramic materials is their low fracture toughness, they possess high compression resistance, high humidity degree, and high Young's modulus.

The advancements in science have introduced a lot of progress in bone tissue engineering compared to the conventional methods used for bone replacements and treatments. Autografts and allografts are the conventional strategies to repair bone defects due to their structural similarity with native bone. However, these approaches have several drawbacks, such as inflammation, pain and graft rejection. To overcome the drawbacks of conventional techniques, researchers developed materials and methods that help to fabricate bone scaffolds that closely resemble the characteristics and function of a human bone [15]. Scaffold-based tissue engineering has gained a lot of attention for bone tissue engineering and regeneration due to their long-term stability, sustained release of soluble factors, cellular support, integration with native bone, etc. [16]. Traditionally, ceramics-based bone scaffolds are produced using methods such as solvent casting, particulate leaching, freeze drying, injection molding, compression molding, electrospinning, and hydrogels [17]. In the techniques like injection molding and compression molding, ceramic materials are mixed with polymers and high pressure is applied to remove air pockets and consolidate the ceramic powder to make dense bone scaffolds with specific geometry [18,19]. However, it is challenging to fabricate scaffolds according to patient requirements, controlled porosity, and pore size distribution using these traditional fabrication methods. As an alternative, 3D printing has been emerging as a viable fabrication method due to numerous advantages, including design flexibility, customizability, reduced material waste, faster production, ability to control porosity and improved mechanical properties [20].

3D printing had its origins in the late 19th century when photo sculpture and geomorphology technologies were established. 3D printing is an additive manufacturing (AM) technique that helps to create three-dimensional objects using a computer-aided design. Fused deposition modeling (FDM), selective laser sintering (SLS), stereolithography, selective laser melting (SLM), inkjet 3D printing, adhesive droplet and powder bed-based AM, digital laser processing, continuous liquid interface production, and other 3D printing techniques were developed between 1980 s and 2010 s based on various working principles [21]. Various 3D printing techniques, like FDM, SLS, stereolithography, etc., are very promising in the fabrication of scaffolds for bone tissue engineering and regeneration. Customized shape, pore size, and enhanced mechanical properties are some of the main advantages of 3D printed bone constructs. Because of the precise control over the production process and the ability to customize the final products, biomedical researchers have been fascinated with 3D printing technology.

This review paper provides a comprehensive overview on steps involved in 3D printing of bone scaffolds, various ceramic biomaterials and additive manufacturing techniques used for fabricating bioactive and osteogenic scaffolds along with their applications and commercial scope. Initially, the pre-requisites for 3D printing and steps involved in 3D printing along with the post-processing steps for fabricating biomimetic bone scaffolds are discussed. Further, various natural and synthetic bioceramic materials used for the fabrication of bone scaffolds and the essential requirements for 3D printing of ceramics are discussed. Additionally, the advantages and disadvantages of 3D printing of ceramic materials using fusion deposition modeling (FDM), selective laser sintering, stereolithography, digital light processing, and 3D bioprinting of ceramic ink are discussed in detail. Furthermore, the use of ceramic based 3D printed bone substitutes for treating variety of clinical condi-

tions such as fractures, cancers, traumatic injuries, osteomyelitis, cartilage repair, and drug delivery. In order to demonstrate the potential of 3D printing ceramic materials for commercial applications, several details about bone scaffold manufacturers and market growth statistics were discussed. Finally, the technological constraints, design considerations, practical challenges and future perspectives associated with the fabrication of 3D printed ceramic bone scaffolds are described.

2. Requirements for 3D printing of ceramics:

Ceramic scaffolds are usually produced by 3D printing a green body, which is then sintered at high temperatures to turn them into solid structures. Ceramic 3D printing for treating bone defects involves the same basic steps as general 3D printing strategies, including pre-processing (before printing), printing, and post-processing (after printing). Pre-processing involves patient defect scanning/imaging, digital implant designing in computer-aided design (CAD) software, material selection, surgical planning, and simulation testing. Ink formulation and parameters optimization are required for printing high-resolution 3D structures during the printing step. Post-processing is required for residual removal and implant strengthening steps through debinding, sintering, coating, surface modification, sterilization, and other basic steps. Before implanting into the patients, the 3D printed scaffolds/implants are tested for strength, durability, biocompatibility, and host-implant interactions to ensure safety and effectiveness. Finally, these printed scaffolds can be used for various applications such as bone, cartilage regeneration, drug delivery, etc. by implanting them at defect site [22]. Satisfying the material/printing requirements in the processing steps is crucial for 3D printing of ceramic materials with good printability, stability, high resolution, and controlled porosity, which could help in directly utilising the 3D printed ceramic implants for clinical applications.

2.1. Pre-processing stage

Advancements in computer-aided design and computer-aided manufacturing (CAD-CAM) have made it possible to design customized scaffolds for bone deformities according to patient requirements. The process of designing a bone implant digitally according to patient needs involves scanning/imaging, reconstructing, designing, fixing analysis, and generating printable files [23]. Implant fabrication starts with digital imaging and CT scanning to create a 3D image of the patient's defect site in Digital Imaging and Communications in Medicine (DICOM) format, followed by a mask-drawing process to design the missing bone part in each 2D image slice, and ultimately designing the bone implant using software, such as 3Matics or Solidworks. Also, modifications in the shape or morphological features of 3D printed bone can be implemented according to the guidance of the surgeons for fixing and better integration with native bone [24]. Moreover, designing 3D bone implants with controlled porosity (pore morphology) and infill patterns are required to achieve better mechanical strength (stiffness), nutrient/waste transport, and cell-material interactions.

To understand the role of 3D model design in customizing bone implants Vijayavenkataraman *et al.*, designed & fabricated gradient bone implant by printing alumina (Al_2O_3) using Lithography-based Ceramics Manufacturing (LCM) technology to mimic the trochanter region of hip bone to reduce the stress shielding effect. A total of 12 unit cell designs were selected from a pool of 90 designs based on their porosity (~50%) and pore size (500–1000 μm) which was achieved by changing the size and thickness of the unit cell and sintered for 48 h to enhance mechanical strength (compression Youngs's modulus – 2–5.5 GPa; fractural strength of 11–133.5 MPa). This method allowed the design of an implant containing four quadrants: medioanterior (MA), lateroanterior (LA), lateroposterior (LP), and medioposterior (MP), with varying trabecular and cortical structures. Using this 3D printing method, gradient 3D structures were successfully fabricated with smooth shape transition and mechanically similar to native hip. The printed structures (10 mm height) consisted of 3 different gradient of regions: region 1 mimicked MA & MP cortical bone with Youngs modulus of 3 GPa, region 2 mimicked trabecular bone with 2 GPa and finally region 3 mimicked LA and LP cortical bone with 5.5 GPa Youngs modulus [25].

2.2. Printing of ceramic materials

Materials like barium titanate, silicon carbide, hydroxyapatite, etc., have gained great importance in 3D printing due to their availability, safety and efficacy. Careful selection of ceramic materials/-composites and optimal concentrations to prepare slurry/ink are required to fabricate bone scaffolds according to the functional requirement of defect site. 3D printing techniques such as FDM, DLP, SLS, SLM, 3D gel printing, etc., has some prerequisite conditions to facilitate high-resolution ceramic printing. The selection and preparation of ceramic slurry as well as additive manufacturing methods are generally determined by implant design [24]. For example, ceramic particles can be suspended or mixed with thermoplastic polymers to form printable filaments for FDM, which are extruded layer-by-layer to form a stable porous 3D structure after solidification. Saranti et al. printed bone scaffolds by producing a PLA filament containing 45S5 BG and carbon dots composites, which was extruded using a desktop filament extruder and printed at 200 °C nozzle temperature [26]. Similarly, for other 3D printing techniques, such as extrusion, DLP, stereolithography, SLA, and SLS technique, the ceramic material should mix with a medium (solvent or dispersant) to form uniform paste or slurry with appropriate viscosity [27]. Further, ball milling of ceramic materials for overnight helps to produce homogenous powder mixture of ceramic composites such as calcium oxide:silicon dioxide:strontium oxide/magnesium oxide ratio (11:5:4) to produce printable ceramic ink without clogging [28]. Additionally, a few other additives like plasticizers (poly(ethylene glycol) 400), binders (polymethacrylate ammonium, hydroxypropyl methylcellulose, polyethyleneimine, etc.), dispersant (BYK-2155, sodium polyacrylate, S18, etc.,) and inorganic electrolyte are used to enhance the printability [29]. Selection of optimal solid content (>40% w/v) & homogeneity of slurry is important as it affects the shear stress, printability and mechanical properties [30–32].

Ceramic paste concentration should be optimal for extrusion-based implant printing to stack multi-layered structures and improve adhesion between layers. Similarly, for SLA technique, ceramic materials need to be suspended as a slurry containing resin, photocurable monomer, initiator and dispersant. Ceramic slurry with a low viscosity (<3 Pa.s) and high solid contents need to be enabled with better photocrosslinking efficiency (low curing depth) to improve printability [33]. For SLM/SLS, the ceramic materials should possess the optimal material density, melting point and higher diffusion rate to produce printable paste. The ceramic components are mixed with polymer based binders (PCL, PLA, etc.,), which binds the ceramic component together during the 3D printing process [34,35].

2.3. Post-processing stage

The 3D printed ceramic implants for bone replacement require following post-processing steps, such as sintering and surface modifications to improve their mechanical properties and biocompatibility. Sintering is the process of compacting and forming a

solid mass by applying pressure and/or heat to the material, causing the particles to bond together and form a solid mass. It induces physical and chemical changes in the printed constructs to achieve high interconnectivity, making them stronger and more durable. Usually, lower temperatures (400–600 °C) during sintering burn out organic binders and pore-forming agents, leaving porous structures. Sintering at higher temperatures fuses ceramic particles, reducing pore size and increasing construct density to produce a stable construct with shrinkage. Hence, parameters like sintering temperature, atmosphere, heating rate, holding time, etc., affect the mechanical properties and shrinkage behavior of the 3D printed ceramic scaffolds. Xiangjia Li *et al.,* reported that 3D printed hydroxyapatite/tricalcium phosphate scaffolds with 30% porosity showed high compressive strength (4.32 MPa) after sintering at 1250 °C temperature compared to scaffolds sintering temperature of 1050 °C (0.13 MPa) [36]. Similarly, Yu Pan et al. reported that the holding time of alumina-based scaffolds for 180 min increased the hardness of scaffolds to 30.1 GPa compared to scaffolds sintered for 30 min (13.6 GPa) which confirmed the role of holding time in improving the mechanical properties of 3D printed constructs [37]. Sintering at higher temperatures or sintering for a longer duration leads to the occurrence of multiple cracks. Based on these observations, 3D printed ceramic scaffolds require careful selection of optimal sintering conditions to achieve the desired mechanical properties and dimensional accuracy without cracking and thermal damage.

During the high-temperature sintering process the 3D printed ceramic materials undergo densification which result in shrinkage. It may be noted that percentage shrinkage of ceramic materials depends on the concentration of ceramic material, ratio between binder and ceramics, sintering temperature, holding time and initial porosity of green body (before sintering). To demonstrate the influence of sintering parameters on shrinkage, Xiangjia Li *et al*., analyzed the relationship between sintering temperature, concentration of ceramics, holding time, and shrinkage ratio. Increasing the concentration of ceramics resulted in a significant reduction in the shrinkage of the green body. Scaffolds prepared with 20% (%wt) HA/TCP ceramic ink shrunk by 45.25%, and scaffolds prepared with 40% (%wt) ceramics shrunk by 17.8% at a sintering temperature of 1150 °C. The height of green bodies shrunk more than the length and width, due to the weak binding forces between layers, where binders get removed easily, causing greater shrinkage in the z-direction (height). Higher microhole density reduces HA/TCP scaffold shrinkage and causes varying shrinkage ratios in both axial (Z) and radial (XY) directions, with greater axial shrinkage due to isotropic stress [36]. Due to extensive particle fusion during sintering, ceramic materials with high melting points shrink more during sintering. Further, the effect of infill density on shrinkage was reported by Uday Kiran Roopavath *et al*., where the scaffolds printed with 100% infill density showed low shrinkage (12 ± 3.7%) compared to 75% (28 ± 3.8%) and 50% (42 ± 4.7%) infill density due to more deposition of materials with 100% infill density [38].

For enhanced tissue regeneration, these printed bone scaffolds can be tailored with surface modifications or bioactive factors to provide a favorable *milieu* for the cells of interest and to integrate with native bone [9]. Recent reports showed surface coating of 3D printed bone scaffolds with oxygen-generating biomaterials such as calcium peroxide (CPO), magnesium peroxide (MPO), sodium percarbonate (SPO) promoted bone regeneration with increased cell viability and proliferation [39–41]. Further, incorporating growth factors such as bone morphogenetic proteins (BMPs - BMP-2, BMP-4, and BMP-7), vascular endothelial growth factor (VEGF), insulin-like growth factor (IGF), fibroblast growth factor (FGF), and platelet-derived growth factor (PDGF) enhanced cell adhesion, proliferation, osteogenic differentiation, and bone formation in defects created in animal models. Ceramic scaffolds for bone regeneration require control over the surface roughness with printing parameters or post-processing techniques to influence osteoblast behavior by increasing contact area and promoting cell adhesion, proliferation, & differentiation through focal adhesion formation. A detailed discussion on various ceramic materials, 3D printing methods used for the fabrication of bone scaffolds, and potential applications of these printed scaffolds is provided in the following sections.

3. Ceramic materials for bone tissue engineering

Ceramics are group of materials made up of inorganic and non-metallic solids such as oxide, nitride, carbide, or boride. Upon exposure to higher temperatures these materials become bone like structures due to formation of ionic and covalent bonds. Usually, ceramics are widely used in the production of semiconductors, electrical insulators, plugs, capacitors, transducers, data storage elements, bone tissue implants, etc. Ceramic materials are highly tensile and form stable bonds with the host tissues. Ceramic scaffolds must be mechanically stable, as they are subjected to various forces, including compressive, tensile, & shear forces, and inadequate mechanical properties might lead to compromised bone healing. The mechanical properties of ceramic scaffolds are significantly influenced by various parameters such as concentration, porosity, pore size, sintering temperatures, interconnectivity between the pores, infill densities in the printed scaffolds, etc. Ceramic scaffolds for bone regeneration require a balance between porosity and mechanical properties, as higher porosity leads to compromises in mechanical performance, while low porosity leads to reduced nutrients/oxygen diffusion, and poor integration with native bone. Choice of ceramic materials for scaffold fabrication usually depends on the application since load-bearing and non-load-bearing bones have very different mechanical requirements. Bioceramics is a class of bioactive materials extensively used in bone tissue engineering to replace or repair damaged bone tissues [42]. Bioceramics can be both natural and synthetic and their key features and applications are mentioned in Table 1.

3.1. Natural bioceramics

Natural bioceramics are ceramic materials that are naturally available for bone scaffold preparation with properties like biocompatibility, low immunogenicity and biodegradability. However, their usage is currently limited because of their weak mechanical characteristics and the possibilities of immunological responses in the body after implantation. Natural bioceramics are prepared from numerous natural sources, including bones from cadavers, scales of fishes & animals, eggshells, etc. There are wide varieties of natural bioceramics, and some of their properties, biocompatibility, and sources, are discussed briefly below.

3.2. Hydroxyapatite

Hydroxyapatite ($Ca_{10}(PO_4)_6(OH)_2$) is a calcium phosphate, which is naturally occurring inorganic compound in the bone and widely used as ceramic material for fabricating bone scaffolds and implants [38]. There are various methods for preparing hydroxyapatite from synthetic and natural sources [75]. The natural hydroxyapatite sources include bones, scales of fishes and other animals, eggshells, etc. In a study by Trakoolwannachai *et al.,* hydroxyapatite was successfully prepared from eggshell waste and a composite was prepared using it along with polycaprolactone (PCL). Hydroxyapatite was successfully prepared by co-precipitating phosphoric acid and calcium oxide from the egg shell [76]. Cahyanto *et al.,* prepared hydroxyapatite from fish bones by deproteiniza-

Table 1
Different ceramic materials and their applications.

Materials	Chemical Formula	Sintering Temperature	Key Features	Applications	Ref
β-Tricalcium phosphate	β-$Ca_3(PO_4)_2$	200–1400 °C	Good biodegradability, bio absorption, low crack/ deformation, low shrinkage, and porosity	Hard tissue repair	[43–49]
Silica carbide	SiC	1860–1950 °C	Excellent strength, good compressive properties, fracture behaviour, microscopic features	Light weight design of structural ceramics	[50–55]
Ferrite	Fe_3O_4	900–1400 °C	Cost-effective, high biocompatibility and magnetic behaviour	Magnetic hyperthermia and bone tissue regeneration	[56,57]
Alumina	Al_2O_3	1500–1800 °C	Biocompatibility, Chemical inertness, inexpensive, easy availability	Joint replacements, bone spacers, dental implants	[58,59]
Hydroxy-apatite	$Ca_{10}(PO_4)_6(OH)_2$	1000–1250 °C	Good cell growth, good compression performance, good biocompatibility	Clinical repair of bone defects	[60–64]
Zirconium oxide	ZrO_2	1000–1450 °C	Good tensile strength, good mechanical properties	Bone repair, bone tissue engineering	[64–66]
Calcium silicate	$CaSiO_3$	1200–1400 °C	Excellent bioactivity, biodegradability and osteoconductivity	Hard tissue regeneration and as coating for metal implants	[67,68]
Barium titanate	$BaTiO_3$	900–1200 °C	Good tensile strength, good biocompatibility	Large bone defects	[62,69–71]
Calcium carbonate	$CaCO_3$	600–1000 °C	Good biocompatibility, bioactivity, high osteoconductivity	Bone tissue engineering, osteoconductive bone substitutes	[72–74]

tion and using a reflex method with KOH and H_3PO_4 solutions [77]. Similarly, hydroxyapatite was prepared naturally from various other sources like pig bone [78], bovine bone [44], and fish scales [79], etc. These hydroxyapatites are less toxic and osteoconductive, facilitating bone cell growth [80] and used as an effective biomaterial for bone fabrication.

3.3. Synthetic bioceramics

Advances in materials science have led to the usage of synthetic ceramics more than natural ceramics for bone tissue engineering applications. Synthetic ceramics are made *in vitro* using the proteins and organic substances found naturally in the body [3]. Most synthetic materials used for making bone grafts are commonly composed of calcium, aluminum and silicon. Ceramics do not occur naturally in body, but they are widely used since they show similar biological responses and present a similar microenvironment as natural bone [81]. For example, the stoichiometry of tricalcium phosphate ceramics is comparable to that of amorphous bone precursors, but the stoichiometry of hydroxyapatite is similar to that of bone minerals [82]. Various synthetic ceramic materials widely used for the preparation of bone scaffolds are explained below.

3.3.1. Tricalcium phosphate

Tricalcium phosphate ($Ca_3(PO_4)_2$) is a bioactive substance commonly used as a component in bone replacement implants since it potentially induces osteoblastic development in progenitor cells. Tricalcium phosphate is a remarkably successful biomaterial for bone regeneration because of its biocompatibility, bioactivity, osteoconductivity, and biodegradability [83]. Drugs embedded or functionalized on the surface of tricalcium phosphate can treat osteoporosis-related fractures, large bone defects, bone tumors, and osteomyelitis [84]. Increased osteoconductivity and osteoinductivity help bone development and mineralization, which aids in bone regeneration. The most distinguishing characteristic of tricalcium phosphate is that it can be produced *in situ* by dissolution precipitation process at body temperature. The process by which a solute in a gaseous, liquid, or solid phase dissolves in a solvent to form a solution is known as the dissolution process [85]. This property contributes to its beneficial characteristics, such as the ability to mold after mixing and its injectable property, which allows for less invasive application and the potential to operate as a medication & delivery vehicle for biological molecules. Injectable tricalcium phosphate was used to heal intrabony defects in humans, an osseous defect with definite morphology [86]. On radiographs, tricalcium phosphate was well-integrated and absorbed in the vertebra with no indications of osteolysis or necrosis. Tricalcium phosphate is blended with materials like collagen, sphingosine 1-phosphate, and metal ions to increase its biochemical characteristics and osteogenic capacity [45,46].

One of the challenges in tricalcium phosphate scaffold preparation is the requirement to optimize the component distribution and microporous structure for enhancing biodegradation & bone defect repair. To address this issue, Chen *et al*., 3D printed a core-shell-typed nonstoichiometric wollastonite macroporous scaffold with a microporous core-shell using 4% and 10% Magnesium (Mg) doped Calcium silicate (CaSi), which formed CSiMg4 and CSiMg10. From the previous research, it was evident that Mg-doped CaSi bioceramics can improve mechanical characteristics, surface biocompatibility, and osteogenesis of the scaffold. In this study, Mg-doped CaSi were prepared by a wet chemical method. CSiMg4 and CSiMg10 were combined with polyvinyl alcohol (PVA) to prepare the core-shell bioceramics, which were 3D printed and sintered for three hours at 1100 °C (Fig. 1A). Four sets of scaffolds were printed with and without pores (by adding polystyrene spheres 20%) and labelled CSiMg4@CSiMg10, CSiMg4@CSiMg10-p, CSiMg10@CSiMg4 and CSiMg10@CSiMg4-p. However, high-density micropores were found in CSiMg4@CSiMg10-p and CSiMg10@CSiMg4-p, despite the fact that macropore structure and interconnectivity were found in all scaffolds (Fig. 1B). Mechanical strength analysis of these scaffolds demonstrated that CSiMg4@CSiMg10 had a greater compressive strength of ~25.8 MPa and an elastic modulus of 784 MPa. Biodissolution test with Tris-HCl showed fast release of Ca, Mg and Si ions and a faster mass loss of ~17–23% after 8 weeks was also observed. New Zealand white rabbits with femoral bone abnormalities were used to evaluate the in vivo efficacy of these scaffolds after 12 weeks of implantation. 3D μCT reconstruction and histological examination revealed that the CSiMg4@CSiMg10-p scaffold had significantly stronger osteogenic abilities compared to other scaffolds (Fig. 1D). After four weeks of implantation, X-ray images demonstrated the integration between the scaffold and host bone tissue. Further, CSiMg10@CSiMg4-p and CSiMg4@CSiMg10-p groups showed significantly increased bone tissue formation and biodegradation at 12 weeks post-implantation (Fig. 1C). Thus, it was shown that a core-shell bioceramic 3D printing approach could be used to produce single-phase or biphasic bioactive ceram-

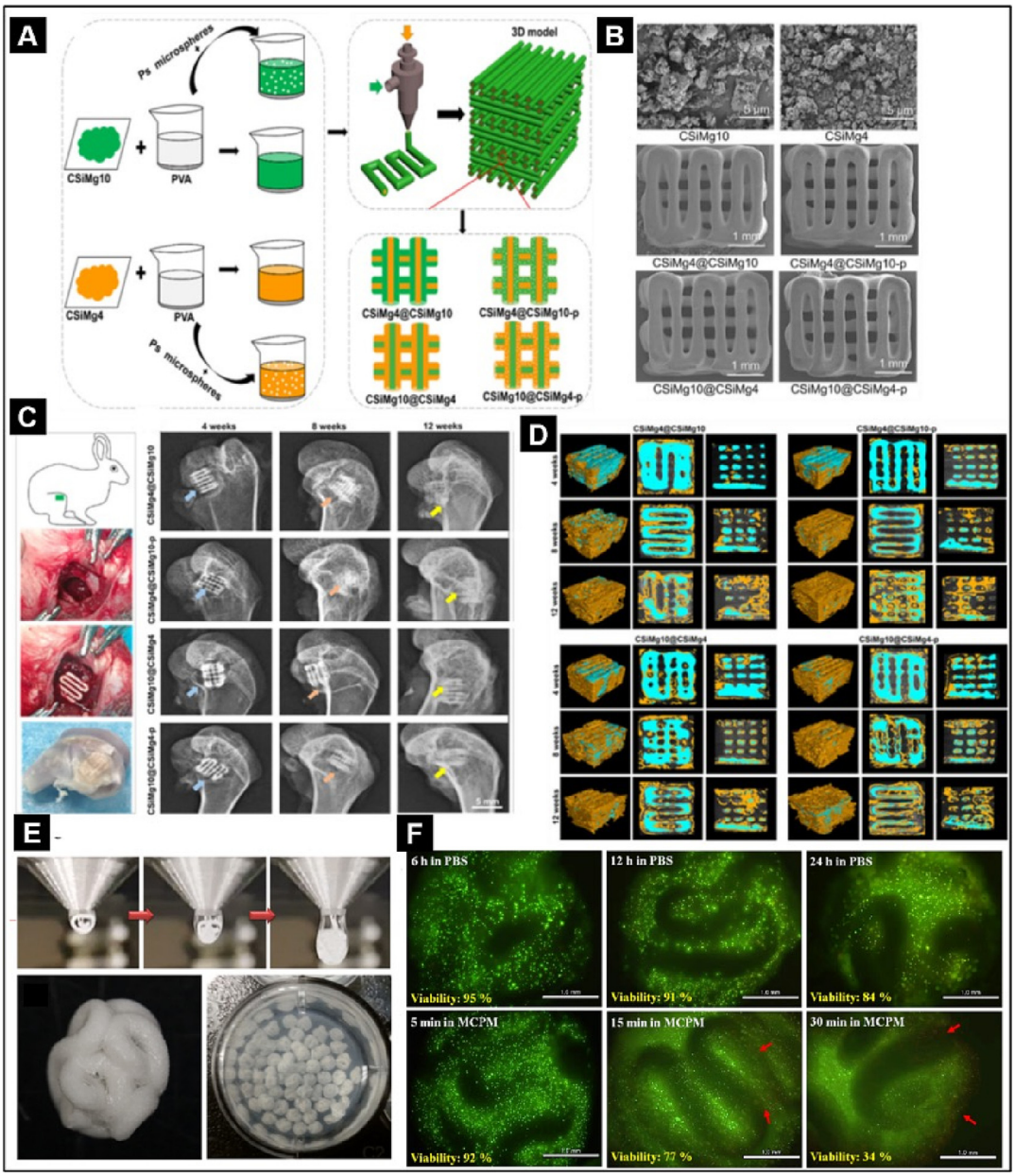

Fig. 1. Various types of scaffolds fabricated using Tricalcium phosphate. [A] Schematic representation of preparation and three–dimensional printing of porous core–shell scaffolds using bioceramics; [B] SEM images of bioceramics powders and 3D printed scaffolds; [C] Implantation of 3D prited scaffolds in femoral bone defect and radiological images of the femoral bone specimens at different time points; [D] 3D and 2D micro–CT images for the animal model filled with bioceramics scaffolds (Blue: bioceramics; yellow: new bone). Reproduced with permission from [87]. [E] Fabrication and Post–fabrication process of coiled ceramic/hydrogel core – shell beads; [F] Live–dead assay of cell–loaded core–shell beads immersed in 1X PBS and MCPM (50 mM) (Live – green & Dead – red). Reproduced with permission from [88]. (For interpretation of the references to color in this figure legend, the reader is referred to the web version of this article.)

ic scaffolds with precisely tuned biodegradation for bone regeneration and repair in certain pathological conditions [87].

Apart from bone healing and repair and, these scaffolds are also used for other applications like drug delivery. Quercetin and bisphosphates are drugs that are commonly used to treat osteoporosis. Raja *et al*., prepared unique coil structured bioceramics using α-tricalcium phosphate (TCP) loaded with quercetin, enclosed in alginate hydrogel beads for cell and drug delivery applications. The alginate hydrogel, which makes the shell, was loaded with preosteoblast (MC3T3-E1) cells. The prepared ceramic paste and the alginate hydrogel were extruded simultaneously through the inner and outer nozzle, respectively. Further, the alginate shell was crosslinked using calcium chloride or monocalcium phosphate monohydrate (MCPM) solution (Fig. 1E). The α-TCP hardened to form calcium-deficient hydroxyl apatite (CDHA) by immersing it in phosphate-buffered saline solution. After 24 h, 84% of the MC3T3-E1 cells remained viable when $CaCl_2$ was utilized as the crosslinker solution. In contrast, MCPM had a much lower survival rate of 34% after 30 min. (Fig. 1F). These scaffolds also showed a good drug release profile since the quercetin was released efficiently with a rate of 3.8 ng/day and 28.4 ng/day by 1 wt% and 5 wt% samples respectively in 120 days. These multifunctional, structured microbeads could be used as new bone graft alternatives for hard tissue regeneration [88]. Although TCP is a bioactive ceramic material due to osteointegration ability, it has low mechanical strength (compressive strength: 2.5–16 MPa) which

makes it only suitable for low to medium load-bearing applications [48].

3.3.2. Zirconium oxide

Zirconium dioxide (ZrO_2), also called zirconia, is a white crystalline zirconium oxide [65]. It has monoclinic crystalline structure, and one of the most popular bioceramics in the market [89]. Scaffolds manufactured using zirconia showed bending strengths ranging from 900 to 1200 MPa and fracture resistance ranging from 9 to 10 MPa [90]. Zirconium oxide has an extremely high melting point of 2715 °C and also is known for its biocompatible nature [91]. It has a wide range of applications, including abrasive items, paint additives, joint implants, dental bridges, etc. Dentistry scaffolds were fabricated using 3D slurry printing technology with zirconium oxide, and a two-stage sintering approach fulfilled the requirements of micro-hardness (1556 HV) and average flexural strength (539.1 MPa) compared to other polymers [92]. Further, studies showed that the efficiency of these scaffolds were further increased by combining it with nano-hydroxyapatite powder [63,93]. The exceptional mechanical properties of ZrO_2, which include high compressive, bending, tensile, and flexible strengths, make it as an ideal material for load-bearing bone applications. However, due to its bioinertness and high stiffness, zirconium oxide is not suitable for applications in which flexibility and osteointegration are critical.

3.3.3. Barium titanate

Barium titanate ($BaTiO_3$) is a well-known piezoelectric ceramic substance commonly used to prepare scaffolds for bone tissue engineering [94]. The piezoelectric effect is important for bone formation, fracture healing, maintaining a charged surface, improving bone cell adhesion and proliferation [95–97]. Increased sintering temperature improves the compressive strength of porous scaffolds, piezoelectric coefficient, biocompatibility, and capacity to build strong interfacial contact with the surrounding bone. Barium titanate scaffolds are effective for bone tissue engineering and other biomedical applications due to their osteogenic differentiation and cytocompatibility [69,98–100]. Sol–gel, mechanical mixing and sintering techniques are used to prepare barium titanate slurries & scaffolds, which have high compressive strength, bending module, elastic property, and Young's modulus [101,102]. Recent studies have shown that scaffolds coated with barium titanate exhibit good antibacterial properties and improved osteogenesis [103]. Barium titanate has high mechanical strength and stiffness, making it a suitable material for load-bearing bone implants. However, the blending of barium titanate with bioactive materials like hydroxyapatite (HA) is essential to enhance bioactivity and implant stability by integrating with host bone tissues.

3.3.4. Silicon carbide

Silicon carbide (SiC) has biomimetic features, such as superior density, strength, and thermo–mechanical properties, making it an important material for biomedical applications, including bone tissue engineering [104]. In its crystalline form, silicon carbide possesses stronger elastic modulus, lower frictional coefficient, extreme hardness, resistance and is chemically inert nature. SiC has a wider bandgap, ranging from 2.4 to 3.2 eV depending on the polytype, improving sensing capability and making it more biocompatible [105]. Low density, high strength, oxidation resistance, excellent thermal shock resistance, high hardness, wear resistance, chemical resistance, low thermal expansion and high thermal conductivity are some of the other interesting characteristics of silicon carbide [106–108]. SiC bioceramics have proven to be good materials for biomedical implants due to their bio-inertness, simplicity of handling, capacity to be molded into any desired shape, chemical & physical stability, and biocompatibility [109]. Several studies have shown that SiC can be used extensively for hip implants and load-bearing bones since it possess superior mechanical properties, slow degradation and high biocompatibility [50,51]. However, due to its low toughness, these scaffolds are susceptible to cracking over time. Therefore, careful design and processing methods are required to ensure long-term stability.

3.3.5. Calcium carbonate

Calcium carbonate ($CaCO_3$) is one of the most common minerals found on the earth and it is an excellent ceramic material to fabricate bone due to good biocompatibility and faster resorption rate. The disadvantage of calcium carbonate as a ceramic material is that it decomposes to calcium oxide (CaO) and carbon dioxide (CO_2) around 600 °C–700 °C, making the sintering process difficult [110]. Amorphous calcium carbonate (ACC) is a biomineral that has been used as a bioink by Shaked et al., for 3D bioprinting of bone scaffolds. ACC paste was prepared by stabilizing it with magnesium by using different binders like glycerol (GLY), ethylene glycol (EG), and triethylene glycol (TEG), which was later 3D printed using Hyrel 3D Engine-SR printer followed by sintering at 150℃ overnight. The chemical composition of the sintered samples was evaluated using energy-dispersive X-ray spectroscopy (EDS), where 50/50 (50% Ca solution and 50 % Mg solution) ACC models exhibited higher incorporation of Mg compared to other concentrations (60/40 & 70/30). It was observed that GLY could promote the formation of larger crystals than EG, and the smallest crystal was formed when TEG was used as a binder. This novel method of 3D printing ACC could emphasize the benefits and open up new possibilities for energy-efficient ceramic 3D printing in various applications [111]. Despite its biocompatibility, biodegradability, and low cost, calcium carbonate has less favorable mechanical properties than commonly used materials like hydroxyapatite (HA) and other ceramics.

3.3.6. Nano hydroxyapatite

Hydroxyapatite (HA) is a calcium apatite mineral $Ca_{10}(PO_4)_6(OH)_2$ with calcium to phosphorus ratio of 1.67. It is a physiologically active, biodegradable calcium phosphate that accounts for nearly 65% of bone mass and the bulk of inorganic components in bone tissue [112–114]. Synthetic HA will become highly crystalline calcium phosphate when treated at high temperatures. However, their physical properties differ slightly, such as microstructure, crystal size, and porosity. After implantation at the bone defect site, HA can directly link with nascent bone tissue, increasing graft vascularization and stem cell proliferation thereby accelerate bone regeneration [3,115]. Due to changes in physical and chemical features of HA crystallinity, microstructures, and solvability, the mechanical & biological aspects of HA-based bone substitutes can be improved by adding Sr^{2+} or Mg^{2+} [116,117]. The mechanical properties of 3D-printed nano-hydroxyapatite scaffolds can be tailored by varying the amount of ceramic material used, and they have been widely used for fabricating both load-bearing and non-load bearing bone implants. Furthermore, according to recent findings, HA bone grafts may aid in the faster healing of critical and non-critical-sized bone defects. Inkjet-based 3D printing, stereolithography (SLA) based 3D printing, extrusion-based 3D printing, and laser-based 3D printing are the four most common 3D printing procedures for printing hydroxyapatite-based bone models [118,119].

Although bioceramic/polymer composites are well-known for producing customized implants, their influence and use in 3D bioprinting are not thoroughly studied. In a study by Lee *et al.*, hydroxyapatite (HA)/gelatin composites were prepared by mixing different concentrations of HA (0%, 60%, 70%, and 80%) with gelatin, their mechanical and biological properties were studied. Maximum compressive strength of 8.4 ± 2.7 MPa was observed in 70% HA

scaffold compared to other conditions similar to cancellous bone. Further, the biological characterization of scaffolds was analyzed by culturing rat adipose-derived mesenchymal stem cells (RASMD) on the scaffolds, where maximum cell proliferation was observed in the scaffolds containing 60% HA. Moreover, osteogenic differentiation was seen greater in scaffolds with 60–80% HA, which was confirmed using ALP (alkaline phosphatase) and ARS (Alizarin Red-S) assays. This study confirmed that bioprinting of bioceramics and hydrogel composite scaffolds had improved shape fidelity, mechanical strength and bioactivity [120]. Zhang *et al.*, used UV curing method to prepare hydroxyapatite (HAP) suspensions. UV oligomers and monomers were combined with HAP powder, and then nano zirconia was added before 3D printing using a DLP printer. Mouse bone mesenchymal stem cells (mBMSCs) were seeded on these printed constructs with a density of 3000 cells/cm^2 and high cell viability was observed using live-dead staining [121]. In another study, Shao *et al.*, prepared a HA slurry and printed scaffolds with dimension of 18 × 18 × 5 mm^3 at three different speeds of 3 mm/s, 5 mm/s, and 8 mm/s using the 3D-gel printing (3D-GP) technique (Fig. 2A). The printability of the HA scaffold was affected by printing parameters such as printing speed, nozzle diameter, and layer height, where 5 mm/s printing speed was optimal for printing 3D scaffolds. The SEM analysis of the prepared scaffold showed the presence of micropores on the surface of the printed lines and the width of the printed lines was similar to the nozzle diameter (Fig. 2B). Fig. 2C shows the image of the green body and sintered sample, which shows uniform pore distribution without any structural defect in both the samples. Further, Tris-HCl degradation test showed 10.38% weight loss after 5 weeks, which indicate that these scaffolds are suitable for bone regeneration with controlled degradation [122].

Polycaprolactone (PCL) is also widely used for bone tissue engineering since it provides a porous architecture that resembles natural bone. Some of the properties of PCL such as hydrophobic nature, low bioactivity and poor mechanical properties limit its potential for bone tissue engineering applications. To overcome these existing challenges, Chlana *et al.*, modified and covered the PCL with nano hydroxyapatite (nHA), a ceramic layer of hydroxyapatite by wet chemical deposition method and further by low-temperature plasma surface modification with hexamethyldisilazane (HMDSZ) monomer. Each strand in printed construct had a diameter of 303–309 μm, and the scaffold had maximum compressive strength of 34 ± 1 MPa. Further, the wettability of the scaffolds was determined using contact angle measurements where PCL-printed scaffolds were hydrophobic with a contact angle of 110 ± 5°, and the PCL-HA scaffolds were hydrophilic with a contact angle of 27 ± 7°. Based on the findings of this study, it can be concluded that the surface modifications using HA improve the wettability of hydrophobic synthetic polymer scaffolds such as PCL [123].

4. 3D printing methods

Ceramic materials are tailored into required shapes from powder with or without binders using standard methods like gel casting, injection molding, machining, etc. The major drawbacks of making ceramics scaffolds are cost and long processing times [124]. Molding is the most common method for fabricating ceramic scaffolds. However, producing intricate geometries and interconnecting porous structures with this procedure is difficult. The rigidity and fragile nature of ceramics make them more difficult to machine processes and hence, these conventional processes fail to make intricate 3D structures using ceramic constituents [125]. 3D printing is a process that allows the facile fabrication of complex geometries and shapes, which is difficult to achieve using the standard fabrication techniques mentioned before [126,127]. The use of 3D printing in ceramic scaffold fabrication brings new prospects for addressing the limitations and challenges of traditional scaffold fabrication approaches. 3D printed ceramic materials are biocompatible, chemically resistant, have high strength-to-weight ratio and good thermal conductivity. In the same way, different 3D printing strategies like FDM, SLS, stereolithography, DLP and 3D gel printing, etc., are widely employed to fabricate bone scaffolds for tissue engineering & clinical research applications. The advantages and disadvantages of various 3D printing methods and their applications in the fabrication of ceramic scaffolds are mentioned in Table 2.

4.1. Fused deposition modelling

Fusion deposition modeling (FDM) is an extrusion-based 3D printing in which thermoplastic polymer filament materials are used to print 3D objects. Four major components of the FDM process include feeding material, print head, gantry and a building surface [145]. The FDM works on the principle of additive concept in which the material is laid down on the surface in a layer-by-layer fashion. 3D printing using FDM is performed by feeding a plastic thread or wiring into an extrusion outlet that controls the flow of material [146]. When thermoplastic filaments are placed in FDM, they melt between rollers and are extruded through a nozzle onto the build surface (Fig. 3A). A great advantage of FDM technology is multi-material printing to ensure good design quality, improved mechanical properties, better adhesive strength and excellent mechanical interlocking. The adhesive strength in FDM technology is determined by the slicing pattern of the substance attached as well as the density of the layers beneath the adjacent surface [128].

The bioactivity and mechanical characteristics of L-polylactic acid (PLLA)/hydroxyapatite (HA) in the fabrication of composite scaffolds using FDM were studied by Zhang *et al.,* for bone repair. The PLLA scaffold has a hydrophobic surface with a contact angle of 95.9°, and the hydrophilicity was increased further with an increase in the concentration of hydroxyapatite (HA 30% – 87.2° and HA 50% – 77.4°) (Fig. 4A). With a compressive strength of 15 MPa, scaffolds containing 50% HA had mechanical properties that were comparable to human cancellous bone (2–12 MPa). Rabbit mesenchymal stem cells (rMSCs) with a density of 5 × 10^4 were used for *in vitro* studies, and the CCK-8 assay showed no cytotoxicity effect of scaffolds after five days of culture. On day 1, the cells adhered to the porous scaffolds and cells grown on 50% nHA scaffolds showed elongated morphology compared to other groups (Fig. 4B). Further, scaffolds were implanted into femur defects (5 mm size) in rabbits for in vivo efficacy analysis. After 4 weeks of implantation, H&E staining results revealed bone tissue formation within the pores of the scaffold, and osteocytes had an oriented distribution which indicated the matured bone tissue (Fig. 4C). Compared to other complex, advanced, and cutting-edge 3D printing technologies, this research provides a low-cost, stable, simple, and quick method for personalized bone scaffold printing, which is unquestionably conducive to the advancement and rapid response of personalized biomaterials in clinical applications [129].

Clinical management of bone defects causes various difficulties, and 3D printing is helping to resolve them to a significant extent. Wang *et al.*, [130] developed a composite bone scaffold using poly-lactic acid (PLA) and nano-hydroxyapatite (nHA) by 3D printing using FDM. The composites were prepared by varying the ratio of nHA, which includes 0% nHA/PLA (Pn0), 10% nHA/PLA (Pn10), 20% nHA/PLA (Pn20), 30% nHA/PLA (Pn30), 40% nHA/PLA (Pn40) and 50% nHA/ PLA (Pn50) of which the 3D printed structure of Pn0 and Pn30 is shown in the Fig. 4D. The composition gradient was evaluated after fabrication, and it was determined that the

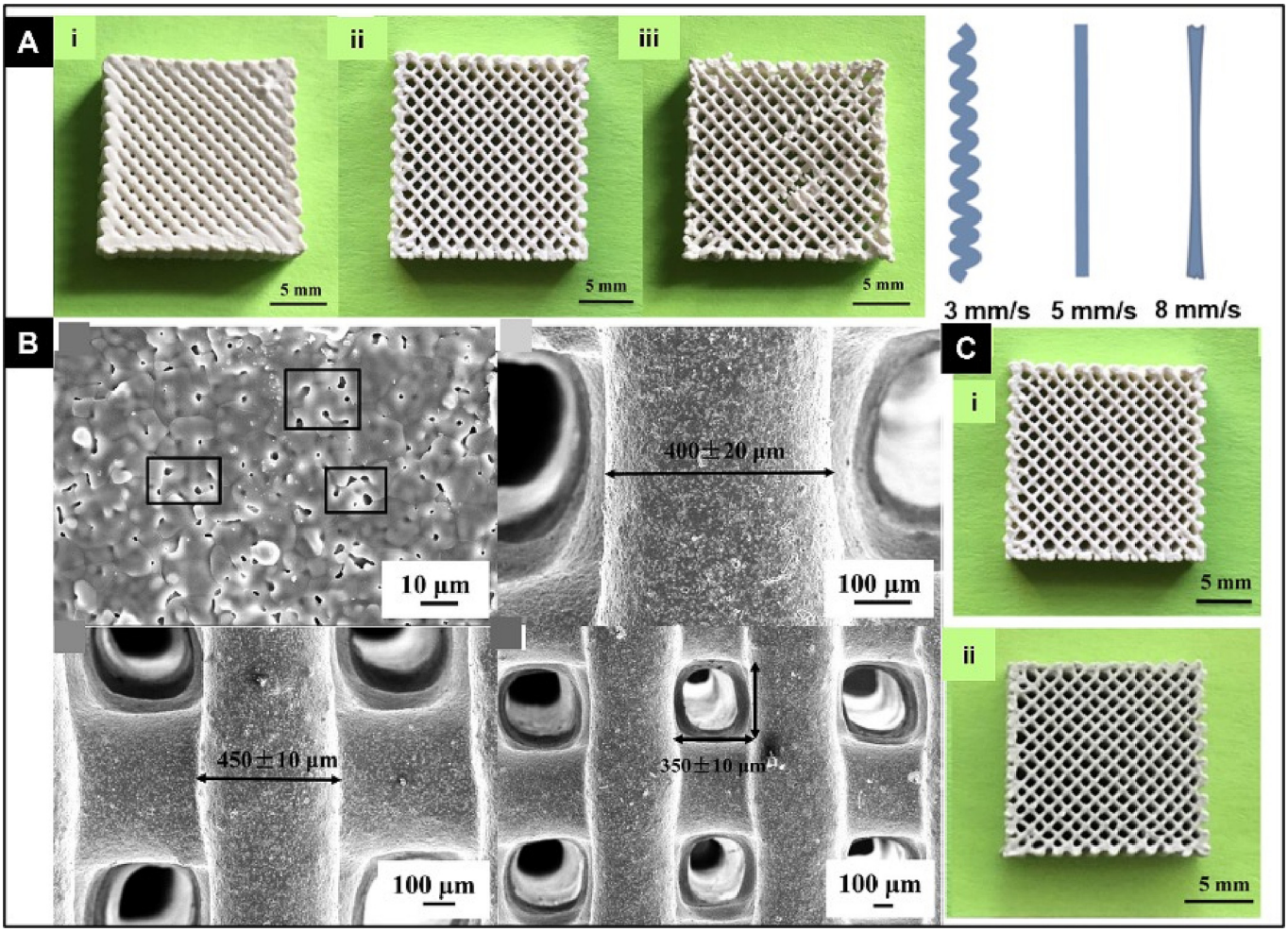

Fig. 2. Various scaffolds fabricated using nano–hydroxyapatite. [A] Ceramic samples printed by 3D gel printing, with different printing speeds: (i) 3 mm/s, (ii) 5 mm/s, and (iii) 8 mm/s. [B] SEM images of 3D printed sintered HA porous scaffolds; [C] HA porous scaffolds fabricated using 3D gel printing; (i) green body, (ii) sintered sample. Reproduced with permission from [122]. (For interpretation of the references to color in this figure legend, the reader is referred to the web version of this article.)

fiber color changed from translucent to white as the concentration of nHA increased. Mechanical tests of printed scaffolds showed that they could maintain their shape and integrity after applying pressure and maintained their elasticity. However, the scaffolds with more than 40% nHA were more brittle and did not maintain their shape after compression. Bone marrow mesenchymal stem cells (BMSCs) grown on scaffolds showed stretched morphology with pseudopodium for seven days without any cytotoxic effect. The Pn0 and Pn30 scaffolds were implanted into the defect of the rabbit femoral bone for 3 months. H&E staining and CT images of the scaffold demonstrated no tissue necrosis and inflammatory responses after implantation, and bone regeneration was maximum where the implant was in contact with the cortical bone. The CT image showed that the fastest-growing new bone was found towards the periphery of the bone defect area, which eventually filled inward and toward the center. At three-time intervals within three months of surgery, the Pn30 group consistently outperformed the Pn0 group in terms of the surface area and volume of new bone development (Fig. 4E). The H&E staining results showed the new bone formation of the bone tunnel within the implanted Pn0 and Pn30 scaffolds at 1, 2 and 3 months after implantation (Fig. 4F). Thus, the PLA and nHA composite scaffold has much potential for healing & treating various bone deformities and injuries.

4.2. Selective laser sintering

Selective laser sintering (SLS) is a 3D printing method that uses a high-power laser to sinter or bind all the components into a solid mass. This method operates with a CO_2 laser that helps to sinter the powder to form the first layer of the solid 3D printed structure (Fig. 3B). A roller is used for the deposition of the new layer of the powder, and the thickness of the corresponding layer increases [147]. Due to rapid cooling and heating rates induced by the high-intensity laser, it is not easy to produce bioceramics using SLS directly. However, this technology is particularly beneficial to fabricate composite scaffolds [132]. The essential parameters to be controlled in this method includes laser power, powder composition, and temperature. SLS is the only method that can be used to produce metal structures for fabricating dental implants. SLS is preferable over stereolithography because it achieves superior dimensional accuracy and does not require the usage of a support structure [148]. However, high temperatures in SLS may result in the decomposition of materials, making it more difficult to remove these substances once the scaffold has been manufactured, which may prevent cell proliferation and trigger inflammatory responses. In addition, the resolution of the product is determined by the size, shape, and arrangement of the dust particles, which is the major drawback of this approach.

Table 2
Different 3D printing methods used in the fabrication of ceramic based bone scaffolds.

Sl. No	Additive manufacturing method	Printing Resolution	Ceramic slurry/ink preparation method	Parameters for optimization	Advantages	Disadvantages	Ref
1.	Fused deposition modelling (FDM)	100 μm – 1 mm	Thermoplastic polymer & ceramic powders mixed to form a continuous filaments to print 3D scaffolds	Printing speed, nozzle temperature, offset and feed rate	Compatible with wide range of materials, easy operation, reproducibility and low – cost	Low resolution and improper adhesion between deposited layers	[128–130]
2.	Selective laser sintering (SLS)	50–250 μm	Powdered bed prepared with equal sized ceramic particles which can withstand the laser power & temperature to ensure defect free constructs	Laser power, powder composition, temperature, size and shape of powder	High resolution, printed constructs possess high mechanical strength, complex structure fabrication using powder as support	Requirement of powder materials, materials should withstand laser heat, shrinkage of the scaffolds, pre- and post-heating treatments for powders	[131–134]
3.	Stereolithography (SLA)	20–100 μm	Mixing of photopolymerizable liquid resin with ceramic materials	Layer height, exposure duration, intensity of light	High resolution, high printing speeds, low wastage of ceramic materials	Photopolymers are required for printing, additional support and post-processing steps	[135–138]
4.	Digital light processing (DLP)	25–100 μm	Vat filled with ceramic powder and liquid photopolymer is exposed to digital arrays of lights to fabricate bone scaffolds	Light intensity, exposure time, type of resin and layer height	High resolution, accuracy and cost-effectiveness	Limited materials availability, requirement of photo reactivity, limited build volume	[137–140]
5.	3D gel printing (3DGP)	100 μm – 1 mm	Homogenous ceramic slurry is prepared by mixing ceramic materials with water-soluble polymer binder solutions	External pressure, nozzle diameter, printing speed and slurry viscosity	Low cost, complex shape printability, high scalability, large size scaffold fabrication	Low-resolution, high-pressure requirements, needle clogging, support material requirements	[87,120,141–143]

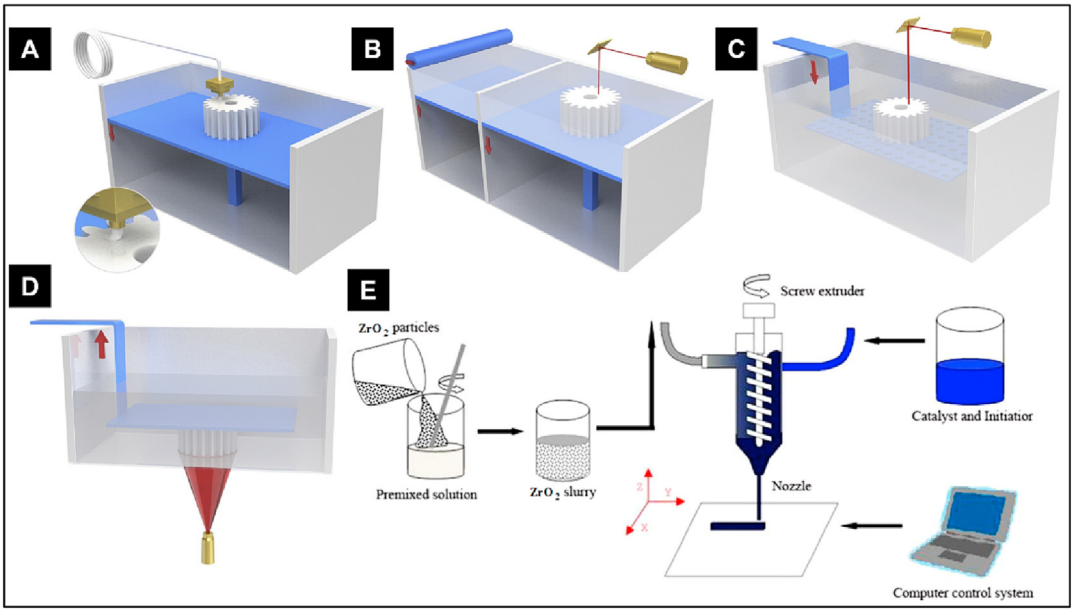

Fig. 3. Different types of 3D printing techniques used for ceramics printing. [A] Fused deposition modelling; [B] Selective laser sintering; [C] Stereolithography; [D] Digital light processing; (Reproduced with permission from [144]); [E] 3D gel printing. (Reproduced with permission from [127]).

Laser melting deposition is another method for manufacturing machine parts in industry and fabrication of ceramic scaffolds. Chioibasu *et al.*, [133] used this method to 3D print bone plates using titanium alloy (Ti6Al4V) and analyzed the physicochemical and biological properties. According to elemental mapping, the distribution of elements on the surface was uniform with no segregations or regions with the poor elemental distribution. The cytocompatibility of the implants were evaluated using Human osteosarcoma cells (SaOs2), which showed an exponential increase (40%) in the cell proliferation rate from day 1 to 7. Thus, the prototype orthopedic bone plates, 3D printed by laser melting deposition has great potential in tissue engineering. Tsai *et al.*, [134] fabricated a composite porous titanium scaffold (Ti-6Al-4V) using magnesium-calcium silicate (Mg-CS), and chitosan (CH) for orthopedic applications. Different types of composite scaffolds were prepared by varying the concentration of calcium silicate (CS0–0%,

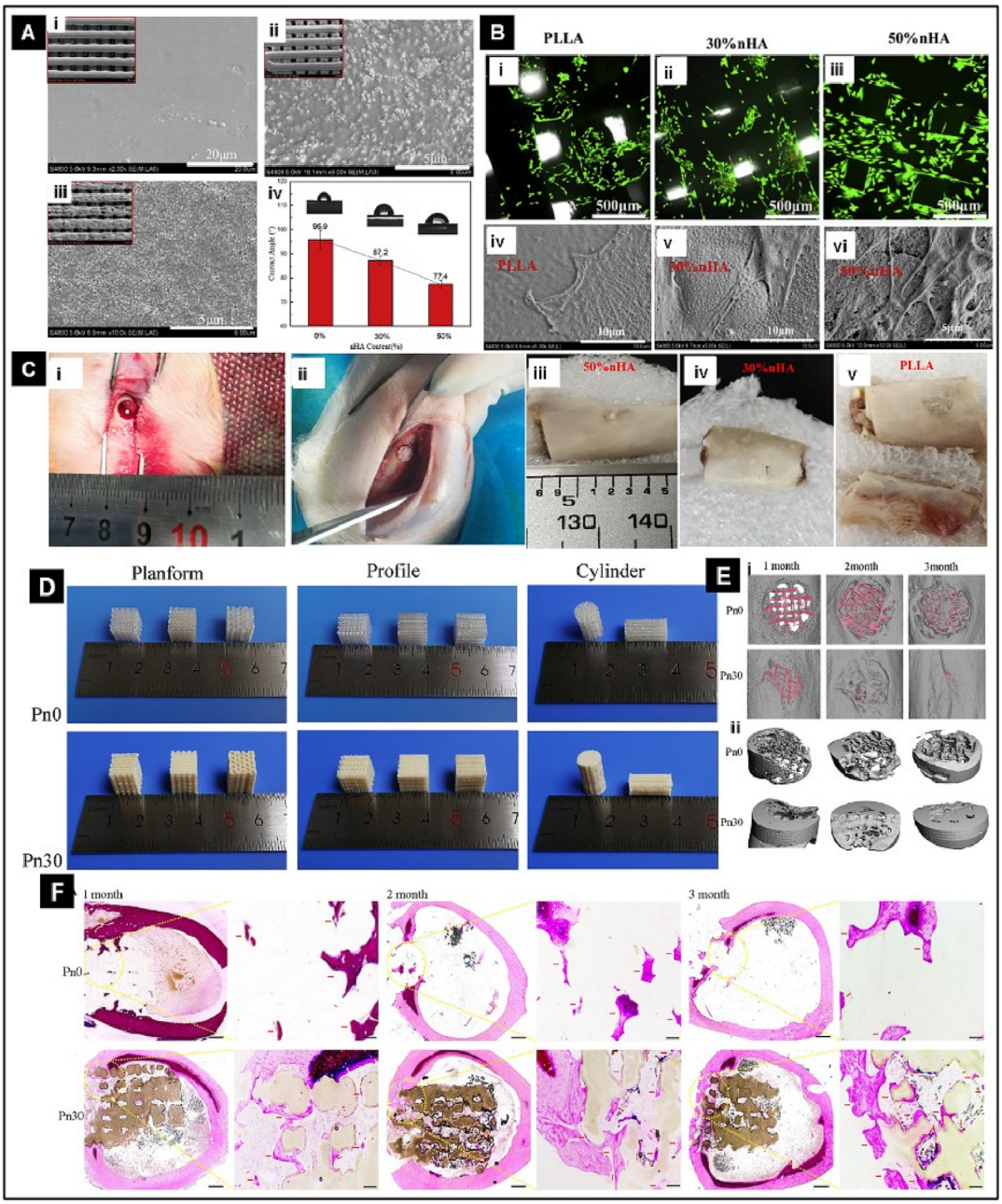

Fig. 4. [A] Morphology of composite scaffolds – (i) PLLA scaffolds; (ii) 30% nHA composite scaffolds; (iii) 50% nHA composite scaffolds and (iv) Water contact angle. [B] *In vitro* evaluation of 3D–printed scaffolds – (i – iii) Cell viability and (iv – vi) SEM images of rMSC cells cultured on different scaffolds at day 1. [C] (i) Creating bone defect model; (ii) Implantation of the scaffold in vivo and (iii – v) harvested after one month. Reproduced with permission from [129]. [D] 3D printed scaffolds of composite materials (Pn0 and Pn30); [E] Rabbit femoral bone defect repair using Pn0 and Pn30 composite scaffolds – (i) 3D micro–CT images of bone implants after 1, 2 and 3 months after implantation (Scaffold – red & bone – grey); (ii) Reconstructed images. [F] H&E staining of the bones slice for identifying new bone formation within the implanted scaffolds (Pn0 and Pn30) after 1, 2, and 3 months of implantation of rabbit femur. Reproduced with permission from [130]. (For interpretation of the references to color in this figure legend, the reader is referred to the web version of this article.)

CS20–0.2%, and CS50–0.5%) (Fig. 5A). The scaffolds showed higher hydrophilic behavior with higher content of Mg-CS (CS20 – 0° & CS50 – 0°) compared to CS0 and Al-4 V scaffolds. The scaffolds showed micro/macro porous architecture and good mechanical properties with compressive strengths between 48.5 ± 1.4 MPa and 50.3 ± 1.6 MPa. However, no significant difference was observed in the mechanical properties of scaffolds between the groups. The scaffolds were immersed in simulated body fluid (SBF), and ion release was studied using inductively coupled plasma atomic emission spectroscopy (ICP-AES) analysis. These results indicated that there was a minimal release of calcium and silicon ions from the scaffolds after 4 weeks of immersion (Ca ions – 1.6 3 ± 0.10 mM (CS20), 1.93 ± 0.05 mM (CS50); Si ions – 0.15 ± 0.04 mM (CS20) to 0.36 ± 0.04 mM (CS50). Human Wharton's Jelly mesenchymal stem cells (WJMSCs) were used to study the extracellular matrix secretion where the expression of COL 1 and FN increased proportionally with increase in CS content in the scaffold. In addition, in comparison to other scaffolds, CS50 scaffolds exhibited higher alkaline phosphatase activity and Alizarin Red staining, which indicated that the Mg-CS/CH-coated Ti-6Al-4V scaffolds with WJMSC promoted superior osteogenic differentiation for three weeks (Fig. 5B). As a result of these findings, novel

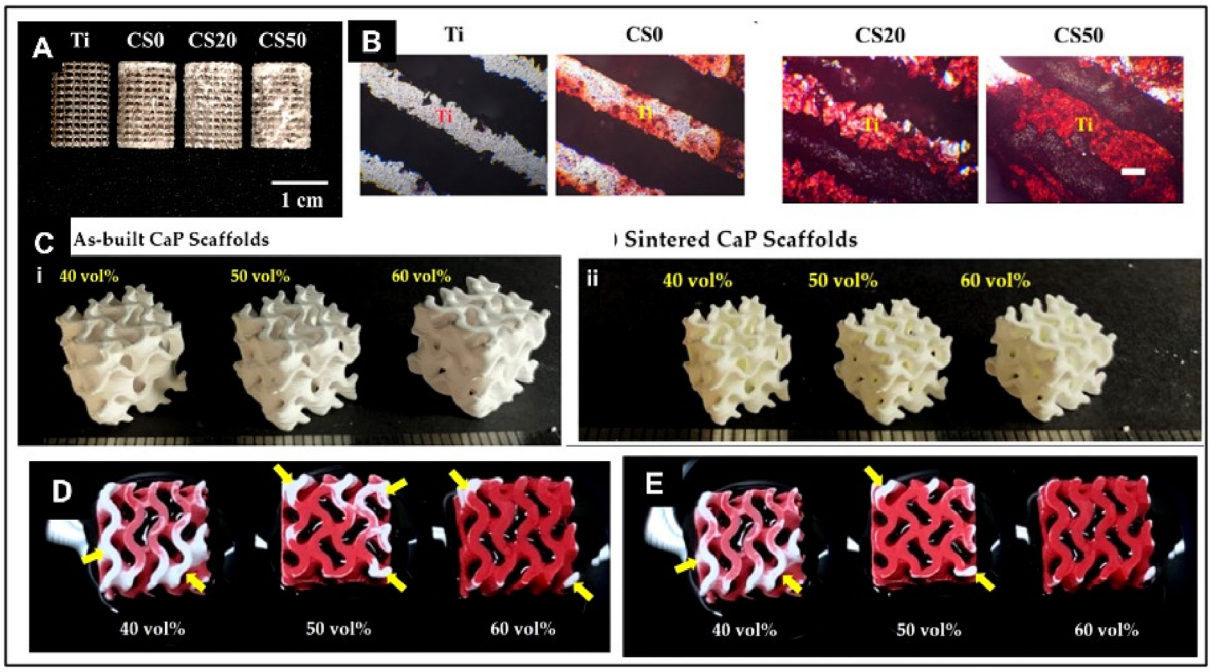

Fig. 5. [A] Macroscopic images of the Mg-CS/CH-coated Ti6-Al-4V scaffolds; [B] Alizarin Red S staining on the Mg-CS/CH-coated Ti-6Al-4V scaffolds with WJMSC for 3 weeks (Reproduced with permission from [134]); [C] Optical images of 3D printed scaffolds – (i) as–built and (ii) sintered CaP scaffolds with hierarchically porous structures and different camphene–camphor amounts (40 vol%, 50 vol%, and 60 vol%). Optical image of porous CaP scaffolds after various immersion times of [D] 10 s and [E] 25 s into the red dye added water. Yellow arrows indicate the regions without water penetration. (Reproduced with permission from [137]). (For interpretation of the references to color in this figure legend, the reader is referred to the web version of this article.)

alternatives may be developed to produce more durable bone scaffolds with improved biological response.

4.3. Stereolithography

Stereolithography (SLA), also known as photo-solidification, is an additive manufacturing technique that uses a photochemical process to print complex 3D structures layer-by-layer (Fig. 3C). SLA consists of a UV-curable photopolymer, a laser unit, galvanometric mirrors, support structures, an elevator, and a recoater blade [149]. The laser unit fires an ultraviolet beam onto a reflecting mirror after filling the vat/tank with liquid resin and imprinting the digital instructions. Galvanometric mirrors direct the UV beam to the resin surface, and the laser creates a layer on the support structure before creating the actual component structure [135]. After the layers are imaged on the resin surface, the elevator system lowers the build platform, and the recoater blade glides over the platform to apply the next layer of resin. This process is continued until the layer-by-layer imaging of the object is completed [150]. A UV curing oven is used to cure the prepared 3D-printed objects, and these layers solidify at the appropriate temperature, resulting in the desired product with excellent surface shine [136].

In a recent study, Zhou *et al.*, used stereolithography for 3D printing of β-TCP scaffolds. Biodegradability of β-TCP, make it an appropriate material for hard tissue regeneration. The surface tension of the β-TCP slurry was increased by adding KH-560 flocculant, which was 3D printed using stereolithography. The total printing duration was 76 min, where the bottom layer was printed in 15 s and subsequent layers were printed in 5 s with each layer thickness of 0.02 mm. Further, the prepared scaffolds were sintered in a muffle furnace at 1050 °C for 8 h with an isostatic press of 200 MPa applied for about 5 min. SEM analysis revealed that the average grain size of the scaffold was 0.7 μm, the slurry with 48% solid loading had 0.68 μm and a density of 85.8%. This study demonstrated that the β-TCP is a promising material for hard tissue regeneration including bone defect treatments [151].

4.4. Digital light processing

Digital light processing (DLP) is a 3D printing technology that uses resins made of photopolymers to create three-dimensional structures under an illumination source (Fig. 3D) [31,152]. A projector screen with digital light, digital micromirror device (DMD), conveyor and a resin tank that contains the printing material are the important components of a DLP [139]. DMD is an art made of many micromirrors that helps to navigate the light beam from the digital light projector [153]. A digital screen is made up of pixels and is employed as the origin of the light beam in DLP [140]. The main advantage of this technique is speed and printing efficiency with great dimensional accuracy, which makes it more preferable method for various 3D printing applications like printing of mouth parts in dental industries like maxilla, mandible, teeth, etc., and also for the production of affordable hearing aids [154].

Kim *et al.*, fabricated calcium phosphate (Ca-P) scaffold with tailored macro porosity and microporous layers for diverse bone scaffold applications to demonstrate the versatility of digital light processing (DLP) using freeze cast ceramic layer as feedstock. Photocurable suspensions were made using camphene-camphor with diurethane dimethacrylate monomers. Photocurable suspensions were freeze-casted and photopolymerized by DLP, resulting in solidification at a controlled temperature of 33–38 °C. Each layer in the printed Ca-P scaffold was about 220 μm, and these were photopolymerized with an exposure time of 20 s which was later made into a gyroid macrostructure with a pore size of about 1 mm × 1. 5 mm, and this was further sintered at 1250℃ for 3 h to make a strong scaffold. The optical image of the scaffold before and after sintering with varying porosity and different concentration of camphene camphor amounts (40 vol%, 50 vol%, 60 vol%) are provided in

Fig. 5C. The microporous structures of the Ca–P scaffolds were increased with the increase in camphene–camphor concentration from 40% to 60%. The water penetration was studied by immersing the scaffolds in water with red dye for easy understanding at different time points of 10 and 25 s. Increased camphene camphor concentration led to increased water penetration due to the elevated microporosity (Fig. 5D & E). MC3T3-E1 cells were used to determine the cytocompatibility of the scaffolds and the scaffold with 60% camphene–camphor concentration had the maximum cell viability. Due to increase in microporosity, the water penetration ability of the Ca–P scaffolds was greater in the 60% camphene–camphor scaffold. These results demonstrated the potential of these scaffolds as scaffolds for bone regeneration [137].

With the digital light processing (DLP) technique, Yao *et al.,* successfully prepared high-performance hydroxyapatite scaffolds with good mechanical properties and densification. A 30 mm × 40 mm × 350 mm solid bar structure model was printed to study the effect of sintering on the three-point bending strength test. The 3D printed samples were sintered at 1100℃, 1150℃, 1200℃, 1250℃ and 1300℃ for 2 h. Samples sintered at 1300℃ showed a density of 97%, bending strength of 92.4 MPa and flexural modulus of 3.24 GPa. *In vitro* experiments using rat bone marrow mesenchymal stem cells (rBMSCs) found no cytotoxicity for up to seven days. The DLP-printed construct with p-cell triply periodic minimum surface (TPMS) showed 74% porosity and 4.09 MPa compressive strength, which satisfies the criteria for cancellous bone substitutes. The results of this study demonstrated that the sintering in wet CO_2 atmosphere increases the densification of the construct and also contributes to the biological growth of the construct since it restrains dihydroxylation and promotes cell adhesion and proliferation, which are critical for early bone formation and osteointegration [138].

4.5. 3D gel printing

3D gel printing (3DGP) is an additive manufacturing technique to fabricate 3D objects, including biological scaffolds [122]. Compared to the other methods, 3D printing using 3DGP offers greater benefits in terms of wide variety of materials and the low cost of printing components. Different materials like metals, ceramics and their composites can be used for making 3D printed products using this method. Another benefit of this method is that it improves printing efficiency by depositing highly concentrated ceramic slurry to complex-shaped parts due to the slurry's good flowability and gelation characteristics [127]. The basic steps in 3DGP involve the preparation of pre-mixed solution and slurry, the addition of initiator or other crosslinking agents, and 3D printing. Besides this, the 3DGP device has four modules – a slurry preparing module, a 3D moving module, a screw extruding module, and a controlling module (Fig. 3E). The screw extruding module helps to extrude the slurry, whereas the 3D moving module helps to move the screw extruding module in 3D motion controlled by the controlling module [141]. Researchers used various bioprinting strategies to fabricate bone-like structures in which extrusion-based bioprinting was widely used due to the ease of fabrication and flexibility in producing complex structures. Further, extrusion-based printing was also employed to create a composite scaffold of hydroxyapatite (HA) and gelatin with more HA concentration to provide a microenvironment for bone tissue regeneration with mechanical and compositional properties similar to a natural bone matrix [120]. Chen *et al.,* 3D printed ceramic scaffolds with calcium silicate (Ca_2SiO_4) doped with magnesium (Mg) using an extrusion-based 3D printer with a coaxial double nozzle system [87]. In a recent study, Raja *et al.,* proposed a novel low-temperature production approach for fabricating calcium-deficient hydroxyapatite (CDHA) 3D scaffold for bone tissue regeneration using extrusion 3D printing. The green body structure was prepared using a paste of α-TCP (tricalcium phosphate) with HPMC solution as a binder and 3D printed by material extrusion. This green body was dried at 37 °C for 24 h, and cementation was carried out in phosphate buffer saline (PBS) solution at 37 °C, which formed the CDHA 3D structure (Fig. 6A). The scaffolds were prepared using different gauge sizes (21G, 23G and 25G) and infills of 50%, 60%, 70% and 80% (Fig. 6B). Further, drug loading efficacy of the scaffolds were studied by loading quercetin in α-TCP scaffold. Shrinking of the CDHA scaffold was visible after the sintering process at 1100 °C for 6 h when compared to the non-sintered (Fig. 6C). But the sintering of the CDHA scaffold with quercetin showed the complete burnout of the quercetin at high temperatures (Fig. 6C & D). Direct drug loading into α-TCP prior to scaffold fabrication revealed uniform drug distribution throughout the scaffold, including its pores. But only partial drug adsorption occurred on the scaffolds, with most of the drug adhering to the pores. Therefore, bone tissue engineering using low-temperature calcium phosphate as biomaterial has excellent potential for clinical applications to treat various bone defects [155]. Similarly, Cho *et al.,* used an extrusion-based 3D printing system to fabricate a macro/microporous bioactive scaffold using $CaO–SiO_2–P_2O_5–B_2O_3$ coated with rhBMP2 to repair critical femoral bone fractures in rabbits using an induced membrane approach. Using the induced membrane approach, the 3D-printed bioactive ceramic scaffold was used to cure femoral bone deficiencies in rabbits (Fig. 6E–G). The gross morphology and histological results of the midsagittal cross-section showed that the mature osseous bridging was only identified in the posteromedial cortex, and the rest of the cortex in the graft was filled with fibrotic tissues (Fig. 6H). Thus, the induced membrane approach showed promising results as a graft to repair critical-sized bone lesions [142].

Jianzhuang *et al.,* prepared a hydroxyapatite scaffold doped with magnesium silicate (MgSiO3) using 3D gel-printing technique and analyzed the influence of $MgSiO_3$ on the rheological properties, printability and dimensional changes. Shear-thinning behavior was observed in all samples where the slurries with high solid loading (50 vol%) showed higher viscosity than the low solid loading (40 & 45 vol%) due to the rapid agglomerations of ceramic particles. Further, a decrease in the viscosity of the $MgSiO_3$ doped slurries (3%, 5%, 8%, 12%) was observed with increasing $MgSiO_3$ concentrations. Moreover, with the increase in $MgSiO_3$ (12%) concentration, the printability of the slurries was decreased due to low viscosity. The morphological features of the prepared scaffolds revealed linked internal structures with a pore size of 350–620 μm and strand widths of 300–400 μm. Finally, the highest compressive strength was observed in the 3% $MgSiO_3$ scaffold with 93.1 MPa, while the lowest compressive strength of 40 MPa was observed in scaffolds prepared using 12% $MgSiO_3$. Increased weight of the $MgSiO_3$ in slurry led to weakened particle bonding, reduced compressive strength and bigger pores on the printed scaffold. The degradation studies of scaffolds in Tris-HCl showed a reduced weight of about 9.91% after 5 weeks in 3% $MgSiO_3$ scaffolds. This study showed the enhanced properties such as printability, mechanical tunability and controlled degradation of $MgSiO_3$ doped ceramic bone scaffolds [143]. Various types of 3D printing techniques used to fabricate bone scaffolds using ceramics were listed with their applications and outcomes in Table 3.

5. Clinical applications

As discussed earlier, bioceramics are materials composed of biocompatible ceramics and bio-glasses, which are used to prepare scaffolds for various biomedical applications [82]. The hardness and porosity of the scaffolds fabricated using bioceramics can be

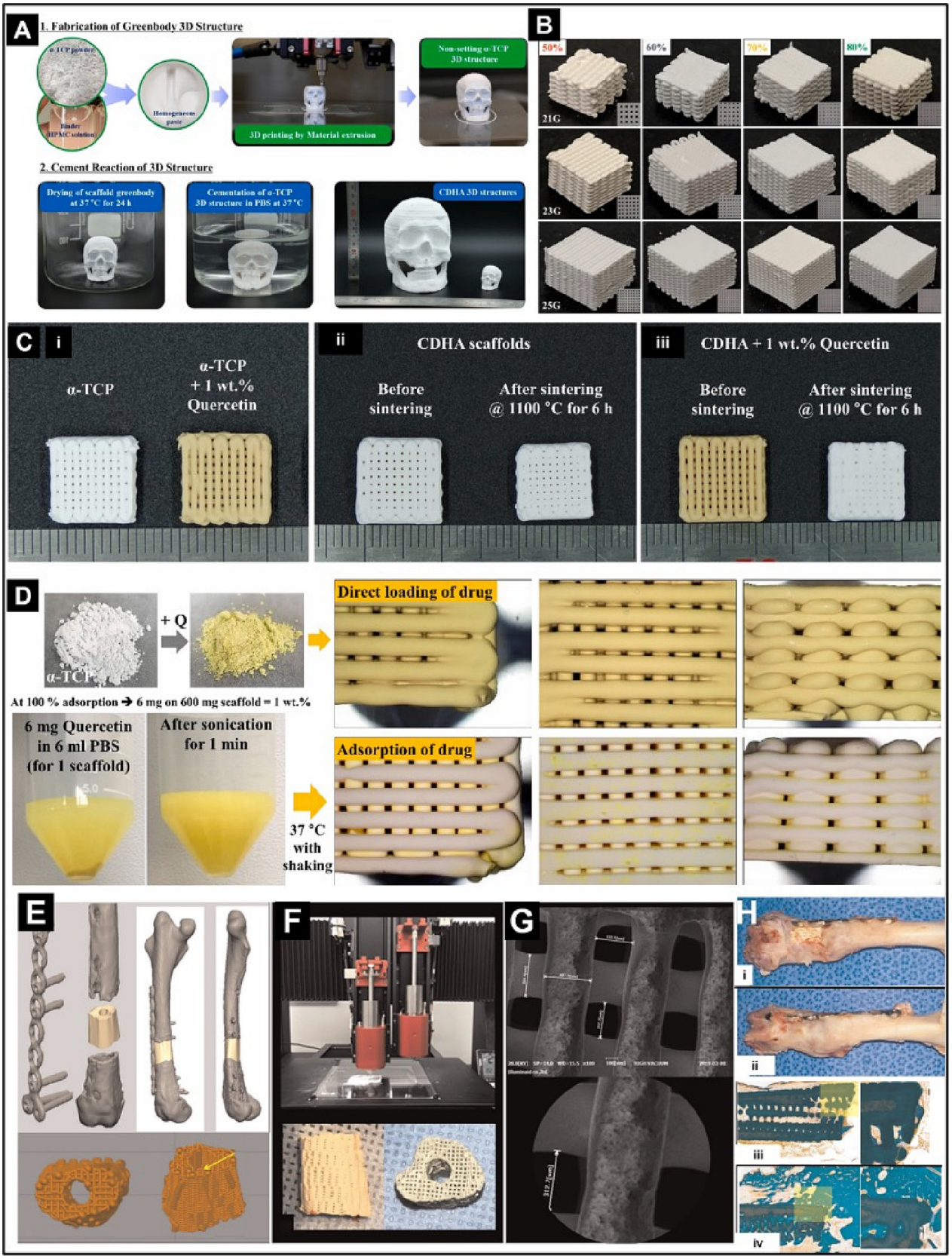

Fig. 6. [A] Schematic representation of two-Step additive manufacturing process for fabrication & hardening of calcium deficient hydroxyapatite scaffolds; [B] Comparison of overall structure of scaffolds printed using different nozzle and infill; [C] (i) Comparison of α-TCP scaffolds and α-TCP with 1 wt% Quercetin loaded scaffolds; (ii) Effect of sintering on CDHA scaffolds; (iii) Effect of sintering on CDHA with 1 wt% Quercetin scaffolds. [D] Visual comparison of drug loaded in α-TCP compared to drug loading on sintered scaffolds by adsorption. Reproduced with permission from [155]. [E & F] Scaffold design and three-dimensional (3D) printing of ceramic scaffolds with material extrusion (ME) type ceramic 3D printer; [G] SEM images of printed scaffolds; [H] Gross photos (i & ii) and midsagittal cross-sectional (iii & iv) histological images. Reproduced with permission from [142].

Table 3
Different types of 3D printing techniques used to fabricate bone scaffolds using ceramics.

3D Printing Technique	Materials Used	Resolution	Speed	Compressive Strength	Applications	Outcomes	Ref
FDM	Polylactic acid/ biphasic calcium phosphate	0.2 mm	40 mm/s	–	Bone substitutes	The structures had high porosity with granule size of < 100 nm, pore size was > 200 μm. The scaffold had good osteoconductive properties, bioresorbable, and biocompatible	[156]
FDM	Polylactic acid/ hydroxy-apatite			58 MPa	Femur fracture treatment	The scaffold promoted rigidity and resistance against external or axial load, increased porosity of 80-85%	[157]
FDM	Poly(ether ether ketone)/calcium hydroxy-apatite/ reduced graphene oxide			Young's modulus of 1000 GPa & tensile strength of 130.5 GPa	Hip implant fabrication	Improved osteogenesis	[158]
FDM	Poly(ether ether ketone)	0.8–1.2 mm	10–30 mm/s	197.83–370.42 MPa	Fabrication of load-bearing bone scaffolds, bone tissue engineering	Scaffolds with uniform and gradient pores, the rough surface of the scaffolds allows the attachment, migration and differentiation of the cells, useful for the fabrication of load bearing bone implants	[159]
FDM	Biphasic calcium phosphate scaffold reinforced with zirconia (ZrO_2)	0.4–0.6 mm	100 mm/min	0.5–1 MPa	Bone tissue and cartilage fabrication	Interconnected porous scaffold fabrication with good mechanical properties, increased expression of bone morphogenic protein-2	[160]
FDM	Polylactic-acid-bioactive glass 18 composite scaffolds	0.2–0.6 mm	–	3–18 MPa	Bone tissue engineering & regeneration applications	Open-porous and osteoinductive scaffold, increased osteogenic differentiation of human adipose-derived stem cells	[161]
FDM	poly(lactic acid), and hydroxy-apatite	0.06 mm	–	1.2–85 MPa	Fabrication of trabecular bone models	Enhanced mechanical properties & strength of the scaffold compared to commonly used synthetic bone models	[162]
Stereolithography	Poly HIPE (High internal phase emulsion)	–	–	–	Induction of osteosarcoma on trabecular bone mimicking the structure	Mimics the hierarchical structure of native tissue with macro porosity	[163]
Stereolithography	Titanium alloy (Ti-6Al-4V)/β-Tricalcium phosphate	–	–	–	Fabrication of hemi-knee joint	Resembled the original structure of the joint with interconnected pores of 250 μm and microchannels of 300 μm	[164]
Stereolithography	β-Tricalcium phosphate/poly (ethylene glycol) diacrylate	0.1 mm	–	–	Bone implants	A biphasic osteochondral scaffold with designed interface and shape was successfully fabricated	[165]
Stereolithography	Colourless photo curable acrylic resin	0.08 mm	–	5 MPa	Anatomically shaped bone implants, bone defect repairing	Oscillatory perfusions were performed for better cell attachment and proliferation	[166]
Stereolithography	Poly(trimeth-ylene carbonate) resins with hydroxy-apatite	0.05 mm	–	–	Bone repair	Increased osteogenic differentiation of human bone marrow stem cells, osteointegration, tailored architecture and functionality of the scaffold	[167]
SLS	13-93 Glass	0.152 mm	76.2–304.8 mm/s	5–11 MPa	Load bearing bone implant fabrication	Scaffolds contains good pore interconnectivity, porosity, mechanical strength & bioactivity	[168]
SLM	β-tricalcium phosphate and poly (D, L)-lactide	–	–	13–23 MPa	Fabrication of biodegradable bone implants	Scaffolds were biodegradable with good bending strength	[169]
DLP	Hydroxy-apatite	–	–	15.25 MPa	Bone repair	Scaffolds with good mechanical properties, porosity and pore size, biocompatible, promote cell proliferation, adhesion and differentiation	[170]
DLP	ZrO_2/HA composite	-	-	39.99–52.25 MPa	Bone repair	Excellent compressive strength, mimics natural cancellous bone	[171]
Inkjet printer	Calcium phosphate	0.11–0.8 mm	4–10 mm/s	1–5.5 MPa	Skull bone tissue reconstruction	High porous structures (60-80%) were implanted in the beagle's skull, and after 8 weeks, new bone tissue formation was observed	[172]
Inkjet printer	Tricalcium phosphate	–	–	–	Bone implant fabrication	Improved bone regeneration and vascularization was observed in the holes of the scaffold. Connective tissue formation was also visible from the scaffold	[173]

(*continued on next page*)

Table 3 (*continued*)

3D Printing Technique	Materials Used	Resolution	Speed	Compressive Strength	Applications	Outcomes	Ref
Ink jet printer	Pure-phase lithium calcium silicate ($Li_2Ca_4Si_4O_{13}$, $L_2C_4S_4$) bioceramic	–	3 mm/s	15–40 MPa	Osteochondral interface reconstruction	Scaffolds with high porosity, improved chondrocyte and rBMSC cell viability, gene expression & excellent osteochondral regeneration	[174]
3D gel printing	β-Tricalcium phosphate/calcium silicate/hydroxy-apatite	0.25 mm	4-6 mm/s	–	Bone regeneration and augmentation of bone implant	Enhanced cell adhesion and differentiation of mBMSCs with increased gene expression of HUVECs	[175]
3D gel printing	Gelatin/ bioactive glass	–	10 mm/s	5.1 ± 0.6 MPa	Bone regeneration implant fabrication	Scaffolds was biocompatible and has good toughness and resilience with high porosity (60-70%)	[176]
3D gel printing	Hydroxy-apatite	–	–	9.34 ± 0.59 MPa	To promote osteogenesis in patients with bone abnormalities such as osteogenesis imperfecta.	Scaffold was biomimetic, promotes cell adhesion, differentiation and proliferation, with excellent permeability and compressive strength	[177]
3D gel printing	β-Tricalcium phosphate/ bioactive glass	–	6.5 mm/s	8 MPa	Osteogenesis, angiogenesis, treatment for calvarial bone defect	Scaffold had good mechanical and biological characteristics with porosity of 56-58%	[178]
3D gel printing	$CaSiO_3$ powder	–	10 mm/s	16.52 MPa	Bone tissue engineering	Good porosity and compressive strength	[179]
3D gel printing	Mg & epoxy resin	–	3-20 mm/s	13.18-20.05 MPa	Bone repair and bone tissue engineering	Scaffolds with high porosity, excellent compressive strength, improved cell adhesion and osteogenesis, good biocompatibility, and degradability	[180]

tailored by varying the concentrations and sintering parameters. The most common use for these bioceramic scaffolds is to create implants to repair bone loss or deformations. Human/clinical applications of 3D printed ceramics or ceramic composite scaffolds in several bone defect reconstructions and their outcomes are described in Table 4. Due to the biocompatible and non-toxic behavior of bioceramics, they avoid the body's natural defensive mechanisms by mimicking the natural bone composition and microenvironment [181]. Other advantages of these bioceramics include high wear resistance, lesser plastic and elastic deformations, high compressional strength, low friction coefficient, biological and chemical corrosion resistance [182]. Studies have shown that these ceramic scaffolds can also promote cell growth, proliferation and tissue regeneration, which subsequently help in various medical applications [125,183]. Apart from bone defect repairing and bone-implant fabrication, these ceramic scaffolds are also applicable in various other fields, and a few of these applications are discussed below.

5.1. Cancer treatment

Osteosarcoma is the most common type of primary bone cancer that usually affects adolescents and young adults, although it can occur at any age. Osteosarcoma often affects long bones and has a rapid growth rate with high metastasis and recurrence rates [184,185]. The current treatment regime includes a combination of tumor resection surgery, multiagent chemotherapy, and/or radiotherapy. However, the results are sometimes unsatisfactory, as remaining cancer cells on the resection margin may be resistant to chemotherapy or insensitive to radiotherapy [186]. Therefore, neoadjuvant therapy such as photothermal therapy (PTT), which utilizes light energy (near-infrared/NIR) to induce localized heat and cause cancer cell necrosis, has been developed in recent years and showing promising results [187]. Moreover, the photothermal agent can be embedded within the 3D printed scaffold used to fill the bone defect after tumor removal surgery, resulting in a comprehensive and efficient treatment of osteosarcoma. Ma *et al*., designed Fe-$CaSiO_3$ (30CS) composite scaffolds by facile ball milling and 3D printing since Fe has excellent fatigue resistance and compressive strength, which are required for load-bearing bone structure and 30CS acts as a great photothermal agent. The 30CS scaffolds were prepared by mixing the iron powder with calcium in different mass percentages of 40, 30, 20, and 10% (Fig. 7A). The basic principle of this scaffold for treating cancer is photothermal and reactive oxygen species (ROS) therapy, which involves the release of iron from the 30CS composite scaffold that inhibits tumor growth. Studies have proved that excess ROS liberation can lead to rapid lipid peroxidation, protein and DNA damage [188]. The compressive strength of the 30CS scaffolds was 126 MPa after sintering at 1350 °C. Saos2 (sarcoma osteogenic) cells were used for *in vitro* studies, and laser irradiation of 30CS scaffolds caused 91.4% of cell death due to cell membrane collapse, coagulative necrosis, protein denaturation, mitochondrial malfunction, and enzyme inactivity. Macroscopic photographs of tumors from six groups on day 15 after implantation of scaffolds and IR thermal images of tumor-bearing mice exposed to 808 nm laser for 600 s are shown in Fig. 7B. Upon NIR irradiation for 10 min, Fe from the 30CS scaffold was released and showed that the ROS produced from the scaffold had antitumor efficiency, which was confirmed by H&E staining. Fig. 7C displays micro-CT scans and histological analyses of the defects in the $CaSiO_3$, Fe, and 30CS groups after 8 weeks of surgery. ROS does not harm the healthy cells as it harms the cancerous cells due to the high concentration of H_2O_2 in tumor cells. Osteogenic differentiation of the scaffold was later verified by observing the upregulation of the bone-related genes or the markers like COLI, OCN, Runx2, and BMP-2 by qRT-PCR on day 7. As a result, the 3D printed Fe-CaSiO3 composite scaffolds can be used as versatile and effective biomaterials for future cortical bone regeneration

Table 4
Human/clinical applications of 3D printed ceramics or ceramic composite scaffolds. [TCP: tricalcium phosphate; CT: computed tomography; mPCL: medical grade polycaprolactone; PCL: polycaprolactone; RIA: Reamer-Irrigator Aspirator®; HA: hydroxyapatite; BCP: Biphasic calcium phosphate; CGFs: concentrated growth factors & PRF: platelet-rich fibrin].

Material(s)	Disease/Condition	Application Type	Total Patients	Results and Follow-up	Ref
α-TCP	Maxillofacial bone deficiencies due to congenital condition or trauma	Maxillofacial bone defect reconstruction	20 patients (18-55 years old)	3D printed bones were applied in 23 regions in 20 patients, with follow-up periods ranging from 12 to 115 months. The success rate was 78%, with CT scans showing graft fusion with native bone. Grafts applied in two regions did not fit well, while three other regions were exposed after one year	[193]
mPCL and TCP scaffold at 80:20 ratio, 3D printed by Osteopore®. The scaffold was filled with RIA bone grafting obtained during surgery	Complex irregular large bone defect due to infected open femoral fracture (6 cm on the medial and 11 cm on the lateral side)	Long bone defect reconstruction	One patient (29 years old)	At 1-year follow-up, the patient experienced no pain under full weight bearing. The X-ray showed adequate bone formation, while CT-scan confirmed near-complete bony fusion and partial degradation of the biodegradable scaffold	[194]
$CaOSiO_2$-$P2O_5$-B_2O_3 glass-ceramic (BGS-7)	Zygomatic bone defects after malarplasty for aesthetic reasons	Maxillofacial bone defect reconstruction	Eight patients (24-53 years old)	At 6 months following surgery, no complications or adverse effects were found. CT scan showed adequate integration (bone fusion) between the implant and native bone in all patients, with a fusion rate reported as high as 77%. The mean implant displacement was only 0.4 mm. All patients (except patient 3, who withdrew from the study in the third month) reported high satisfaction scores (9/10) for both aesthetics and function	[24]
30 %HA-70% β-TCP BCP 3D-printed scaffold	Alveolar bone defect	Dental bone defect augmentation	One patient	Seven years following implantation, microCT and histology biopsies showed residual scaffold 25.6% (not fully resorbed), regenerated bone 59.2%, and soft tissue 15.2%. Interestingly, the 3D-printed BCP scaffold still preserved the correct bone microarchitecture despite not participating in mastication for 7 years	[195]
mPCL-TCP scaffold at 80:20 ratio, 3D printed by Osteopore®	Tibial bone defects after infection and malignancy, post-traumatic calvarial defect, and congenital mandibular bone deficiency. Defect sizes varied from 2,564 to 149,285 cm^3 (36 cm long)	Massive bone defect reconstruction	Four patients (12-27 years old)	In all cases, sufficient bone regeneration was seen within 12 months after surgery. Quality of life (QOL) assessments were performed 1–4 years after reconstruction, with 75% of patients reporting improved QOL and having returned to work, while one patient reported lower QOL due to a more complex underlying medical condition (malignancy)	[196]
PCL and β-TCP at 8:2 ratio	Complex zygomatico-maxillary defects due to malignancy, degeneration, or trauma	Maxillofacial bone defect reconstruction	Eight patients (19–50 years old)	Overall, jaw stability was achieved, and no occlusal complication was found. At 6 months after reconstruction, CT scans showed an average of 79.71% volume conformity between pre–operative and post-operative implant volume. The average de novo bone formation volume was 2.15 mm^3. Bone volume fraction (de novo bone formation ratio to the total implant within the area of interest) ranged from 7 to 66%. However, one patient had an implant exposure after radiotherapy	[197]
CaO-SiO_2-P_2O_5-B_2O_3 glass-ceramics (BGS-7)	Hypoplasia of the zygomatic bone	Maxillofacial bone defect reconstruction	One patient (30 years old)	Fourteen months following surgery, sufficient new bone formation was confirmed via cone-beam CT, and implant integration with the native bone was achieved. No displacement of the 3D-printed ceramics implant was found. The patient reported no complications and was satisfied	[198]
Nano-hydroxyapatite	Ridge resorption prevention following	Dental bone	30 patients	At four months after surgery, adequate	[199]

(*continued on next page*)

Table 4 (*continued*)

Material(s)	Disease/Condition	Application Type	Total Patients	Results and Follow-up	Ref
	tooth removal due to periodontitis	substitute (bone void fillers)	randomized into two groups (3D printed nHA and Nano Bone®)	new bone formation was observed in both groups. Equivalent residual graft, fibrous connective tissue, and alveolar bone resorption were seen in both groups. The 3D printed nHA group showed less soft tissue surface resorption than NanoBone®, although it was not statistically significant	
mPCL-TCP scaffold at 80:20 ratio, 3D printed by Osteopore®	Non-union and malunion due to complex lower extremities fractures (defect volume 29.89 to 165.72 cm^3)	Long bone defect reconstruction	Four patients (23-42 years old)	Significant bone formation was shown in all patients under 12 months following scaffold implantation. Two patients could walk pain-free without any assistive device support under 12 months. Two other patients could bear full weight bearing with crutches at 6-7 months follow-up	[200]
HA only in 3 patients, and HA incorporated with CGFs and PRF membrane in 9 patients	Alveolar bone defect (horizontal ridge deficiency)	Dental bone defect augmentation	12 patients (mean age 53.5 years)	The success rate was 83% (10 out of 12 patients). Adequate bone volume was achieved within 6 months, with histological findings showing full integration of the 3D printed graft in the graft site and new blood vessel formation at the interface between native and neo-bone	[201]

and cancer treatment, serving as a universal platform for material science, tissue engineering, and tumor therapy [189].

3D printed bioceramics scaffold made of tricalcium phosphate (TCP) coated with TiN (TN) microparticles at different concentrations and doxorubicin (DOX), which is a drug used for chemotherapy at different concentrations, was used by Dang *et al.,* as synergistic therapy for osteosarcoma. Digital photographs and SEM images of TCP, TCP–1TN, TCP–2TN, and TCP–3TN scaffolds are shown in Fig. 7D. These scaffolds were subjected to NIR light with various power densities to examine the effect of power density on the photothermal performance of scaffolds. The TCP scaffolds were not able to transform the NIR light to heat since the temperature of the TCP scaffold was only 23.8 ± 0.73 °C, whereas the temperature of the TCP-TN scaffold ranged from 78.55 ± 1.92 °C to 113.99 ± 1.76 °C. These findings reveal that TiN nanoparticles absorbed NIR substantially, with a photothermal conversion efficiency of 48%. K7M2wt cells were used for the *in vitro* studies and no cytotoxicity was observed. Further, cell growth was similar to the control group in TCP-TN scaffolds, and after NIR emission, the cell viability drastically reduced, which showed its photothermal therapeutic efficiency. Whereas in the DOX coated scaffold, the cell viability reduced with an increase in DOX concentration, and this was due to the cumulative release of DOX from the scaffold. BALB/c nude mouse models were used to develop osteosarcoma by injecting K7M2wt cells. Further, the tumor area was exposed to NIR for 10 min to develop a photothermal effect in which TCP-TN had no therapeutic effect on the tumor. Scaffolds implanted with DOX-coated TCP did not develop osteosarcoma and tumor growth since DOX killed the osteosarcoma tumor cells. H&E staining showed a dense and complete tumor tissue formation in TiN coated TCP scaffold, whereas the TCP-DOX was observed with loose tissue and disappeared tumor cells (Fig. 7F). These findings could lead to the development of multifunctional local implantations for tumor eradication following surgical treatments with minimal side effects [190].

Different studies have proved that transition metals are great photothermal agents for treating tumors. Liu *et al.,* utilized this property of the transition metals and made scaffolds with Ca-Si-based bioactive glass-ceramic (BGC) doped with elements like Cu, Fe, Mn and Co. The scaffold degradation was studied in Tris-HCl, which showed a mass loss of 21.3%, 15.9%, 4%, 8.8% and 19.9% in Cu-BGC, Fe-BGC, Mn-BGC, Co-BGC and BGC respectively in 28 days. To evaluate its photothermal behavior, scaffolds were irradiated with NIR for 5 min, where the doped scaffolds showed an increase in temperature, demonstrating that BGC had no photothermal property. The photothermal anti-tumor property of the scaffolds was studied by growing Saos-2 cells. After 808 nm laser irradiation for 15 min, the cell survival rate was 1.2% in the Cu-BGC group, 17.6% in the Fe-BGC group, 37.4% in the Mn-BGC group and 43.1% for the Co-BGC group. In contrast, the survival rate in the BGC scaffold was the same before and after irradiation, about 98.1%. It was also observed that, as the laser power increased, the survival rate in all the doped scaffolds was less than 5%. *In vivo* tests were conducted in nude mice by injecting Saos-2 cells at a density of 5×10^6 to create tumors. Then, the scaffolds were implanted and further irradiated with NIR. As expected, the temperature was higher in those implanted with element-doped scaffolds compared to only BCG scaffolds. After the treatment, the fluorescence intensity in the mice treated with Cu-BGC was found to be the lowest, showing its potential in tumor therapy. As a result, elements-doped bioactive glass-ceramics show much potential for photothermal tumor therapy and bone regeneration [191].

Various studies have proved that photo/magnetothermal joint treatment is more advantageous in killing tumor cells than single photothermal or magnetothermal treatment. Therefore, Zhuang *et al.*, 3D printed akermanite (AKT) bioceramics doped with iron at different concentrations to fabricate bone scaffolds with good osteogenic activity for treating bone tumors. The scaffolds were 3D printed after mixing Fe-AKT with sodium alginate and Pluronic F-127 solution to produce ceramic ink, extruded using a 3D plot-

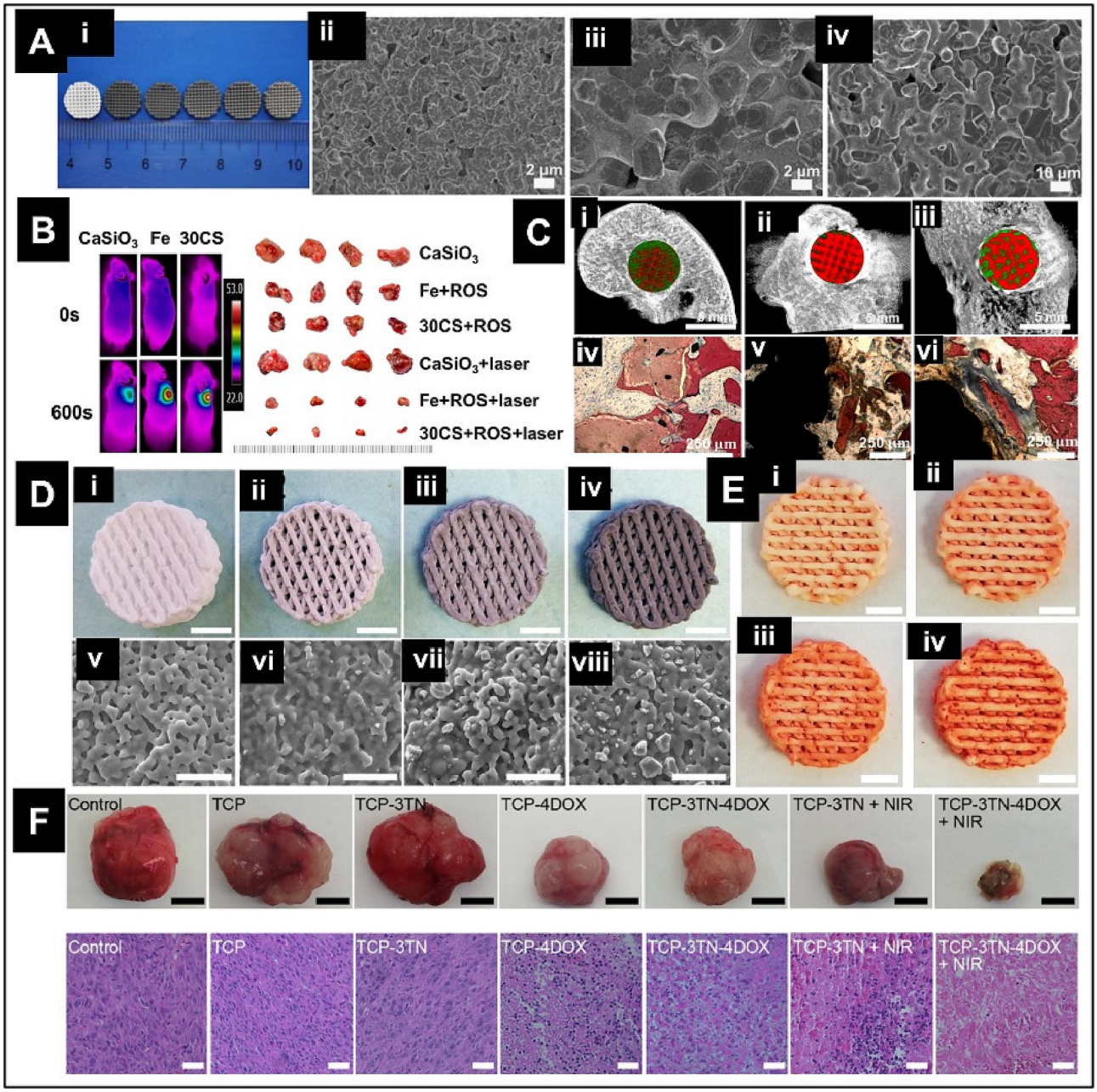

Fig. 7. Different 3D printed ceramic scaffolds are used for treating bone cancers. [A] (i) Macroscopic images of 3D printed scaffolds ($CaSiO_3$, 40CS, 30CS, 20CS, 10CS, and Fe). SEM images of scaffolds sintered at 1350 °C; (ii) $CaSiO_3$, (iii) Fe, (iv) 30CS. [B] IR thermal images of tumor-bearing mice under irradiation by an 808 nm laser for 600 s & macroscopic images of tumors from the six groups on day 15. [C] Micro-CT images & histological analysis of the defects in the $CaSiO_3$, Fe, and 30CS groups 8 weeks post-surgery. Reproduced with permission from [189]. [D] Digital photographs and SEM images of (i, v) TCP; (ii, vi) TCP – 1TN; (iii, vii) TCP – 2TN and (iv, viii) TCP – 3TN scaffolds. [E] Digital photographs of (i) TCP – 1DOX; (ii) TCP – 2DOX; (iii) TCP – 3DOX and (iv) TCP – 4DOX. [F] Photographs of the harvested tumor on day 18 and H & E staining images of tumor tissues from mice with different treatments. Reproduced with permission from [190].

ting system based on the Nano-Plotter and sintered at 1250 °C for 3 h. The degradation studies were performed in Tris-HCl for 3 weeks, and the mass loss observed for AKT, 1Fe-AKT, 2Fe-AKT and 3Fe-AKT was about 28.04, 23.23, 22.34, and 28.61% respectively. The photothermal properties of the scaffolds were studied by irradiating the infrared beam on the scaffolds, and the temperature emitted by scaffolds increased as the concentration of the iron doped in the scaffold increased. The viability of LM-8 cells incorporated into the scaffolds was less than 2% after photo/magnetothermal treatment, and the cell viability was determined to be 59.2% and 81.6% after photothermal and magnetothermal treatment, which revealed that most tumor cells were killed after photo/magnetothermal treatment. Cell adhesion and proliferation on scaffolds were studied using rabbit bone mesenchymal stem cells (rBMSCs), where the cells cultured on the 3Fe-AKT scaffold possessed a higher cell proliferation rate. RUNX2, OPN, OCN, and BMP2 genes of rBMSCs cultured on Fe-doped AKT scaffolds were greater in osteogenic differentiation than in control groups. Since AKT scaffolds had good apatite-formation capacity, the results revealed that iron doping in AKT did not affect the apatite-formation ability of the scaffold materials [192].

5.2. Hip implant fabrications

Among various types of bone implants, ceramic implants are widely used to treat bone defects and injuries due to their potential in biomimicking natural bone [3]. Various diseases and conditions lead to defects and injuries in hip bone, including arthritis, dysplasia, trauma, etc. In severe or end-stage conditions, the treatment often leads to bone's surgical replacements with metal implants. However, several reports showed that the debris from these metal implants might cause metallosis, a condition where local tissue reaction and/or systemic organ manifestations occur due to the damaging effect of metal wear particles. It may range from localized dermatitis, rashes, swelling, pain, inflammations, pseudotumor, organ dysfunction, etc [202,203]. Therefore, ceramic bone implants are cutting-edge discovery for different medical attention since they have less immunogenicity and mimic natural bone [82]. Various ceramic materials such as zirconium, hydroxyapatite, bioactive glass, etc., can be used for fabricating hip implants or prostheses.

As discussed, zirconia is the most commonly used ceramic material for preparing hip prostheses and implants due to its long-term wear resistance and good biocompatibility. Zhu *et al.,* prepared zirconia ceramic-based implants for the hip joint with antibacterial properties. The ceramic slurry of zirconium oxide (ZrO_2) and ZrO_2 doped with zinc oxide (ZnO) nanoparticles were prepared and 3D printed using Makerbot Z18 3D printer and sintered at 1000 °C for 10 h, followed by 1200 °C for 2 h. The antibacterial properties of the ZnO doped and non-doped ZrO_2 samples were studied using *Escherichia coli* (*E. coli*, ATCC 25922) and *Staphylococcus aureus* (*S. aureus*, ATCC 25923) strains. From plate counting results, ZrO_2-ZnO samples exhibited greater antibacterial efficiency with a killing rate of 91.7 ± 1.1% and 99.8 ± 0.25% for gram-negative and gram-positive strains respectively. Further, the cytotoxicity of these scaffolds was analyzed using osteoblasts, and 80% of cells were viable after 7 days. Ceramic scaffolds were implanted in a rabbit hip region and analyzed their efficacy after 4 weeks. *In vivo* analysis revealed that the implant did not dislocate and demonstrated the formation of new bone tissue. All these results showed that the ZrO_2-ZnO ceramics are biocompatible and have great potential for producing customized implants [204].

The cup positioning in the hip is very important since it affects the whole-body balance, hip rotation, and pelvis movement. Therefore, a defect or injury in this part creates a problem in maintaining patient quality of life. Acetabular cups are used for hip cup replacement treatment and are made of ceramics or metal with a thin polyethylene liner. Baino *et al*., prepared Al_2O_3/ ZrO_2 composite cups with a trabecular layer (S50B2) using the sponge replication method by forming a spongy layer over the ceramic cup to promote implant osteointegration. Further, the trabecular glass-derived layer between the ceramic acetabular cup and the host bone can minimize the stiffness mismatch at their interface, allowing ceramic-on-ceramic coupling with its well-known anti-wear qualities [205].

5.3. Cartilage repair

Osteoarthritis (OA) is the most prevalent form of arthritis, which is caused by ageing, wear and tear on the joints, and affects the lives of millions of people worldwide. OA causes cartilage lesions where the protective cartilage covering the bone ends gradually deteriorates and causes pain and swelling [206]. Osteoarthritis can harm any joint, most frequently affecting the knees, hips, hands, and spine joints [207]. Over the years, numerous surgical therapeutic techniques have been developed to regenerate cartilage, including mesenchymal stem cell transplantation and micro fracturing. However, secondary trauma and the low survival rate of exogenous stem cells after the treatment limit such treatments. Cartilage regeneration is challenging due to the lack of lymphatic and blood vessels, which limits the ability of the chondrocytes to grow and migrate [208]. However, various tissue engineering strategies have been used recently to focus on different cell sources, such as chondrocytes, fibroblasts, and stem cells for cartilage repair and regeneration. In addition, different types of biomaterials including ceramics & their interactions with cells and signalling molecules that aid in cartilage development are also studied by various researchers [209].

To fabricate bioactive scaffolds for cartilage and subchondral interface, Deng *et al.,* developed a $Sr_5(PO_4)_2SiO_4$ (SPS) bioactive ceramic scaffolds using an extrusion 3D printing. These scaffolds were incorporated with strontium (Sr) and silicon (Si) ions as their release from the scaffold play an important role in osteochondral defect reconstruction. Chondrocytes cultured on the scaffolds showed increased expression of chondrocyte-specific genes (COL II, Aggrecan, SOX9, and N-cadh) compared to control. The constructs were implanted in a rabbit osteochondral defect model and the results were assessed after 12 weeks. Further, specimens were well integrated with native tissues and showed hyaline cartilage-like tissue without showing an inflammatory response. These results imply that SPS scaffolds can aid in rebuilding osteochondral defects and effectively recreate the intricate interface between cartilage and subchondral bone, which represents a viable method for regenerating osteochondral defects [210].

Similarly, Lin *et al.,* prepared copper-incorporated bioactive glass-ceramics tetraethyl orthosilicate/$(C_2H_5O)_4Si$ (Cu-BGC) scaffolds using an extrusion-based 3D printer to investigate the scaffold's anti-arthritis and cartilage regeneration capability. They found that after 12 weeks of implantation in rabbit osteochondral defect models, hyaline-like tissue (neocartilage) and neo-bone completely covered the defect area in BGC and Cu-BGC groups, with Cu-BGC group showing well-integrated and orderly continuous neo-cartilage tissue compared to BGC group. In contrast, the control group showed incomplete neo-bone and fibrous tissue instead of hyaline-like tissue. They also observed that Cu-BGC ionic extracts increased the level of collagen II, aggrecan, and SOX9 via HIF (hypoxia inducible factor) pathway activation, thus promoting cartilage repair. Meanwhile, the anti-arthritis effect of the 3D printed construct was evidenced by better/higher ICRS (International Cartilage Repair Society) score in Cu-BCG group compared to BCG and control groups. Cu^{2+} ions release triggered a switch of macrophages' tendency toward the anti-inflammatory M2 phenotype rather than pro-inflammatory M1 phenotype, resulting in inhibition of pro-inflammatory cytokines (TNF-α and IL-18) and enhancement of the anti-inflammatory cytokine (IL-10). Thus, Cu-BGC scaffolds not only promote cartilage repair but also prevent further osteoarthritis-related inflammation [211].

5.4. Drug delivery

Drug delivery is transporting a pharmaceutical substance to its target location using different strategies, formulations, manufacturing techniques, storage systems, etc [212]. The conventional method for drug delivery includes simple oral, topical, inhaled, or injection methods. However, due to lack of target specificity, these conventional treatment methods affect the other undesired cells or tissues/organs in our body, which extensively leads to the different undesired side effects [213]. Ceramic-based materials are recently explored as drug delivery vehicle for controlled release to treat cancer, pulmonary infections, etc [214,215].

Poor selectivity of the drug or the pharmacologically active substances to the specific target site is the most important demerit of conventional drug delivery methods. Therefore, using implanted target delivery devices or systems for drug delivery is prevalent.

Loca *et al*., used porous hydroxyapatite with 8 mg of gentamicin sulfate prepared by vacuum impregnation for drug delivery and bone regeneration applications. The gentamicin release was observed *in vitro* by dissolution in media. After 1 h of dissolution, 40% of the active substance was transferred from the ceramic scaffold to the dissolution media, and 75% of the drug was released within 12 h. To reduce the gentamicin release, the scaffold was coated with poly(lactic acid) (PLA), poly(ε-caprolactone) (PCL) and poly(vinyl alcohol) (PVA). It was noted that a kind of globular coating was formed after evaporation from PVA, whereas a porous polymer type of coating was formed by higher evaporation from PCL and PLA. A sustained drug release within 72 h was observed while using PCL or PLA, whereas 40 h was taken for the drug release in PVA-coated scaffolds. Thus, these porous bioceramic scaffolds are a good carrier for drug delivery [216].

Composite scaffolds are widely used in the current scenario more recurrently for most applications, including drug delivery. Therefore, Zhang *et al*., prepared a composite bone scaffold using hydroxyapatite microtubes (HMT) and chitosan (CHS) incorporated with gentamicin sulfate (GS). The drug release studies were performed by dispersing the scaffold in PBS, and the antibacterial tests were performed using the disk diffusion method against Staphylococcus aureus (*S. aureus*) and Escherichia coli (*E. coli*). It was noted that about 40% of the drug was released in 20 h, and the total drug was released approximately after 7 days. The antibiotic resistance test showed good potential in killing *S. aureus* and *E. coli* as the HMTs in the scaffolds released GS molecules, and the GS-loaded HMT-CHS composite scaffold displayed a distinct circular zone of inhibition for both *E. coli* and *S. aureus*. Other medicines and proteins, such as bone morphology protein-2 (BMP-2) to stimulate osteogenesis and vascular endothelial growth factor to promote vascularization, can be loaded onto HMTs in addition to antibiotics. Therefore, HMTs show potential as a carrier that can be used for various purposes, including drug delivery [217].

6. Commercial 3D printed ceramic implants

Ceramic reinforced metal implants are currently front runners among the bone implants for clinical applications. The global market for ceramic 3D printing is expected to reach USD 384 million by 2025. Specifically, the 3D ceramic implants are at the second highest compound annual growth rate of 26.5% in the health sector. It is expected to grow from USD 25 million in 2020 to USD 82 million by 2025 [218]. To provide further insights, globally available commercial 3D printed ceramic or non-ceramic bone implants with their material composition are outlined in Table 5. Currently, clinically available metal implants have major complications such as low osteointegration, high Young's modulus compared to human bones, and metal ions leaching effects due to hypersensitivity increases the risk of bone disruption upon long-term implantation [219,220]. Ceramic-based implants emerged as a viable alternative to metal implants by exhibiting higher osteointegration, cytocompatibility, corrosion resistance, and bone formation capabilities. Personalized 3D printed bone implants in clinical use such as OssDsign® Cranial, Cranioplug® and OssDsign® Catalyst are manufactured by OSSDSIGN [221]. This is a Sweden based manufacturer company, which is involved in designing and 3D printing of personalized 3D implants for cranial repair. Through direct communication or collaboration with the CAD design engineers and surgeons, custom 3D implants are designed and manufactured based on the clinical requirements. This manufacturing option facilitates the development of a perfect implant design to fit the defect and provide easy handling to the surgeons. The steps involved in this process are CT imaging of patient (3D file), CAD implant designing, design approval & validation and finally product fabrication & shipping within four weeks after approval. According to 2022 report, approximately 1500 cases with patient-specific implants (PSI) were successfully implanted worldwide [222]. OssDsign cranial implant comprises HA mosaic tiles (composition of β-tricalcium phosphate/β-calcium pyrophosphate, monetite and brushite) with a 1 mm inner separation gap mounted on 3D printed titanium mesh support, which is used to treat occipital defects. Bloom *et al*., had performed a 7-year follow up study in patients implanted with PSI to assess the implant functionality. In 2017, OssDsign implant and deep inferior epigastric perforator (DIEP) free tissue coverage reconstruction surgery was performed to treat osteomyelitis in a patient. To this end, 3D models were designed from the patient CT images and the 3D printed PSI were implanted in the patient. This custom implant treatment provided a single operative key treatment with longer integration time to treat chronic disorders. It was also observed with more advantages than the usual autologous and poly(ether ether ketone) (PEEK) based treatments. After surgery, the implant had the inherent ability to allow new bone formation without any wound healing issues. Using this treatment, reoccurrence of surgery was completely avoided with continuous wound dressing and frequent health care [223]

Likewise, another commercially available 3D printed bone implants are Osteoplug™ and Osteomesh™. It is an FDM printed porous bioresorbable polycaprolactone (PCL) composite construct to promote bone regeneration. These implants are suitable to treat orbital fractures, dental sockets, buccal defects, craniosynostosis, septal extension, mandible reconstruction, etc [223]. Recently few studies have explored the use of surface coating of 3D printed implants to augment bone regeneration. Al-Maawi *et al*., used this 3D printed PCL mesh coated with platelet-rich fibrin (PRF) matrix to improve cell adhesion and further maturation & interactions. This biocoating of blood-derived components promoted the usage of autologous bio-cues (growth factors) for better integration of implant to the host bone. For uniform coating, 7 × 7 mm mesh were incubated with two differently isolated PRF conditions such as low and high RCF centrifugation (PRF_{High} and PRF_{Low}) for 30 min at 37 °C. Morphological evaluation of the coated mesh confirmed the presence of fibrin network formation over the surface, which could promote the myoblast cell interaction for adhesion, migration and proliferation. *In vitro* studies were performed by culturing human osteoblast cells on PRF-coated and non-coated Osteopore™ (Op). On day 7 of culture, the 3D printed PCL mesh with PRF_{Low} coated surface was observed with higher cell proliferation and alkaline phosphatase activity of ~300%. The osteogenic differentiation marker (osteopontin) expression was also absorbed higher in PRF_{Low} coated mesh. Further, quantification of released growth factors using ELISA confirmed the presence of higher biological growth factors (vascular endothelial growth factor, osteoprotegerin, transforming growth factor β1, platelet-derived growth factor). These results confirmed the feasibility of improving bone growth on the biocoated 3D printed mesh for personalized bone implant treatment [224].

Unlike the 3D printed thermoplastic or metallic ceramic composites, ceramic-based hydrogel bioinks facilitates cell printing for 3D bone construct fabrication. Hence, personalized bone tissue fabrication with patient derived cells could be effectively utilized for regenerative medicine applications. For bioprinting, bioink composition with and without ceramic composites are explored much to promote faster bone growth formation and better bone integration. Some of the commercially available bioinks are GelXA (Cellink), CELLINK® BONE (Cellink), TissueFab® bioink bone (Sigma), 3D Printing hydroxyapatite ink (Sigma), Hyperelastic Bone™ (Dimension Inx), bone decelluloid™ (T&R biofab), etc. [225,226]. Among these bioinks, CELLINK® BONE is made of nanofibrillated cellulose/sodium alginate with tricalcium phosphate. TissueFab® bioink bone is also a ceramic-based hydrogel bioink comprising

Table 5
List of commercially available 3D printed ceramic & non-ceramic bone implants with chemical composition & salient features for bone regeneration applications.

Manu-facturer	Commercial Name	Composition & Additive Manufacturing Technique	Applications & Salient Features	Ref
Ceramic 3D printed implant				
Cerhum, Belgium	MyBone	Synthetic hydroxyapatite 3D printing technology developed by Cerhum	• Maxillofacial, dental, cranial, orthopaedics and spine implants • 1–5 MPa Compressive strength, osteointegration, osteoconductive, limits pain and promote vascularization	[228]
T&R Biofab, Korea	TnR Mesh Plus (Square type) TnR Mesh Dental PlusTnR PSI Plus (Maxilla-Orbital type) TnR PSI Plus (Maxilla-Orbital Zygomatic type) TnR PSI Plus (Maxilla-Orbital Zygomatic type) TnR PSI Plus (Frontal Orbital type)	Polycaprolactone & β-TCP FDM	• Dental barrier for gingiva and alveolar bone • Custom cranio-maxillofacial defects biocompatible, osteoinductive, osteoconductive	[229]
Ossiform-We Print Bone™, Denmark	P3D Bone	β-tricalcium phosphate and stearic acid Melt extrusion printing	• Bone implant • Osteointegration, osteoconductive, bioresorption and vascularized bone formation	[230,231]
Non-Ceramic 3D printed implant				
Osteopore®, Singapore	Osteoplug™ Osteomesh™	PolycaprolactoneFDM (Fused Deposition Modelling)	• Orbital reconstruction • Biocompatible, osteoconductive and promote vascularization	[232,233]
OsteoFab® Technology, USA	OsteoFab® Patient Specific Facial Device OsteoFab® Suture Anchor OsteoFab® Patient Specific Cranial Device OsteoFab® patient Specific Cranial Devices Single Stage Surgery SpineFab® VBR System	PEKK polymer (PolyEtherKetoneKetone) Selective Laser Sintering (SLS) technology by OsteoFab® 3D printer	• Facial bone implant, cranial implant, thoracolumbar spine replacement, etc., • Biocompatible, load bearing, durable, osteointegration	[234]
Zimmer Biomet, USA	OsseoTi® Porous Metal Technology	Ti6Al4V alloy	• Bone implant • Mimic human cancellous bone, biocompatible, corrosion resistance, osteointegration, osteoconductive, 475 μm pore size (70% porosity) and vascularized bone formation	[235]
LRS Implants, South Africa	LRS CiS - Custom 3D-Printed Ankle Fusion Cage LRS CiS - Custom 3D-Printed Femoral Truss Cage	Ti6Al4V Metal 3D Printer (Direct Metal Laser Sintering)	• Mid shaft femoral implant, ankle fusion and other bone implants	[236]

Gelatin methacryloyl (GelMA)/hydroxyapatite. Besides mineralized bioinks, natural polymer-based bioinks are also used in 3D bioprinting of bone constructs. Glaser *et al.,* recently used the extrusion bioprinting technique to fabricate a cellular bone construct. They have used bone morphogenic protein-6 (BMP-6) expressing induced pluripotent stem cells-derived mesenchymal progenitor cells and commercial bone-specific bioink from CELLINK (CELLINK® BONE and GelXA). Both the bioink vary in their chemical composition and crosslinking mechanism to print 3D bone construct. In specific, CELLINK® BONE (Ink-Bone) is a ceramic composite comprising of tricalcium phosphate in sodium alginate/nanofibrillated cellulose bioink. Using Cellink Bio X TM 3D printer, bioinks with the cell density of 10 million cells/mL was used to print a bone construct (10 × 10 × 2 mm sized grid pattern) using the printing parameters of 25-30 kPa pressure, 10 mm/s printing speed and 22G needle. The printed constructs had line width of about 200 to 300 μm and the separation distance between the strands of 700 to 800 μm. *In vitro* studies were performed using three different cell sources such as bone marrow-derived mesenchymal progenitor cells (MPC), iPSCs-derived MPC derived from neural crest (iNCC-MPCs) and mesodermal lineage (iMSCs) to study the importance of choice of cell source for improved bone growth. After 28 days of culture *in vitro*, constructs printed with ink-bone bioink containing MPCs was observed with increased gene expressions (osteocalcin and osteonectin) and high collagen 1 protein expression indicating high-quality bone formation with higher connectivity (bone strength) than GelXA. Thus, ceramic based bioink mimicking the native bone matrix could promote osteogenesis in MPCs. Additionally, micro-CT (micro- computed topography) analysis confirmed that the Ink-Bone with BM-MSC showed higher connectivity density, increased trabecular number and improved BV/TV (bone volume/total volume) levels, which confirmed higher bone formation. *In vivo* efficacy of both bioinks with BMP-6 expressing MPCs were studied (BM-MSC, iMSCs and iNCC-MPCS) in calvarial defect model (NOD/SCID mice). After 8 weeks of implantation, MicroCT data showed increased bone volume in the groups treated with ink-bone containing iNCC-MPC-BMP6. This study provides evidence on the efficacy of cell source and importance of their choices in functional maturation of bone constructs i*n vivo* [227].

7. Conclusions and future perspectives

The gold standard procedure for the treatment of bone defects/fractures caused by trauma/injury is the usage of autologous and non-autologous bone grafts. These methods lead to permanent

bone damage in the case of higher immune response, graft rejection and graft unavailability. Hence, tissue-engineered bone grafts/implants have been developed for the functional bone recovery in shorter period without any delay in treatment. In humans, the biological composition of the bones comprises of mineralized collagen fibrils which indicate the presence of both proteins and ceramic (biominerals) components [237]. Based on the type of bone and its functionality, the ECM composition varies in three major components such as protein (collagen), ceramic (HA), and carbohydrates ratio to provide mechanical support. Ceramic materials have excellent stiffness and similarities to the mineral components of native bone and thus can provide a scaffolding support for the adhesion, proliferation and differentiation of bone cells [238]. Due to these interesting features, ceramic based biomaterials have gained more interest towards the development of scaffolds for bone regeneration. Based on the bone porosity, bone types are categorized as cortical (5–15% porous) and trabecular bone (40–95% porous). The elastic moduli of trabecular bone is 10–20 GPa and cortical bone is 20–23 GPa [239]. Hence, designing bone-specific implants with specific porosity and mechanical properties identical to bone graft is more important in developing tissue engineered products. Bioceramic reinforced scaffolds were observed to reduce the adverse effect on bone regeneration, and it could neutralize the acidic degradation of the polymeric scaffolds. A bioceramic bone implant has to withstand the whole-body load and hence needs to possess higher hardness (1000–2000 HV), fracture toughness (4–10 MPa. $m^{1/2}$), elastic modulus (50–200 GPa), ultimate tensile strength (>200 GPa), corrosion resistance, ageing resistance, wear resistance and durability [240]. Although ceramic scaffolds developed using traditional tissue fabrication techniques have shown great promise for bone tissue engineering, they fail to exactly control the internal pore arrangements and overall architectures of bone scaffolds. Conventional scaffold fabrication techniques are inadequate to support regeneration of bones located in different parts of the body because of differences in their chemical composition, mechanical properties, and structural features. Therefore, advanced fabrication tools like 3D printing have been recently explored to fabricate ceramic based bone scaffolds and implants for regenerative medicine applications including reconstruction of skull, spine, maxillofacial, hip, foot, tibia, knee, etc. Hence, this review captures the latest research on well established bioceramics for bone, bioceramic material properties and recent development in the use of ceramics in additive manufacturing of bone implants. Further different types of 3D printing/3D bioprinting techniques in fabricating ceramic-based constructs are elaborately explained with their printing strategies and bone implant development.

Personalized medicine is a big revolution in the medicinal field since it provides freedom of treating patients based on their own requirements and cell source to avoid several complications including implant rejection, secondary surgery requirements, and implant design mismatch. Bone defects caused due to tumor, trauma, and injuries could be irregular in shape and dimensions. Oftentimes, autologous or allogenic sources of bones may not be an ideal surgical solution to treat such clinical conditions. With the advent of cutting-edge research in modern clinical imaging tools, digital manufacturing techniques, 3D printing is fully capable to fabricate customized bone scaffolds or implants to remodel craniofacial injuries, maxillofacial defects, and other bone injuries in an aesthetic fashion with reduced recovery time [241]. Precise designing of personalized implants could be achieved using the additive manufacturing process. 3D printing method provides accurate control in tailoring geometry, porosity, hardness and composition of bone implants. Clinically, 3D printed bone implant usage is still in the nascent stage.

Currently, the biomimetic approach to fabricate a functional and fully biomimetic 3D tissue equivalent structure with an appropriate cell source is still under research. As per World Health Organization (WHO) report, elderly population is expected to double to 1.4 billion by 2030 from 901 million by 2015. Hence, age-related medical problems and need for their clinal solutions will be on the rise in the coming years. This review also emphasizes the fact that there will be a huge demand for bone joint replacement, dental replacement, cardiovascular surgeries, and other implants to treat/improve human functionality in the years to come [242]. In recent reports based on bone implant market share, USA has the dominant place in usage of bone implants (mostly for orthopaedic treatment and joint replacement). Secondly, European market and followed by Asia-Pacific, Middle East and Africa are leading consumers of bone implants across the globe. It is also observed that bioceramics (alumina, hydroxyapatite, beta-tricalcium phosphate, bioglass, carbon, zirconia and zirconia-toughened alumina) are the second most globally used bone implant for treating injured patients [243]. The market size of bone implants was calculated as USD 17.99 billion in 2020 and it is expected to reach USD 73.81 billion by 2028 [244].

Most of the commercially available bone implants are only material-based implants (acellular). To augment the applications of these implants, suitable strategies should be in place to address the challenges in combining stem cell-based cell therapy along with implants. These cellularized implant strategies could promote faster bone healing, however the cell seeding or cellular bioprinting concept is still in the research level. Hence, the choice of new ceramic bioink composition (composites) and bioprinting strategies are major concerns in regenerative medicine. Bioinks such as magnesium doped polycaprolactone/strontium carbonate nanoparticle-gelatin methacryloyl (Mg-PCL/Sr-GelMA), alginate/methacrylated decellularized bone ECM, type-I collagen/β-TCP, methacrylated glycol chitosan, etc., are some of the recently developed bone specific bioinks with well-observed bone regeneration ability [245–248]. Bone constructs printed with these bioinks have been observed with increased proliferation, osteogenic differentiation, osteogenic gene expression (ALP, OCN, BMP-2, OPN), alkaline phosphatase (ALP) activity and calcium deposition. However, these hydrogel-based bone constructs cannot withstand the load and mechanical stress of the host tissue during implantation. Hence, a mechanically stable and load-bearing ceramic implants with therapeutic cells sources are required. This challenge could be addressed by joint research innovation ventures with a team of scientists from multi-disciplinary fields. By this way, a novel ceramic bioink could be developed which will be compatible with cells to print biomimetic bone for load bearing bone tissue engineering applications.

3D printed ceramics-based bone implants have great advantages to treat bone defects compared to metal-based personalized implants. Usually, metal-based implants are harder than natural human bone, leading to the stress shielding effect at the bone interface due to mechanical mismatch between the implant and native bone [249]. This problem could be addressed using bioceramic implants with tailored mechanical properties & porosity to mimic the microenvironment of native bone. The printing accuracy, resolution, and implant strength mainly depend on the choice of ceramic material, printable ink composition, scaffold design, and printing parameters [87]. Further, 3D printing of ceramics with hydrogel and biological cues for cell integration is possible with the low temperature-based 3D printing approach. However, mostly ceramic printing conditions require a harsh printing environment (high temperature or low pH) or post-processing steps for implant fabrication. Bioprinting a cellular ceramic implant is more challenging. Designing and developing a 3D printer facilitating a feasible cell printing environment will also help to improve personalized bone tissue equivalents. A few limitations that need to be addressed to increase ceramic implant usage globally are

high cost, lower structure reliability, printing failure and vascularization [250]. Moreover, additive manufacturing is an expensive technique involving computer-aided designing, 3D printer operation cost, material cost, sterilization, packaging and transportation cost. Comparatively, the price of 3D printed bone grafts is high when compared to mold-based fabrication method. Further, laser-based additive manufacturing techniques are more expensive than extrusion/melt printing. Hence, the printing type has a major breakpoint in deciding the implant cost, which needs to be addressed in the future. Printed ceramic composites could undergo shrinkage, drying, microcracking, and pattern distortion after the drying/sintering. Post-processing phase of the ceramic implant is more critical, where a higher chance of material failure may occur without knowledge. Also, the shrinkage effects of the ceramic implants should be considered while designing the initial CAD file for future design matches. The wide availability of bioceramic materials, including β-tricalcium phosphate, nano-hydroxyapatite, silica carbide, zirconium oxide, barium titanate, and calcium carbonate, could help resolve material failure issues. Moreover, a combination of ceramic materials, incorporation of nanomaterials could be considered in the future to further augment the material characteristics suitable for bespoke implant development. In most of the cases, the failure of ceramic implants could be due to exposure to high-stress or cyclic loading over a longer duration. To overcome these failures, strategies for better designing of ceramic implants and doping the ceramic implants with metals are currently developed to improve durability, therapeutic efficiency, osteoconductivity and anti-bacterial activity [251,252]. Hence printing and processing optimization for the material choice will result in efficient scaffold fabrication with reliable solutions for the above-mentioned challenges in the years to come.

CRediT authorship contribution statement

Harshavardhan Budharaju: Writing – original draft. **Shruthy Suresh:** Writing – original draft. **Muthu Parkkavi Sekar:** Writing – original draft. **Brigita De Vega:** Writing – original draft. **Swaminathan Sethuraman:** Writing – original draft, Writing – review & editing. **Dhakshinamoorthy Sundaramurthi:** Conceptualization, Writing – review & editing, Funding acquisition. **Deepak M. Kalaskar:** Conceptualization, Writing – review & editing, Funding acquisition.

Data availability

No data was used for the research described in the article.

Declaration of Competing Interest

The authors declare that they have no known competing financial interests or personal relationships that could have appeared to influence the work reported in this paper.

Acknowledgements

The authors wish to acknowledge Nano Mission, Department of Science & Technology (DST) (SR/NM/TP-83/2016 (G)), and Prof. T. R. Rajagopalan R & D Cell of SASTRA Deemed University for financial and infrastructural support. We also wish to acknowledge ATGC grant, Department of Biotechnology (DBT) (BT/ATGC/127/SP41147/2021) and Adhoc funding, Indian Council of Medical Research (ICMR) (17x3/Adhoc/23/2022-ITR) for financial support. The authors are thankful to the Council of Scientific & Industrial Research (CSIR), Government of India for the senior research fellowship (09/1095/(0051)19-EMR-I) and Indian Council of Medical Research (ICMR) for the senior research fellowship (3/1/1(4)/CVD/2020-NCD-1). We thank the Indonesian Endowment Fund for Education (202111220807913) for supporting Brigita De Vega for her PhD scholarship.

References

[1] A.-M. Wu, C. Bisignano, S.L. James, G.G. Abady, A. Abedi, E. Abu-Gharbieh, R.K. Alhassan, V. Alipour, J. Arabloo, M. Asaad, W.N. Asmare, A.F. Awedew, M. Banach, S.K. Banerjee, A. Bijani, T.T.M. Birhanu, S.R. Bolla, L.A. Cámera, J.-C. Chang, D.Y. Cho, M.T. Chung, R.A.S. Couto, X. Dai, L. Dandona, R. Dandona, F. Farzadfar, I. Filip, F. Fischer, A.A. Fomenkov, T.K. Gill, B. Gupta, J.A. Haagsma, A. Haj-Mirzaian, S. Hamidi, S.I. Hay, I.M. Ilic, M.D. Ilic, R.Q. Ivers, M. Jürisson, R. Kalhor, T. Kanchan, T. Kavetskyy, R. Khalilov, E.A. Khan, M. Khan, C.J. Kneib, V. Krishnamoorthy, G.A. Kumar, N. Kumar, R. Lalloo, S. Lasrado, S.S. Lim, Z. Liu, A. Manafi, N. Manafi, R.G. Menezes, T.J. Meretoja, B. Miazgowski, T.R. Miller, Y. Mohammad, A. Mohammadian-Hafshejani, A.H. Mokdad, C.J.L. Murray, M. Naderi, M.D. Naimzada, V.C. Nayak, C.T. Nguyen, R. Nikbakhsh, A.T. Olagunju, N. Otstavnov, S.S. Otstavnov, J.R. Padubidri, J. Pereira, H.Q. Pham, M. Pinheiro, S. Polinder, H. Pourchamani, N. Rabiee, A. Radfar, M.H.U. Rahman, D.L. Rawaf, S. Rawaf, M.R. Saeb, A.M. Samy, L. Sanchez Riera, D.C. Schwebel, S. Shahabi, M. A. Shaikh, A. Soheili, R. Tabarés-Seisdedos, M.R. Tovani-Palone, B.X. Tran, R.S. Travillian, P.R. Valdez, T.J. Vasankari, D.Z. Velazquez, N. Venketasubramanian, G.T. Vu, Z.-J. Zhang, T. Vos, Global, regional, and national burden of bone fractures in 204 countries and territories, 1990–2019: a systematic analysis from the Global Burden of Disease Study 2019, Lancet Healthy Longevity 2 (9) (2021) e580–e592.

[2] E. Kironde, P. Sekimpi, I. Kajja, P. Mubiri, Prevalence and patterns of traumatic bone loss following open long bone fractures at Mulago Hospital, OTA Int.: Open Access J. Orthop. Trauma. 2 (2019) e015.

[3] A.R. Amini, C.T. Laurencin, S.P. Nukavarapu, Bone tissue engineering: recent advances and challenges, Crit. Rev. Biomed. Eng. 40 (2012) 363–408, https://doi.org/10.1615/critrevbiomedeng.v40.i5.10.

[4] R. Kaliaraj, S. Gandhi, D. Sundaramurthi, S. Sethuraman, U.M. Krishnan, A biomimetic mesoporous silica–polymer composite scaffold for bone tissue engineering, J. Porous Mater. 25 (2) (2018) 397–406.

[5] M.N. Collins, G. Ren, K. Young, S. Pina, R.L. Reis, J.M. Oliveira, Scaffold fabrication technologies and structure/function properties in bone tissue engineering, Adv. Funct. Mater. 31 (21) (2021) 2010609.

[6] M.P. Sekar, H. Budharaju, A. Zennifer, S. Sethuraman, D. Sundaramurthi, Four dimension printing in healthcare, in: 3D Printing in Medicine, Elsevier, 2023, pp. 337–359.

[7] D. Sundaramurthi, L.R. Jaidev, L.N. Ramana, S. Sethuraman, U.M. Krishnan, Osteogenic differentiation of stem cells on mesoporous silica nanofibers, RSC Adv. 5 (2015) 69205–69214, https://doi.org/10.1039/C5RA07014G.

[8] M. Thangadurai, A. Ajith, H. Budharaju, S. Sethuraman, D. Sundaramurthi, Advances in electrospinning and 3D bioprinting strategies to enhance functional regeneration of skeletal muscle tissue, Biomater. Adv. 142 (2022), https://doi.org/10.1016/j.bioadv.2022.213135 213135.

[9] H. Budharaju, A. Zennifer, S. Sethuraman, A. Paul, D. Sundaramurthi, Designer DNA biomolecules as a defined biomaterial for 3D bioprinting applications, Mater. Horiz. 9 (2022) 1141–1166, https://doi.org/10.1039/D1MH01632F.

[10] J. Li, M. Chen, X. Fan, H. Zhou, Recent advances in bioprinting techniques: approaches, applications and future prospects, J. Transl. Med. 14 (2016) 271, https://doi.org/10.1186/s12967-016-1028-0.

[11] N. Shayesteh Moghaddam, M. Taheri Andani, A. Amerinatanzi, C. Haberland, S. Huff, M. Miller, M. Elahinia, D. Dean, Metals for bone implants: safety, design, and efficacy, Biomanuf. Rev. 1 (2016) 1, https://doi.org/10.1007/s40898-016-0001-2.

[12] E. Barua, A.B. Deoghare, P. Deb, S. Das Lala, Naturally derived biomaterials for development of composite bone scaffold: A review, IOP Conf. Series: Mater. Sci. Eng. 377 (2018), https://doi.org/10.1088/1757-899X/377/1/012013 012013.

[13] A. Zennifer, A. Subramanian, S. Sethuraman, Design considerations of bioinks for laser bioprinting technique towards tissue regenerative applications, Bioprinting. 27 (2022) e00205.

[14] M. Vallet-Regí, A.J. Salinas, Ceramics as bone repair materials, Second Edi., Elsevier Ltd, 2019. https://doi.org/10.1016/b978-0-08-102451-5.00006-8.

[15] W. Wang, K.W.K. Yeung, Bone grafts and biomaterials substitutes for bone defect repair: A review, Bioact. Mater. 2 (2017) 224–247, https://doi.org/10.1016/J.BIOACTMAT.2017.05.007.

[16] M. Alonzo, F. Alvarez Primo, S. Anil Kumar, J.A. Mudloff, E. Dominguez, G. Fregoso, N. Ortiz, W.M. Weiss, B. Joddar, Bone tissue engineering techniques, advances, and scaffolds for treatment of bone defects, Curr. Opin. Biomed. Eng. 17 (2021), https://doi.org/10.1016/j.cobme.2020.100248 100248.

[17] D. Cao, S. Malakooti, V.N. Kulkarni, Y. Ren, H. Lu, Nanoindentation measurement of core–skin interphase viscoelastic properties in a sandwich glass composite, Mech. Time-Depend. Mater. 25 (2021) 353–363, https://doi.org/10.1007/s11043-020-09448-y.

[18] D. Cao, S. Malakooti, V.N. Kulkarni, Y. Ren, Y. Liu, X. Nie, D. Qian, D.T. Griffith, H. Lu, The effect of resin uptake on the flexural properties of compression molded sandwich composites, Wind Energy 25 (2022) 71–93, https://doi.org/10.1002/we.2661.

[19] X. Wang, T. Xu, M.J. de Andrade, I. Rampalli, D. Cao, M. Haque, S. Roy, R.H. Baughman, H. Lu, The interfacial shear strength of carbon nanotube sheet modified carbon fiber composites, in: 2021: pp. 25–32. https://doi.org/10.1007/978-3-030-59542-5_4.
[20] M. Bahraminasab, Challenges on optimization of 3D-printed bone scaffolds, Biomed. Eng. Online 19 (2020) 69, https://doi.org/10.1186/s12938-020-00810-2.
[21] C. Wang, W. Huang, Y. Zhou, L. He, Z. He, Z. Chen, X. He, S. Tian, J. Liao, B. Lu, Y. Wei, M. Wang, 3D printing of bone tissue engineering scaffolds, Bioact. Mater. 5 (2020) 82–91, https://doi.org/10.1016/j.bioactmat.2020.01.004.
[22] M. Sadia, B. Arafat, W. Ahmed, R.T. Forbes, M.A. Alhnan, Channelled tablets: An innovative approach to accelerating drug release from 3D printed tablets, J. Control. Release 269 (2018) 355–363, https://doi.org/10.1016/J.JCONREL.2017.11.022.
[23] N. Kladovasilakis, P. Charalampous, A. Boumpakis, T. Kontodina, K. Tsongas, D. Tzetzis, I. Kostavelis, P. Givissis, D. Tzovaras, Development of biodegradable customized tibial scaffold with advanced architected materials utilizing additive manufacturing, J. Mech. Behav. Biomed. Mater. 141 (2023), https://doi.org/10.1016/J.JMBBM.2023.105796 105796.
[24] U.-L.-L. Lee, J.-Y.-Y. Lim, S.-N.-N. Park, B.-H.-H. Choi, H. Kang, W.-C.-C. Choi, A clinical trial to evaluate the efficacy and safety of 3D printed bioceramic implants for the reconstruction of zygomatic bone defects, Materials. 13 (2020) 4515, https://doi.org/10.3390/ma13204515.
[25] S. Vijayavenkataraman, L.Y. Kuan, W.F. Lu, 3D-printed ceramic triply periodic minimal surface structures for design of functionally graded bone implants, Mater. Des. 191 (2020), https://doi.org/10.1016/J.MATDES.2020.108602 108602.
[26] A. Saranti, A. Tiron-Stathopoulos, L. Papaioannou, C. Gioti, A. Ioannou, M.A. Karakassides, K. Avgoustakis, I. Koutselas, K. Dimos, 3D-printed bioactive scaffolds for bone regeneration bearing carbon dots for bioimaging purposes, Smart Mater. Med. 3 (2022) 12–19, https://doi.org/10.1016/J.SMAIM.2021.11.002.
[27] W. Liu, M. Li, J. Nie, C. Wang, W. Li, Z. Xing, Synergy of solid loading and printability of ceramic paste for optimized properties of alumina via stereolithography-based 3D printing, J. Mater. Res. Technol. 9 (2020) 11476–11483, https://doi.org/10.1016/J.JMRT.2020.08.038.
[28] Y.H. Lin, A.K.X. Lee, C.C. Ho, M.J. Fang, T.Y. Kuo, M.Y. Shie, The effects of a 3D-printed magnesium-/strontium-doped calcium silicate scaffold on regulation of bone regeneration via dual-stimulation of the AKT and WNT signaling pathways, Biomater. Adv. 133 (2022), https://doi.org/10.1016/J.MSEC.2022.112660 112660.
[29] H. Wu, L. Chao, Q. Zhang, Y. Yi, C. Jiao, Y. Ye, L. Shen, J. Zhao, G. Wu, C. Wang, Design and 3D printing of ceramic maxillofacial prosthesis with gradient pores based on Voronoi-Tessellation principle, Mater. Today Commun. 33 (2022), https://doi.org/10.1016/J.MTCOMM.2022.104559 104559.
[30] K. Liu, X. Wu, J. Liu, H. Yang, M. Li, T. Qiu, H. Dai, Design and manufacture of a customized, large-size and high-strength bioactive HA osteoid composite ceramic by stereolithography, Ceram. Int. 49 (2023) 11630–11640, https://doi.org/10.1016/J.CERAMINT.2022.12.010.
[31] B. Zhang, X. Gui, P. Song, X. Xu, L. Guo, Y. Han, L. Wang, C. Zhou, Y. Fan, X. Zhang, Three-dimensional printing of large-scale, high-resolution bioceramics with micronano inner porosity and customized surface characterization design for bone regeneration, ACS Appl. Mater. Interfaces 14 (2022) 8804–8815, https://doi.org/10.1021/acsami.1c22868.
[32] H. Li, L. Song, J. Sun, J. Ma, Z. Shen, Dental ceramic prostheses by stereolithography-based additive manufacturing: potentials and challenges, 118 (2018) 30–36. https://doi.org/10.1080/17436753.2018.1447834.
[33] Z. Huang, L.Y. Liu, J. Yuan, H. Guo, H. Wang, P. Ye, Z. Du, Y. Zhao, H. Zhang, C.L. Gan, Stereolithography 3D printing of Si3N4 cellular ceramics with ultrahigh strength by using highly viscous paste, Ceram. Int. 49 (2023) 6984–6995, https://doi.org/10.1016/J.CERAMINT.2022.10.137.
[34] Y.R. Wu, J.H. He, L.J. Cheng, J.M. Wu, Y.S. Shi, Effects of AlN inorganic binder on the properties of porous Si3N4 ceramics prepared by selective laser sintering, Ceram. Int. 48 (2022) 29900–29906, https://doi.org/10.1016/J.CERAMINT.2022.06.255.
[35] Y. Xu, W. Ding, M.G. Chen, H. Du, T. Qin, Synergistic fabrication of micro-nano bioactive ceramic-optimized polymer scaffolds for bone tissue engineering by in situ hydrothermal deposition and selective laser sintering, 33 (2022) 2104–2123. https://doi.org/10.1080/09205063.2022.2096526.
[36] X. Li, Y. Yuan, L. Liu, Y.S. Leung, Y. Chen, Y. Guo, Y. Chai, Y. Chen, 3D printing of hydroxyapatite/tricalcium phosphate scaffold with hierarchical porous structure for bone regeneration, Bio-Design Manuf. 3 (2020) 15–29, https://doi.org/10.1007/s42242-019-00056-5.
[37] Y. Pan, H. Li, Y. Liu, Y. Liu, K. Hu, N. Wang, Z. Lu, J. Liang, S. He, Effect of holding time during sintering on microstructure and properties of 3D printed alumina ceramics, Front. Mater. 7 (2020), https://doi.org/10.3389/fmats.2020.00054.
[38] U.K. Roopavath, S. Malferrari, A. Van Haver, F. Verstreken, S.N. Rath, D.M. Kalaskar, Optimization of extrusion based ceramic 3D printing process for complex bony designs, Mater. Des. 162 (2019) 263–270, https://doi.org/10.1016/j.matdes.2018.11.054.
[39] F.S. Hosseini, A.A. Abedini, F. Chen, T. Whitfield, C.C. Ude, C.T. Laurencin, Oxygen-generating biomaterials for translational bone regenerative engineering, ACS Appl. Mater. Interfaces (2023), https://doi.org/10.1021/acsami.2c20715.
[40] S. Suvarnapathaki, X. Wu, T. Zhang, M.A. Nguyen, A.A. Goulopoulos, B. Wu, G. Camci-Unal, Oxygen generating scaffolds regenerate critical size bone defects, Bioact. Mater. 13 (2022) 64–81, https://doi.org/10.1016/j.bioactmat.2021.11.002.
[41] S. Suvarnapathaki, X. Wu, D. Lantigua, M.A. Nguyen, G. Camci-Unal, Breathing life into engineered tissues using oxygen-releasing biomaterials, NPG Asia Mater. 11 (2019) 65, https://doi.org/10.1038/s41427-019-0166-2.
[42] M. Roy, A. Bandyopadhyay, S. Bose, Ceramics in bone grafts and coated implants, materials and devices for bone disorders. (2017) 265–314. https://doi.org/10.1016/B978-0-12-802792-9.00006-9.
[43] Y. Zhang, H. Shao, T. Lin, J. Peng, A. Wang, Z. Zhang, L. Wang, S. Liu, X. Yu, Effect of Ca/P ratios on porous calcium phosphate salt bioceramic scaffolds for bone engineering by 3D gel-printing method, Ceram. Int. 45 (2019) 20493–20500, https://doi.org/10.1016/j.ceramint.2019.07.028.
[44] C.Y. Ooi, M. Hamdi, S. Ramesh, Properties of hydroxyapatite produced by annealing of bovine bone, Ceram. Int. 33 (2007) 1171–1177, https://doi.org/10.1016/J.CERAMINT.2006.04.001.
[45] Y. Cao, L. Xiao, Y. Cao, A. Nanda, C. Xu, Q. Ye, 3D printed β-TCP scaffold with sphingosine 1-phosphate coating promotes osteogenesis and inhibits inflammation, Biochem. Biophys. Res. Commun. 512 (2019) 889–895, https://doi.org/10.1016/j.bbrc.2019.03.132.
[46] D.K. Lee, M.-R. Ki, E.H. Kim, C.-J. Park, J.J. Ryu, H.S. Jang, S.P. Pack, Y.K. Jo, S.H. Jun, Biosilicated collagen/β-tricalcium phosphate composites as a BMP-2-delivering bone-graft substitute for accelerated craniofacial bone regeneration, Biomater. Res. 25 (2021) 13, https://doi.org/10.1186/s40824-021-00214-w.
[47] M.Z.A. Khiri, K.A. Matori, M.H.M. Zaid, C.A.C. Abdullah, N. Zainuddin, I.M. Alibe, N.A.A. Rahman, S.A.A. Wahab, A.Z.K. Azman, N. Effendy, Crystallization behavior of low-cost biphasic hydroxyapatite/β-tricalcium phosphate ceramic at high sintering temperatures derived from high potential calcium waste sources, Results Phys. 12 (2019) 638–644, https://doi.org/10.1016/j.rinp.2018.12.025.
[48] M. Bohner, B.L.G. Santoni, N. Döbelin, β-tricalcium phosphate for bone substitution: Synthesis and properties, Acta Biomater. 113 (2020) 23–41, https://doi.org/10.1016/j.actbio.2020.06.022.
[49] Y. Ma, H. Dai, X. Huang, Y. Long, 3D printing of bioglass-reinforced β-TCP porous bioceramic scaffolds, J. Mater. Sci. 54 (2019) 10437–10446, https://doi.org/10.1007/s10853-019-03632-3.
[50] H. Li, K. Xue, N. Kong, K. Liu, J. Chang, Silicate bioceramics enhanced vascularization and osteogenesis through stimulating interactions between endothelia cells and bone marrow stromal cells, Biomaterials 35 (2014) 3803–3818, https://doi.org/10.1016/j.biomaterials.2014.01.039.
[51] S. Visbal, J. Lira-Olivares, T. Sekino, K. Niihara, B.K. Moon, S.W. Lee, Mechanical properties of Al2O3-TiO2-SiC nanocomposites for the femoral head of hip joint replacement, Mater. Sci. Forum 486–487 (2005) 197–200, https://doi.org/10.4028/WWW.SCIENTIFIC.NET/MSF.486-487.197.
[52] X. Guo, H. Yang, Sintering and microstructure of silicon carbide ceramic with Y3Al5O12 added by sol-gel method, J. Zhejiang Univ.-Sci. B 6 (2005) 213–218, https://doi.org/10.1631/jzus.2005.B0213.
[53] M. Petousis, N. Vidakis, N. Mountakis, S. Grammatikos, V. Papadakis, C.N. David, A. Moutsopoulou, S.C. Das, Silicon carbide nanoparticles as a mechanical boosting agent in material extrusion 3D-printed polycarbonate, Polymers 14 (2022) 3492, https://doi.org/10.3390/polym14173492.
[54] R. He, N. Zhou, K. Zhang, X. Zhang, L. Zhang, W. Wang, D. Fang, Progress and challenges towards additive manufacturing of SiC ceramic, J. Adv. Ceram. 10 (2021) 637–674, https://doi.org/10.1007/s40145-021-0484-z.
[55] H. Mei, X. Yin, J. Zhang, W. Zhao, Compressive properties of 3D printed polylactic acid matrix composites reinforced by short fibers and SiC nanowires, Adv. Eng. Mater. 21 (2019) 1800539, https://doi.org/10.1002/adem.201800539.
[56] F. Alam, H.N. Das, A.K.M.A. Hossain, Effects of sintering temperature on the magnetic properties of Cr substituted Mn-Zn ferrite, in: 2012 7th International Conference on Electrical and Computer Engineering, 2012, pp. 443–446, https://doi.org/10.1109/ICECE.2012.6471582.
[57] F. Yang, X. Zhang, Z. Guo, A.A. Volinsky, 3D gel-printing of Sr ferrite parts, Ceram. Int. 44 (2018) 22370–22377, https://doi.org/10.1016/j.ceramint.2018.08.364.
[58] H. Hasoon Al-Moameri, Z. Majid Nahi, D. Raheem Rzaij, N.T. Al-Sharify, A review on the biomedical applications of alumina, J. Eng. Sustain. Develop. 24 (2022) 28–36, https://doi.org/10.31272/jeasd.24.5.5.
[59] D. Landek, L. Ćurković, I. Gabelica, M. Kerolli Mustafa, I. Žmak, Optimization of sintering process of alumina ceramics using response surface methodology, Sustainability 13 (2021) 6739, https://doi.org/10.3390/su13126739.
[60] J. Radhakrishnan, A. Manigandan, P. Chinnaswamy, A. Subramanian, S. Sethuraman, Gradient nano-engineered in situ forming composite hydrogel for osteochondral regeneration, Biomaterials 162 (2018) 82–98, https://doi.org/10.1016/j.biomaterials.2018.01.056.
[61] G.M. Cunniffe, T. Gonzalez-Fernandez, A. Daly, B.N. Sathy, O. Jeon, E. Alsberg, D.J. Kelly, Three-dimensional bioprinting of polycaprolactone reinforced gene activated bioinks for bone tissue engineering, Tissue Eng. A 23 (2017) 891–900, https://doi.org/10.1089/ten.tea.2016.0498.
[62] C. Polley, T. Distler, R. Detsch, H. Lund, A. Springer, A.R. Boccaccini, H. Seitz, 3D printing of piezoelectric barium titanate-hydroxyapatite scaffolds with interconnected porosity for bone tissue engineering, Materials 13 (2020) 1–16, https://doi.org/10.3390/MA13071773.
[63] M.N. Aboushelib, R. Shawky, Osteogenesis ability of CAD/CAM porous zirconia scaffolds enriched with nano-hydroxyapatite particles, Int. J. Implant Dent. 3 (2017), https://doi.org/10.1186/s40729-017-0082-6.

[64] G. Muralithran, S. Ramesh, The effects of sintering temperature on the properties of hydroxyapatite, Ceram. Int. 26 (2000) 221–230, https://doi.org/10.1016/S0272-8842(99)00046-2.

[65] M. Kozakiewicz, T. Gmyrek, R. Zajdel, B. Konieczny, Custom-made zirconium dioxide implants for craniofacial bone reconstruction, Materials 14 (2021) 840, https://doi.org/10.3390/ma14040840.

[66] L. Jiang, Y. Liao, Q. Wan, W. Li, Effects of sintering temperature and particle size on the translucency of zirconium dioxide dental ceramic, J. Mater. Sci. - Mater. Med. 22 (2011) 2429–2435, https://doi.org/10.1007/s10856-011-4438-9.

[67] K.-Y. Tsai, H.-Y. Lin, Y.-W. Chen, C.-Y. Lin, T.-T. Hsu, C.-T. Kao, Laser sintered magnesium-calcium silicate/poly-ε-caprolactone scaffold for bone tissue engineering, Materials 10 (2017) 65, https://doi.org/10.3390/ma10010065.

[68] L. de Siqueira, C.G. de Paula, R.F. Gouveia, M. Motisuke, E. de Sousa Trichês, Evaluation of the sintering temperature on the mechanical behavior of β-tricalcium phosphate/calcium silicate scaffolds obtained by gelcasting method, J. Mech. Behav. Biomed. Mater. 90 (2019) 635–643, https://doi.org/10.1016/j.jmbbm.2018.11.014.

[69] D. Luciana Aurora Soares do Amaral, R. de Souza Salomão Zanette, G. Torres de Souza, S. Augusto da Silva, J. Adriano Kopke de Aguiar, R. Fortes Marcomini, A. Márcio Resende do Carmo, B. Valentim Nogueira, R. José da Silva Barros, F. de Sá Silva, M. de Oliveira Santos, M. Munk, H. de Mello Brandão, C. Magno da Costa Maranduba, Induction of osteogenic differentiation by demineralized and decellularized bovine extracellular matrix derived hydrogels associated with barium titanate, Biologicals 66 (2020) 9–16.

[70] U. Ulfa, K. Kusumandari, Y. Iriani, The effect of temperature and holding time sintering process on microstructure and dielectric properties of barium titanate by co-precipitation method, AIP Conf. Proc. 2202 (2019), https://doi.org/10.1063/1.5141649.

[71] H. Naghib-zadeh, C. Glitzky, I. Dörfel, T. Rabe, Low temperature sintering of barium titanate ceramics assisted by addition of lithium fluoride-containing sintering additives, J. Eur. Ceram. Soc. 30 (2010) 81–86, https://doi.org/10.1016/j.jeurceramsoc.2009.07.005.

[72] A.D. Woldetsadik, S.K. Sharma, S. Khapli, R. Jagannathan, M. Magzoub, Hierarchically porous calcium carbonate scaffolds for bone tissue engineering, ACS Biomater Sci. Eng. 3 (2017) 2457–2469, https://doi.org/10.1021/ACSBIOMATERIALS.7B00301/ASSET/IMAGES/LARGE/AB-2017-00301R_0006.JPEG.

[73] A. Chróścicka, Z. Jaegermann, P. Wychowański, A. Ratajska, J. Sadło, G. Hoser, S. Michałowski, M. Lewandowska-Szumiel, Synthetic calcite as a scaffold for osteoinductive bone substitutes, Ann. Biomed. Eng. 44 (7) (2016) 2145–2157.

[74] B. Kim, H.J. Kang, J. Lee, Improvement of the compressive strength of a cuttlefish bone-derived porous hydroxyapatite scaffold via polycaprolactone coating, J. Biomed. Mater. Res. Part B: Appl. Biomater. 101 (2013) 1302–1309, https://doi.org/10.1002/jbm.b.32943.

[75] S. Yang, B. Zhu, P. Yin, L. Zhao, Y. Wang, Z. Fu, R. Dang, J. Xu, J. Zhang, N. Wen, Integration of human umbilical cord mesenchymal stem cells-derived exosomes with hydroxyapatite-embedded hyaluronic acid-alginate hydrogel for bone regeneration, ACS Biomater Sci. Eng. 6 (2020) 1590–1602, https://doi.org/10.1021/acsbiomaterials.9b01363.

[76] V. Trakoolwannachai, P. Kheolamai, S. Ummartyotin, Characterization of hydroxyapatite from eggshell waste and polycaprolactone (PCL) composite for scaffold material, Compos. Part B: Eng. 173 (2019), https://doi.org/10.1016/J.COMPOSITESB.2019.106974 106974.

[77] A. Cahyanto, E. Kosasih, D. Aripin, Z. Hasratiningsih, Fabrication of hydroxyapatite from fish bones waste using reflux method, IOP Conf. Series: Mater. Sci. Eng. 172 (2017) 012006, https://doi.org/10.1088/1757-899X/172/1/012006.

[78] A.M. Janus, M. Faryna, K. Haberko, A. Rakowska, T. Panz, Chemical and microstructural characterization of natural hydroxyapatite derived from pig bones, Microchim. Acta 161 (3-4) (2008) 349–353.

[79] W. Pon-On, P. Suntornsaratoon, N. Charoenphandhu, J. Thongbunchoo, N. Krishnamra, I.M. Tang, Hydroxyapatite from fish scale for potential use as bone scaffold or regenerative material, Mater. Sci. Eng. C, Mater. Biol. Appl. 62 (2016) 183–189, https://doi.org/10.1016/J.MSEC.2016.01.051.

[80] S. Mondal, U. Pal, A. Dey, Natural origin hydroxyapatite scaffold as potential bone tissue engineering substitute, Ceram. Int. 42 (2016) 18338–18346, https://doi.org/10.1016/J.CERAMINT.2016.08.165.

[81] T.T. Roberts, A.J. Rosenbaum, Bone grafts, bone substitutes and orthobiologics: The bridge between basic science and clinical advancements in fracture healing, Organogenesis 8 (4) (2012) 114–124.

[82] N. Eliaz, N. Metoki, Calcium phosphate bioceramics: A review of their history, structure, properties, coating technologies and biomedical applications, Materials 10 (4) (2017) 334, https://doi.org/10.3390/MA10040334.

[83] S. Bin Sulaiman, T.K. Keong, C.H. Cheng, A. Bin Saim, R.B.H. Idrus, Tricalcium phosphate/hydroxyapatite (TCP-HA) bone scaffold as potential candidate for the formation of tissue engineered bone, Indian J. Med. Res. 137 (2013) 1093–1101. https://pubmed.ncbi.nlm.nih.gov/23852290.

[84] Ş. Dragosloveanu, C. Dragosloveanu, H. Stanca, D. Cotor, A. Andrei, C. Dragosloveanu, C. Stoica, Tricalcium phosphate and hydroxyapatite treatment for benign cavitary bone lesions: A prospective clinical trial, Exp. Ther. Med. 20 (2020) 1, https://doi.org/10.3892/etm.2020.9345.

[85] K. Ishikawa, Bone substitute fabrication based on dissolution-precipitation reactions, Materials. 3 (2010) 1138–1155. https://doi.org/10.3390/ma3021138.

[86] K. Cheng, W. Zhu, X. Weng, L. Zhang, Y. Liu, C. Han, W. Xia, Injectable tricalcium phosphate/calcium sulfate granule enhances bone repair by reversible setting reaction, Biochem. Biophys. Res. Commun. 557 (2021) 151–158, https://doi.org/10.1016/j.bbrc.2021.03.145.

[87] Y. Chen, J. Huang, J. Liu, Y. Wei, X. Yang, L. Lei, L. Chen, Y. Wu, Z. Gou, Tuning filament composition and microstructure of 3D-printed bioceramic scaffolds facilitate bone defect regeneration and repair, Regenerative, Biomaterials 8 (2021), https://doi.org/10.1093/rb/rbab007 rbab007.

[88] N. Raja, H. Park, Y.J. Choi, H.S. Yun, Multifunctional calcium-deficient hydroxyl apatite-alginate core-shell-structured bone substitutes as cell and drug delivery vehicles for bone tissue regeneration, ACS Biomater Sci. Eng. 7 (2021) 1123–1133, https://doi.org/10.1021/acsbiomaterials.0c01341.

[89] M.C. Tanzi, S. Farè, G. Candiani, Biomaterials and Applications, in: Foundations of Biomaterials Engineering, Elsevier, 2019, pp. 199–287, https://doi.org/10.1016/B978-0-08-101034-1.00004-9.

[90] E. Kontonasaki, P. Giasimakopoulos, A.E. Rigos, Strength and aging resistance of monolithic zirconia: an update to current knowledge, Jap. Dental Sci. Rev. 56 (2020) 1–23, https://doi.org/10.1016/j.jdsr.2019.09.002.

[91] H. Xiao-jian, S. Tao, P. Bao-wu, Z. Han-chang, Research on characteristic parameter of Ta-Zro2 fiber blackbody cavity temperature sensor, Int. J. Signal Process. Image Process. Pattern Recogn. 9 (2016) 287–296, https://doi.org/10.14257/ijsip.2016.9.2.24.

[92] X. Zhang, X. Wu, J. Shi, Additive manufacturing of zirconia ceramics: a state-of-the-art review, J. Mater. Res. Technol. 9 (2020) 9029–9048, https://doi.org/10.1016/j.jmrt.2020.05.131.

[93] G. Abedi, A. Jahanshahi, M.H. Fathi, I. Sohrabi Haghdost, A. Veshkini, Study of nano-hydroxyapatite/zirconia stabilized with yttria in bone healing: Histopathological study in rabbit model, Pol. J. Pathol. 65 (2014) 40–47, https://doi.org/10.5114/pjp.2014.42668.

[94] M. Acosta, N. Novak, V. Rojas, S. Patel, R. Vaish, J. Koruza, G.A. Rossetti, J. Rödel, BaTiO 3 -based piezoelectrics: Fundamentals, current status, and perspectives, Appl. Phys. Rev. 4 (4) (2017) 041305.

[95] J. Jacob, N. More, K. Kalia, G. Kapusetti, Piezoelectric smart biomaterials for bone and cartilage tissue engineering, Inflamm. Regener. 38 (2018) 2, https://doi.org/10.1186/s41232-018-0059-8.

[96] J. Reis, C. Frias, C. Canto e Castro, M.L. Botelho, A.T. Marques, J.A.O. Simões, F. Capela e Silva, J. Potes, A new piezoelectric actuator induces bone formation *in vivo*: A preliminary study, J. Biomed. Biotechnol. 2012 (2012) 613403. https://doi.org/10.1155/2012/613403.

[97] M. Cerrolaza, V. Duarte, D. Garzón-Alvarado, Analysis of bone remodeling under piezoelectricity effects using boundary elements, J. Bionic Eng. 14 (2017) 659–671, https://doi.org/10.1016/S1672-6529(16)60432-8.

[98] A. Rocca, A. Marino, V. Rocca, S. Moscato, G. de Vito, V. Piazza, B. Mazzolai, V. Mattoli, T.J. Ngo-Anh, G. Ciofani, Barium titanate nanoparticles and hypergravity stimulation improve differentiation of mesenchymal stem cells into osteoblasts, Int. J. Nanomed. 10 (2015) 433–445, https://doi.org/10.2147/IJN.S76329.

[99] H.-Y. Yao, Y.-W. Lin, T.-H. Chang, Dielectric properties of batio3-epoxy nanocomposites in the microwave regime, Polymers 13 (9) (2021) 1391.

[100] F.A. Ismail, R.A. Maulat Osman, M.S. Idris, S. Taking, Z.A. Zahid Jamal, M.H.A. Wahid, Dielectric and microstructural properties of $BaTiO_3$ and Ba 0.9925 Er 0.0075 TiO_3 ceramics, EPJ Web Conf. 162 (2017) 01051, https://doi.org/10.1051/epjconf/201716201051.

[101] J. Grandgirard, D. Poinsot, L. Krespi, J.P. Nénon, A.M. Cortesero, Costs of secondary parasitism in the facultative hyperparasitoid Pachycrepoideus dubius: Does host size matter?, Entomol Exp. Appl. 103 (2002) 239–248, https://doi.org/10.1023/A.

[102] Z. Zhou, Z. Yang, Q. Yuan, Barium titanate ceramic inks for continuous ink-jet printing synthesized by mechanical mixing and sol-gel methods, Trans. Nonferrous Met. Soc. Chin. 18 (2008) 150–154, https://doi.org/10.1016/S1003-6326(08)60027-8.

[103] I. Sanaullah, H.N. Khan, A. Sajjad, S. Khan, A.N. Sabri, S. Naseem, S. Riaz, Improved osteointegration response using high strength perovskite BaTiO3 coatings prepared by chemical bath deposition, J. Mech. Behav. Biomed. Mater. 138 (2023), https://doi.org/10.1016/j.jmbbm.2022.105635 105635.

[104] M. López-Álvarez, C. Rodríguez-Valencia, J. Serra, P. González, Bio-inspired ceramics: promising scaffolds for bone tissue engineering, Procedia Eng. 59 (2013) 51–58, https://doi.org/10.1016/j.proeng.2013.05.093.

[105] W. Liu, Q. Li, X. Yang, X. Chen, X. Xu, Correction: Synthesis and characterization of n-doped sic powder with enhanced photocatalytic and photoelectrochemical performance, Catalysts. 10 (2020) 1–2. https://doi.org/10.3390/catal10101155.

[106] H. Abderrazak, E.S.B. Hadj Hmi, Silicon carbide: synthesis and properties, in: Properties and Applications of Silicon Carbide, InTech, 2011. https://doi.org/10.5772/15736.

[107] Z. Ma, J. Li, F. Cao, J. Yang, R. Liu, D. Zhao, Porous silicon carbide coated with tantalum as potential material for bone implants, Regenerative, Biomaterials 7 (2020) 453–459, https://doi.org/10.1093/rb/rbaa021.

[108] M. Lopez-Alvarez, J. Serra, A. De, P. Gonzalez, Marine-based carbon and silicon carbide scaffolds with patterned surface for tissue engineering applications, in: Advances in Ceramics - Electric and Magnetic Ceramics, Bioceramics, Ceramics and Environment, InTech, 2011. https://doi.org/10.5772/22046.

[109] P. González, J.P. Borrajo, J. Serra, S. Liste, S. Chiussi, B. León, K. Semmelmann, A. de Carlos, F.M. Varela-Feria, J. Martínez-Fernández, A.R. de Arellano-López, Extensive studies on biomorphic SiC ceramics properties for medical

applications, Key Eng. Mater. 254–256 (2003) 1029–1032, https://doi.org/10.4028/www.scientific.net/KEM.254-256.1029.
[110] F. He, J. Zhang, F. Yang, J. Zhu, X. Tian, X. Chen, In vitro degradation and cell response of calcium carbonate composite ceramic in comparison with other synthetic bone substitute materials, Mater. Sci. Eng. C 50 (2015) 257–265, https://doi.org/10.1016/J.MSEC.2015.02.019.
[111] H. Shaked, I. Polishchuk, A. Nagel, Y. Bekenstein, B. Pokroy, Long-term stabilized amorphous calcium carbonate—an ink for bio-inspired 3D printing, Mater. Today Bio. 11 (2021), https://doi.org/10.1016/j.mtbio.2021.100120 100120.
[112] A. El-Ghannam, P. Ducheyne, Bioactive ceramics, in: P.-B.-T.-C.-B. Ducheyne (Ed.), Comprehensive Biomaterials, Elsevier, Oxford, 2011, pp. 157–179, https://doi.org/10.1016/B978-0-08-055294-1.00021-0.
[113] S. Fernando, M. McEnery, S.A. Guelcher, 16 - Polyurethanes for bone tissue engineering, in: S.L. Cooper, J.B.T.-A. in: P.B. Guan (Eds.), Woodhead Publishing, 2016: pp. 481–501. https://doi.org/https://doi.org/10.1016/B978-0-08-100614-6.00016-0.
[114] B. Lowe, J.G. Hardy, L.J. Walsh, Optimizing nanohydroxyapatite nanocomposites for bone tissue engineering, ACS Omega 5 (2020) 1–9, https://doi.org/10.1021/acsomega.9b02917.
[115] J.R. García, A.J. García, Biomaterial-mediated strategies targeting vascularization for bone repair, Drug Deliv. Transl. Res. 6 (2016) 77–95, https://doi.org/10.1007/s13346-015-0236-0.
[116] H. Yu, P.J. VandeVord, L. Mao, H.W. Matthew, P.H. Wooley, S.-Y. Yang, Improved tissue-engineered bone regeneration by endothelial cell mediated vascularization, Biomaterials 30 (2009) 508–517, https://doi.org/10.1016/j.biomaterials.2008.09.047.
[117] I. Macías, N. Alcorta-Sevillano, A. Infante, C.I. Rodríguez, Cutting edge endogenous promoting and exogenous driven strategies for bone regeneration, Int. J. Mol. Sci. 22 (14) (2021) 7724, https://doi.org/10.3390/ijms22147724.
[118] L. Wu, X. Pei, B. Zhang, Z. Su, X. Gui, C. Gao, L. Guo, H. Fan, Q. Jiang, L. Zhao, C. Zhou, Y. Fan, X. Zhang, 3D-printed HAp bone regeneration scaffolds enable nano-scale manipulation of cellular mechanotransduction signals, Chem. Eng. J. 455 (2023), https://doi.org/10.1016/j.cej.2022.140699 140699.
[119] Y. Xu, F. Zhang, W. Zhai, S. Cheng, J. Li, Y. Wang, Unraveling of advances in 3D-printed polymer-based bone scaffolds, Polymers 14 (2022) 566. https://doi.org/10.3390/POLYM14030566.
[120] H. Lee, J.M. Yoo, S.Y. Nam, Additive fabrication and characterization of biomimetic composite bone scaffolds with high hydroxyapatite content, Gels 7 (2021) 100, https://doi.org/10.3390/gels7030100.
[121] J. Zhang, D. Huang, S. Liu, X. Dong, Y. Li, H. Zhang, Z. Yang, Q. Su, W. Huang, W. Zheng, W. Zhou, Zirconia toughened hydroxyapatite biocomposite formed by a DLP 3D printing process for potential bone tissue engineering, Mater. Sci. Eng. C 105 (2019), https://doi.org/10.1016/j.msec.2019.110054 110054.
[122] H. Shao, J. He, T. Lin, Z. Zhang, Y. Zhang, S. Liu, 3D gel-printing of hydroxyapatite scaffold for bone tissue engineering, Ceram. Int. 45 (2019) 1163–1170, https://doi.org/10.1016/j.ceramint.2018.09.300.
[123] A. Chlanda, P. Oberbek, M. Heljak, Ż. Górecka, K. Czarnecka, K.S. Chen, M.J. Woźniak, Nanohydroxyapatite adhesion to low temperature plasma modified surface of 3D-printed bone tissue engineering scaffolds - qualitative and quantitative study, Surf. Coat. Technol. 375 (2019) 637–644, https://doi.org/10.1016/j.surfcoat.2019.07.070.
[124] Y. Lakhdar, C. Tuck, J. Binner, A. Terry, R. Goodridge, Additive manufacturing of advanced ceramic materials, Prog. Mater Sci. 116 (2021), https://doi.org/10.1016/j.pmatsci.2020.100736 100736.
[125] N. Kamboj, A. Ressler, I. Hussainova, Bioactive ceramic scaffolds for bone tissue engineering by powder bed selective laser processing: A review, Materials 14 (2021) 5338, https://doi.org/10.3390/ma14185338.
[126] H. Budharaju, A. Subramanian, S. Sethuraman, Recent advancements in cardiovascular bioprinting and bioprinted cardiac constructs, Biomater. Sci. 9 (2021) 1974–1994, https://doi.org/10.1039/d0bm01428a.
[127] H. Shao, D. Zhao, T. Lin, J. He, J. Wu, 3D gel-printing of zirconia ceramic parts, Ceram. Int. 43 (2017) 13938–13942, https://doi.org/10.1016/j.ceramint.2017.07.124.
[128] T.N.A.T. Rahim, A.M. Abdullah, H. Md Akil, Recent developments in fused deposition modeling-based 3D printing of polymers and their composites, Polym. Rev. 59 (2019) 589–624, https://doi.org/10.1080/15583724.2019.1597883.
[129] B. Zhang, L. Wang, P. Song, X. Pei, H. Sun, L. Wu, C. Zhou, K. Wang, Y. Fan, X. Zhang, 3D printed bone tissue regenerative PLA/HA scaffolds with comprehensive performance optimizations, Mater. Des. 201 (2021), https://doi.org/10.1016/j.matdes.2021.109490 109490.
[130] W. Wang, B. Zhang, M. Li, J. Li, C. Zhang, Y. Han, L. Wang, K. Wang, C. Zhou, L. Liu, Y. Fan, X. Zhang, 3D printing of PLA/n-HA composite scaffolds with customized mechanical properties and biological functions for bone tissue engineering, Compos. B Eng. 224 (2021), https://doi.org/10.1016/j.compositesb.2021.109192 109192.
[131] A.-V. Do, B. Khorsand, S.M. Geary, A.K. Salem, 3D printing of scaffolds for tissue regeneration applications, Adv. Healthc. Mater. 4 (2015) 1742–1762, https://doi.org/10.1002/adhm.201500168.
[132] F. Lupone, E. Padovano, M. Pietroluongo, S. Giudice, O. Ostrovskaya, C. Badini, Optimization of selective laser sintering process conditions using stable sintering region approach, Express Polym. Lett. 15 (2021) 177–192, https://doi.org/10.3144/EXPRESSPOLYMLETT.2021.16.
[133] D. Chioibasu, A. Achim, C. Popescu, G. Stan, I. Pasuk, M. Enculescu, S. Iosub, L. Duta, A. Popescu, Prototype orthopedic bone plates 3D printed by laser melting deposition, Materials 12 (6) (2019) 906, https://doi.org/10.3390/ma12060906.
[134] C.-H. Tsai, C.-H. Hung, C.-N. Kuo, C.-Y. Chen, Y.-N. Peng, M.-Y. Shie, Improved bioactivity of 3D printed porous titanium alloy scaffold with chitosan/magnesium-calcium silicate composite for orthopaedic applications, Materials 12 (2) (2019) 203, https://doi.org/10.3390/ma12020203.
[135] G. Ding, R. He, K. Zhang, N. Zhou, H. Xu, Stereolithography 3D printing of SiC ceramic with potential for lightweight optical mirror, Ceram. Int. 46 (2020) 18785–18790, https://doi.org/10.1016/J.CERAMINT.2020.04.196.
[136] H. Wu, Y. Cheng, W. Liu, R. He, M. Zhou, S. Wu, X. Song, Y. Chen, Effect of the particle size and the debinding process on the density of alumina ceramics fabricated by 3D printing based on stereolithography, Ceram. Int. 42 (2016) 17290–17294, https://doi.org/10.1016/J.CERAMINT.2016.08.024.
[137] J.-W. Kim, J.-B. Lee, Y.-H. Koh, H.-E. Kim, Digital light processing of freeze-cast ceramic layers for macroporous calcium phosphate scaffolds with tailored microporous frameworks, Materials 12 (18) (2019) 2893, https://doi.org/10.3390/ma12182893.
[138] Y. Yao, W. Qin, B. Xing, N. Sha, T. Jiao, Z. Zhao, High performance hydroxyapatite ceramics and a triply periodic minimum surface structure fabricated by digital light processing 3D printing, J. Adv. Ceram. 10 (2021) 39–48, https://doi.org/10.1007/s40145-020-0415-4.
[139] F. Li, X.u. Ji, Z. Wu, C. Qi, J. Iai, Q. Xian, B. Sun, Digital light processing 3D printing of ceramic shell for precision casting, Mater. Lett. 276 (2020) 128037, https://doi.org/10.1016/J.MATLET.2020.128037.
[140] A. Reid, J.C. Jackson, J.F.C. Windmill, Voxel based method for predictive modelling of solidification and stress in digital light processing based additive manufacture, Soft Matter 17 (2021) 1881–1887, https://doi.org/10.1039/D0SM01968B.
[141] X. Ren, H. Shao, T. Lin, H. Zheng, 3D gel-printing—An additive manufacturing method for producing complex shape parts, Mater. Des. 101 (2016) 80–87, https://doi.org/10.1016/j.matdes.2016.03.152.
[142] J.W. Cho, B.S. Kim, D.H. Yeo, E.J. Lim, S. Sakong, J. Lim, S.N. Park, Y.H. Jeong, T. G. Jung, H. Choi, C.W. Oh, H.J. Kim, J.W. Park, J.K. Oh, 3D-printed, bioactive ceramic scaffold with rhBMP-2 in treating critical femoral bone defects in rabbits using the induced membrane technique, J. Orthop. Res. 39 (2021) 2671–2680, https://doi.org/10.1002/jor.25007.
[143] J. He, H. Shao, T. Lin, Effect of magnesium silicate on 3D gel-printing of hydroxyapatite ceramic composite scaffold, Int. J. Appl. Ceram. Technol. 16 (2019) 494–502, https://doi.org/10.1111/ijac.13133.
[144] Z. Chen, Z. Li, J. Li, C. Liu, C. Lao, Y. Fu, C. Liu, Y. Li, P. Wang, Y. He, 3D printing of ceramics: A review, J. Eur. Ceram. Soc. 39 (2019) 661–687, https://doi.org/10.1016/j.jeurceramsoc.2018.11.013.
[145] S.C. Daminabo, S. Goel, S.A. Grammatikos, H.Y. Nezhad, V.K. Thakur, Fused deposition modeling-based additive manufacturing (3D printing): techniques for polymer material systems, Mater. Today Chem. 16 (2020), https://doi.org/10.1016/J.MTCHEM.2020.100248 100248.
[146] P.K. Penumakala, J. Santo, A. Thomas, A critical review on the fused deposition modeling of thermoplastic polymer composites, Compos. B Eng. 201 (2020), https://doi.org/10.1016/J.COMPOSITESB.2020.108336 108336.
[147] A. Awad, F. Fina, A. Goyanes, S. Gaisford, A.W. Basit, 3D printing: Principles and pharmaceutical applications of selective laser sintering, Int. J. Pharm. 586 (2020), https://doi.org/10.1016/J.IJPHARM.2020.119594 119594.
[148] S. Song, Z. Gao, B. Lu, C. Bao, B. Zheng, L. Wang, Performance optimization of complicated structural SiC/Si composite ceramics prepared by selective laser sintering, Ceram. Int. 46 (2020) 568–575, https://doi.org/10.1016/J.CERAMINT.2019.09.004.
[149] J. Huang, Q. Qin, J. Wang, A review of stereolithography: processes and systems, Processes 8 (2020) 1138. https://doi.org/10.3390/PR8091138.
[150] H. Xing, B. Zou, Q. Lai, C. Huang, Q. Chen, X. Fu, Z. Shi, Preparation and characterization of UV curable Al2O3 suspensions applying for stereolithography 3D printing ceramic microcomponent, Powder Technol. 338 (2018) 153–161, https://doi.org/10.1016/J.POWTEC.2018.07.023.
[151] T. Zhou, L. Zhang, Q. Yao, Y. Ma, C. Hou, B. Sun, C. Shao, P. Gao, H. Chen, SLA 3D printing of high quality spine shaped β-TCP bioceramics for the hard tissue repair applications, Ceram. Int. 46 (2020) 7609–7614, https://doi.org/10.1016/j.ceramint.2019.11.261.
[152] C. Schmidleithner, S. Malferrari, R. Palgrave, D. Bomze, M. Schwentenwein, D. M. Kalaskar, Application of high resolution DLP stereolithography for fabrication of tricalcium phosphate scaffolds for bone regeneration, Biomed. Mater. (Bristol) 14 (4) (2019) 045018.
[153] C. Schmidleithner, D.M. Kalaskar, Stereolithography, in: 3D Printing, InTech, 2018. https://doi.org/10.5772/intechopen.78147.
[154] C.I. Higgins, T.E. Brown, J.P. Killgore, Digital light processing in a hybrid atomic force microscope, In situ, nanoscale characterization of the printing process, Addit. Manuf. 38 (2021), https://doi.org/10.1016/J.ADDMA.2020.101744 101744.
[155] N. Raja, A. Sung, H. Park, H. suk Yun, Low-temperature fabrication of calcium deficient hydroxyapatite bone scaffold by optimization of 3D printing conditions, Ceram. Int. 47 (2021) 7005–7016. https://doi.org/10.1016/j.ceramint.2020.11.051.
[156] P. Nevado, A. Lopera, V. Bezzon, M.R. Fulla, J. Palacio, M.A. Zaghete, G. Biasotto, A. Montoya, J. Rivera, S.M. Robledo, H. Estupiñan, C. Paucar, C. Garcia, Preparation and in vitro evaluation of PLA/biphasic calcium

phosphate filaments used for fused deposition modelling of scaffolds, Mater. Sci. Eng. C 114 (2020), https://doi.org/10.1016/j.msec.2020.111013 111013.
[157] S. Esmaeili, H. Akbari Aghdam, M. Motififard, S. Saber-Samandari, A.H. Montazeran, M. Bigonah, E. Sheikhbahaei, A. Khandan, A porous polymeric-hydroxyapatite scaffold used for femur fractures treatment: fabrication, analysis, and simulation, Eur. J. Orthop. Surg. Traumatol.: Orthopedie Traumatologie. 30 (2020) 123–131, https://doi.org/10.1007/S00590-019-02530-3.
[158] B.I. Oladapo, S.A. Zahedi, S.O. Ismail, Mechanical performances of hip implant design and fabrication with PEEK composite, Polymer 227 (2021), https://doi.org/10.1016/J.POLYMER.2021.123865 123865.
[159] X. Song, D. Shi, P. Song, X. Han, Q. Wei, C. Huang, Fused deposition modeling of poly(ether ether ketone) scaffolds, High Temp. Mater. Processes 40 (2021) 1–11, https://doi.org/10.1515/HTMP-2021-0009/MACHINEREADABLECITATION/RIS.
[160] M.W. Sa, B.N.B. Nguyen, R.A. Moriarty, T. Kamalitdinov, J.P. Fisher, J.Y. Kim, Fabrication and evaluation of 3D printed BCP scaffolds reinforced with ZrO 2 for bone tissue applications, Biotechnol. Bioeng. 115 (2018) 989–999, https://doi.org/10.1002/BIT.26514.
[161] T. Distler, N. Fournier, A. Grünewald, C. Polley, H. Seitz, R. Detsch, A.R. Boccaccini, Polymer-bioactive glass composite filaments for 3D scaffold manufacturing by fused deposition modeling: fabrication and characterization, Front. Bioeng. Biotechnol. 8 (2020), https://doi.org/10.3389/FBIOE.2020.00552/FULL.
[162] D. Wu, A. Spanou, A. Diez-Escudero, C. Persson, 3D-printed PLA/HA composite structures as synthetic trabecular bone: A feasibility study using fused deposition modeling, J. Mech. Behav. Biomed. Mater. 103 (2020), https://doi.org/10.1016/J.JMBBM.2019.103608 103608.
[163] A. Malayeri, C. Sherborne, T. Paterson, S. Mittar, I.O. Asencio, P.V. Hatton, F. Claeyssens, Osteosarcoma growth on trabecular bone mimicking structures manufactured via laser direct write, Int. J. Bioprint. 2 (2016) 67–77, https://doi.org/10.18063/IJB.2016.02.005.
[164] J. He, D. Li, B. Lu, Z. Wang, T. Zhang, Custom fabrication of a composite hemi-knee joint based on rapid prototyping, Rapid Prototyp. J. 12 (2006) 198–205, https://doi.org/10.1108/13552540610682705/FULL/PDF.
[165] X. Wu, Q. Lian, D. Li, Z. Jin, Biphasic osteochondral scaffold fabrication using multi-material mask projection stereolithography, Rapid Prototyp. J. 25 (2019) 277–288, https://doi.org/10.1108/RPJ-07-2017-0144.
[166] D. Du, T. Asaoka, T. Ushida, K.S. Furukawa, Fabrication and perfusion culture of anatomically shaped artificial bone using stereolithography, Biofabrication 6 (2014), https://doi.org/10.1088/1758-5082/6/4/045002 045002.
[167] O. Guillaume, M.A. Geven, C.M. Sprecher, V.A. Stadelmann, D.W. Grijpma, T.T. Tang, L. Qin, Y. Lai, M. Alini, J.D. de Bruijn, H. Yuan, R.G. Richards, D. Eglin, Surface-enrichment with hydroxyapatite nanoparticles in stereolithography-fabricated composite polymer scaffolds promotes bone repair, Acta Biomater. 54 (2017) 386–398, https://doi.org/10.1016/J.ACTBIO.2017.03.006.
[168] K.C.R. Kolan, M.C. Leu, G.E. Hilmas, R.F. Brown, M. Velez, Fabrication of 13–93 bioactive glass scaffolds for bone tissue engineering using indirect selective laser sintering, Biofabrication 3 (2) (2011) 025004, https://doi.org/10.1088/1758-5082/3/2/025004.
[169] M. Lindner, S. Hoeges, W. Meiners, K. Wissenbach, R. Smeets, R. Telle, R. Poprawe, H. Fischer, Manufacturing of individual biodegradable bone substitute implants using selective laser melting technique, J. Biomed. Mater. Res. A 97A (2011) 466–471, https://doi.org/10.1002/JBM.A.33058.
[170] Z. Liu, H. Liang, T. Shi, D. Xie, R. Chen, X. Han, L. Shen, C. Wang, Z. Tian, Additive manufacturing of hydroxyapatite bone scaffolds via digital light processing and in vitro compatibility, Ceram. Int. 45 (2019) 11079–11086, https://doi.org/10.1016/J.CERAMINT.2019.02.195.
[171] Y. Cao, T. Shi, C. Jiao, H. Liang, R. Chen, Z. Tian, A. Zou, Y. Yang, Z. Wei, C. Wang, L. Shen, Fabrication and properties of zirconia/hydroxyapatite composite scaffold based on digital light processing, Ceram. Int. 46 (2020) 2300–2308, https://doi.org/10.1016/j.ceramint.2019.09.219.
[172] B. Zhang, H. Sun, L. Wu, L. Ma, F. Xing, Q. Kong, Y. Fan, C. Zhou, X. Zhang, 3D printing of calcium phosphate bioceramic with tailored biodegradation rate for skull bone tissue reconstruction, Bio-Design Manuf. 2 (2019) 161–171, https://doi.org/10.1007/s42242-019-00046-7.
[173] K. Igawa, M. Mochizuki, O. Sugimori, K. Shimizu, K. Yamazawa, H. Kawaguchi, K. Nakamura, T. Takato, R. Nishimura, S. Suzuki, M. Anzai, U.-i. Chung, N. Sasaki, Tailor-made tricalcium phosphate bone implant directly fabricated by a three-dimensional ink-jet printer, J. Artif. Organs 9 (4) (2006) 234–240.
[174] L. Chen, C. Deng, J. Li, Q. Yao, J. Chang, L. Wang, C. Wu, 3D printing of a lithium-calcium-silicate crystal bioscaffold with dual bioactivities for osteochondral interface reconstruction, Elsevier Ltd 196 (2019) 138–150.
[175] X. Liu, Y. Miao, H. Liang, J. Diao, L. Hao, Z. Shi, N. Zhao, Y. Wang, 3D-printed bioactive ceramic scaffolds with biomimetic micro/nano-HAp surfaces mediated cell fate and promoted bone augmentation of the bone–implant interface in vivo, Bioact. Mater. 12 (2022) 120–132, https://doi.org/10.1016/J.BIOACTMAT.2021.10.016.
[176] C. Gao, M.N. Rahaman, Q. Gao, A. Teramoto, K. Abe, Robotic deposition and in vitro characterization of 3D gelatin-bioactive glass hybrid scaffolds for biomedical applications, J. Biomed. Mater. Res. Part A 101 (2013) 2027–2037, https://doi.org/10.1002/JBM.A.34496.
[177] G. Chen, Y.i. Sun, F. Lu, A. Jiang, D. Subedi, P. Kong, X. Wang, T. Yu, H. Chi, C. Song, K. Liu, P. Qi, J. Yan, Y.e. Ji, A three-dimensional (3D) printed biomimetic hierarchical scaffold with a covalent modular release system for osteogenesis, Korean J. Couns. Psychother. 104 (2019) 109842.
[178] Y. Zhang, L. Xia, D. Zhai, M. Shi, Y. Luo, C. Feng, B. Fang, J. Yin, J. Chang, C. Wu, Mesoporous bioactive glass nanolayer-functionalized 3D-printed scaffolds for accelerating osteogenesis and angiogenesis, Nanoscale 7 (2015) 19207–19221, https://doi.org/10.1039/C5NR05421D.
[179] Z. Zhang, H. Shao, T. Lin, Y. Zhang, J. He, L. Wang, 3D gel printing of porous calcium silicate scaffold for bone tissue engineering, J. Mater. Sci. 54 (2019) 10430–10436, https://doi.org/10.1007/s10853-019-03626-1.
[180] T. Lin, X. Wang, L. Jin, W. Li, Y. Zhang, A. Wang, J. Peng, H. Shao, Manufacturing of porous magnesium scaffolds for bone tissue engineering by 3D gel-printing, Mater. Des. 209 (2021), https://doi.org/10.1016/j.matdes.2021.109948 109948.
[181] M.G. Raucci, D. Giugliano, L. Ambrosio, Fundamental properties of bioceramics and biocomposites, in: I.V. Antoniac (Ed.), Handbook of Bioceramics and Biocomposites, Springer International Publishing, Cham, 2016, pp. 35–58, https://doi.org/10.1007/978-3-319-12460-5_3.
[182] L.L. Hench, Bioceramics: from concept to clinic, J. Am. Ceram. Soc. 74 (1991) 1487–1510, https://doi.org/10.1111/j.1151-2916.1991.tb07132.x.
[183] M.P. Nikolova, M.S. Chavali, Recent advances in biomaterials for 3D scaffolds: A review, Bioact. Mater. 4 (2019) 271–292, https://doi.org/10.1016/j.bioactmat.2019.10.005.
[184] S. Smeland, S.S. Bielack, J. Whelan, M. Bernstein, P. Hogendoorn, M.D. Krailo, R. Gorlick, K.A. Janeway, F.C. Ingleby, J. Anninga, I. Antal, C. Arndt, K.L.B. Brown, T. Butterfass-Bahloul, G. Calaminus, M. Capra, C. Dhooge, M. Eriksson, A.M. Flanagan, G. Friedel, M.C. Gebhardt, H. Gelderblom, R. Goldsby, H.E. Grier, R. Grimer, D.S. Hawkins, S. Hecker-Nolting, K. Sundby Hall, M.S. Isakoff, G. Jovic, T. Kühne, L. Kager, T. von Kalle, E. Kabickova, S. Lang, C.C. Lau, P.J. Leavey, S.L. Lessnick, L. Mascarenhas, R. Mayer-Steinacker, P.A. Meyers, R. Nagarajan, R.L. Randall, P. Reichardt, M. Renard, C. Rechnitzer, C.L. Schwartz, S. Strauss, L. Teot, B. Timmermann, M.R. Sydes, N. Marina, Survival and prognosis with osteosarcoma: outcomes in more than 2000 patients in the EURAMOS-1 (European and American Osteosarcoma Study) cohort, Eur. J. Cancer. 109 (2019) 36–50. https://doi.org/10.1016/j.ejca.2018.11.027.
[185] A. Misaghi, A. Goldin, M. Awad, A.A. Kulidjian, Osteosarcoma: a comprehensive review, SICOT-J. 4 (2018) 12, https://doi.org/10.1051/sicotj/2017028.
[186] X. Zhao, Q. Wu, X. Gong, J. Liu, Y. Ma, Osteosarcoma: a review of current and future therapeutic approaches, Biomed. Eng. Online 20 (2021) 24, https://doi.org/10.1186/s12938-021-00860-0.
[187] J. Sun, F. Xing, J. Braun, F. Traub, P.M. Rommens, Z. Xiang, U. Ritz, Progress of phototherapy applications in the treatment of bone cancer, Int. J. Mol. Sci. 22 (2021) 11354, https://doi.org/10.3390/ijms222111354.
[188] M. Nita, A. Grzybowski, The role of the reactive oxygen species and oxidative stress in the pathomechanism of the age-related ocular diseases and other pathologies of the anterior and posterior eye segments in adults, Oxid. Med. Cell. Longev. 2016 (2016) 1–23.
[189] H. Ma, T. Li, Z. Huan, M. Zhang, Z. Yang, J. Wang, J. Chang, C. Wu, 3D printing of high-strength bioscaffolds for the synergistic treatment of bone cancer, NPG Asia Mater. 10 (2018) 31–44, https://doi.org/10.1038/s41427-018-0015-8.
[190] W. Dang, K. Yi, E. Ju, Y. Jin, Y. Xu, H. Wang, W.-C. Chen, K. Wang, Y. Wang, Y. Tao, M. Li, 3D Printed bioceramic scaffolds as a universal therapeutic platform for synergistic therapy of osteosarcoma, ACS Appl. Mater. Interfaces 13 (2021) 18488–18499, https://doi.org/10.1021/acsami.1c00553.
[191] Y. Liu, T. Li, H. Ma, D. Zhai, C. Deng, J. Wang, S. Zhuo, J. Chang, C. Wu, 3D-printed scaffolds with bioactive elements-induced photothermal effect for bone tumor therapy, Acta Biomater. 73 (2018) 531–546, https://doi.org/10.1016/j.actbio.2018.04.014.
[192] H. Zhuang, R. Lin, Y. Liu, M. Zhang, D. Zhai, Z. Huan, C. Wu, Three-dimensional-printed bioceramic scaffolds with osteogenic activity for simultaneous photo/magnetothermal therapy of bone tumors, ACS Biomater Sci. Eng. 5 (2019) 6725–6734, https://doi.org/10.1021/acsbiomaterials.9b01095.
[193] H. Saijo, Y. Fujihara, Y. Kanno, K. Hoshi, A. Hikita, U. Chung, T. Takato, Clinical experience of full custom-made artificial bones for the maxillofacial region, Regener. Ther 5 (2016) 72–78, https://doi.org/10.1016/j.reth.2016.08.004.
[194] P. Kobbe, M. Laubach, D.W. Hutmacher, H. Alabdulrahman, R.M. Sellei, F. Hildebrand, Convergence of scaffold-guided bone regeneration and RIA bone grafting for the treatment of a critical-sized bone defect of the femoral shaft, Eur. J. Med. Res. 25 (2020) 70, https://doi.org/10.1186/s40001-020-00471-w.
[195] C. Mangano, A. Giuliani, I. De Tullio, M. Raspanti, A. Piattelli, G. Iezzi, Case report: histological and histomorphometrical results of a 3-D printed biphasic calcium phosphate ceramic 7 years after insertion in a human maxillary alveolar ridge, Front. Bioeng. Biotechnol. 9 (2021), https://doi.org/10.3389/fbioe.2021.614325.
[196] G. Castrisos, I. Gonzalez Matheus, D. Sparks, M. Lowe, N. Ward, M. Sehu, M.-L. Wille, Y. Phua, F. Medeiros Savi, D. Hutmacher, M. Wagels, Regenerative matching axial vascularisation of absorbable 3D-printed scaffold for large bone defects: A first in human series, J. Plast. Reconstr. Aesthet. Surg. 75 (2022) 2108–2118, https://doi.org/10.1016/j.bjps.2022.02.057.
[197] W.-S. Jeong, Y.-C. Kim, J.-C. Min, H.-J. Park, E.-J. Lee, J.-H. Shim, J.-W. Choi, Clinical application of 3D-printed patient-specific polycaprolactone/beta tricalcium phosphate scaffold for complex zygomatico-maxillary defects, Polymers 14 (2022) 740, https://doi.org/10.3390/polym14040740.
[198] H. Jo, U.-L. Lee, Zygoma augmentation with 3D printed bioactive glass-ceramic implant, J. Craniofac. Surg. 33 (2022) e521–e523, https://doi.org/10.1097/SCS.0000000000008527.

[199] P. Kijartorn, J. Wongpairojpanich, F. Thammarakcharoen, J. Suwanprateeb, B. Buranawat, Clinical evaluation of 3D printed nano-porous hydroxyapatite bone graft for alveolar ridge preservation: A randomized controlled trial, J. Dent. Sci. 17 (2022) 194–203, https://doi.org/10.1016/j.jds.2021.05.003.
[200] M. Laubach, S. Suresh, B. Herath, M.-L. Wille, H. Delbrück, H. Alabdulrahman, D.W. Hutmacher, F. Hildebrand, Clinical translation of a patient-specific scaffold-guided bone regeneration concept in four cases with large long bone defects, J. Orthop. Transl. 34 (2022) 73–84, https://doi.org/10.1016/j.jot.2022.04.004.
[201] P. Mekcha, J. Wongpairojpanich, F. Thammarakcharoen, J. Suwanprateeb, B. Buranawat, Customized 3D printed nanohydroxyapatite bone block grafts for implant sites: a case series, J. Prosthodont. Res. 67 (2) (2022) 311–320.
[202] M. Merola, S. Affatato, Materials for hip prostheses: A review of wear and loading considerations, Materials 12 (3) (2019) 495.
[203] C.C. Ude, C.J. Esdaille, K.S. Ogueri, H.-M. Kan, S.J. Laurencin, L.S. Nair, C.T. Laurencin, The mechanism of metallosis after total hip arthroplasty, Regener. Eng. Transl. Med. 7 (2021) 247–261, https://doi.org/10.1007/s40883-021-00222-1.
[204] Y. Zhu, K. Liu, J. Deng, J. Ye, F. Ai, H. Ouyang, T. Wu, J. Jia, X. Cheng, X. Wang, 3D printed zirconia ceramic hip joint with precise structure and broad-spectrum antibacterial properties, Int. J. Nanomed. 14 (2019) 5977–5987, https://doi.org/10.2147/IJN.S202457.
[205] F. Baino, J. Minguella, N. Kirk, M.A. Montealegre, C. Fiaschi, F. Korkusuz, G. Orlygsson, V.B. Chiara, Novel full-ceramic monoblock acetabular cup with a bioactive trabecular coating: design, fabrication and characterization, Ceram. Int. 42 (2016) 6833–6845, https://doi.org/10.1016/J.CERAMINT.2016.01.065.
[206] J.N. Katz, K.R. Arant, R.F. Loeser, Diagnosis and treatment of hip and knee osteoarthritis: A review, J. Am. Med. Assoc. 325 (2021) 568–578, https://doi.org/10.1001/JAMA.2020.22171.
[207] C.G. Solomon, L. Sharma, Osteoarthritis of the knee, N. Engl. J. Med. 384 (1) (2021) 51–59.
[208] S. Jiang, W. Guo, G. Tian, X. Luo, L. Peng, S. Liu, X. Sui, Q. Guo, X.u. Li, Clinical application status of articular cartilage regeneration techniques: tissue-engineered cartilage brings new hope, Stem Cells Int. 2020 (2020) 1–16.
[209] C. Chung, J.A. Burdick, Engineering cartilage tissue, Adv. Drug Deliv. Rev. 60 (2) (2008) 243–262.
[210] C. Deng, H. Zhu, J. Li, C. Feng, Q. Yao, L. Wang, J. Chang, C. Wu, Bioactive scaffolds for regeneration of cartilage and subchondral bone interface, Theranostics 8 (7) (2018) 1940–1955.
[211] R. Lin, C. Deng, X. Li, Y. Liu, M. Zhang, C. Qin, Q. Yao, L. Wang, C. Wu, Copper-incorporated bioactive glass-ceramics inducing anti-inflammatory phenotype and regeneration of cartilage/bone interface, Theranostics 9 (2019) 6300–6313, https://doi.org/10.7150/thno.36120.
[212] H. Wen, H. Jung, X. Li, Drug delivery approaches in addressing clinical pharmacology-related issues: opportunities and challenges, AAPS J. 17 (6) (2015) 1327–1340.
[213] A. Tewabe, A. Abate, M. Tamrie, A. Seyfu, E.A. Siraj, Targeted drug delivery — From magic bullet to nanomedicine: principles, challenges, and future perspectives, J. Multidiscip. Healthc. 14 (2021) 1711, https://doi.org/10.2147/JMDH.S313968.
[214] A. Vazda, W. Xia, H. Engqvist, The use of heat to deliver fentanyl via pulmonary drug delivery, Int. J. Pharm.: X. 3 (2021), https://doi.org/10.1016/j.ijpx.2021.100096 100096.
[215] A. Vazda, W. Xia, H. Engqvist, Oral administration of zolpidem tartrate in an abuse-deterrent formulation versus an immediate release formulation in beagle dogs, Scand. J. Mater. Sci. (2021) 1–6, https://doi.org/10.2340/scandjms.v1.41.
[216] D. Loca, J. Locs, K. Salma, J. Gulbis, I. Salma, L. Berzina-Cimdina, Porous hydroxyapatite bioceramic scaffolds for drug delivery and bone regeneration, IOP Conf. Series: Mater. Sci. Eng. 18 (19) (2011) 192019.
[217] Y.G. Zhang, Y.J. Zhu, F. Chen, T.W. Sun, A novel composite scaffold comprising ultralong hydroxyapatite microtubes and chitosan: preparation and application in drug delivery, J. Mater. Chem. B 5 (2017) 3898–3906, https://doi.org/10.1039/C6TB02576E.
[218] 3D Printing Ceramics Market Global Forecast to 2025 | MarketsandMarkets, Market Research Report. (n.d.). https://www.marketsandmarkets.com/Market-Reports/3d-printing-ceramic-market-26085601.html.
[219] G.S. Kaliaraj, T. Siva, A. Ramadoss, Surface functionalized bioceramics coated on metallic implants for biomedical and anticorrosion performance – a review, J. Mater. Chem. B 9 (2021) 9433–9460, https://doi.org/10.1039/D1TB01301G.
[220] L. Shanmuganantha, M.U. Aslam Khan, A.B. Sulong, M.I. Ramli, A. Baharudin, H.M. Ariffin, S.I. Abd Razak, M.H. Ng, Characterization of titanium ceramic composite for bone implants applications, Ceram. Int. 48 (2022) 22808–22819, https://doi.org/10.1016/J.CERAMINT.2022.04.140.
[221] J. Olson, HCMC prints 3-D implant to repair fractured skull bone - StarTribune.com, MINNEAPOLIS. (2018). https://www.startribune.com/hcmc-prints-3-d-implant-to-repair-fractured-skull-bone/475742743/ (accessed August 9, 2022).
[222] OssDsign AB (publ) publishes Q1 2022 Interim Report - OssDsign AB, OssDsign. (2022). https://news.cision.com/ossdsign-ab/r/ossdsign-ab–publ–publishes-q1-2022-interim-report,c3573073 (accessed August 9, 2022).
[223] O. Bloom, N. Goddard, B. Yannoulias, S. Eccles, The successful use of a bespoke OssDsign cranial plate to reconstruct an occipital defect following excision of a recurrent epithelioid sarcoma, JPRAS Open 24 (2020) 71–76, https://doi.org/10.1016/J.JPRA.2020.01.002.
[224] T. Jaenisch, K. Heiss, N. Fischer, C. Geiger, F.R. Bischoff, G. Moldenhauer, L. Rychlewski, A. Sié, B. Coulibaly, P.H. Seeberger, L.S. Wyrwicz, F. Breitling, F.F. Loeffler, High-density peptide arrays help to identify linear immunogenic B-cell epitopes in individuals naturally exposed to malaria infection, Mol. Cell. Proteomics 18 (2019) 642–656, https://doi.org/10.1074/mcp.RA118.000992.
[225] MERCK, TissueFab® bioink Bone, (n.d.). https://www.sigmaaldrich.com/IN/en/product/aldrich/915637 (accessed August 9, 2022).
[226] J. Walladbegi, C. Schaefer, E. Pernevik, S. Sämfors, G. Kjeller, P. Gatenholm, G. K. Sándor, L. Rasmusson, Three-dimensional bioprinting using a coaxial needle with viscous inks in bone tissue engineering - an in vitro study, Ann. Maxillofac. Surg. 10 (2020) 370, https://doi.org/10.4103/AMS.AMS_288_20.
[227] J.D. Glaeser, X. Bao, G. Kaneda, P. Avalos, P. Behrens, K. Salehi, A. Chen, W. Jiang, C. Castaneda, iPSC-neural crest derived cells embedded in 3D printable bio-ink promote cranial bone defect repair, (2022). https://doi.org/10.21203/rs.3.rs-1562664/v1.
[228] CERHUM, Applications MyBone Solution, (2022). https://www.cerhum.com/solution/applications (accessed August 10, 2022).
[229] H. Park, J.W. Choi, W.S. Jeong, Clinical application of three-dimensional printing of polycaprolactone/beta-tricalcium phosphate implants for cranial reconstruction, J. Craniofac. Surg. 33 (2022) 1394, https://doi.org/10.1097/SCS.0000000000008595.
[230] T. Thygesen, C. Slots, M.B. Jensen, N. Ditzel, M. Kassem, L. Langhorn, M. Andersen, Comparison of off-the-shelf β-tricalcium phosphate implants with novel resorbable 3D printed implants in mandible ramus of pigs, Bone 159 (2022), https://doi.org/10.1016/J.BONE.2022.116370 116370.
[231] Ossiform, P3D Bone, (n.d.). https://ossiform.com/p3d-bone.aspx (accessed August 11, 2022).
[232] L. Teo, S.H. Teoh, Y. Liu, L. Lim, B. Tan, J.-T. Schantz, L.L. Seah, A novel bioresorbable implant for repair of orbital floor fractures, Orbit 34 (2015) 192–200, https://doi.org/10.3109/01676830.2015.1015263.
[233] Surgeons | Osteopore, (n.d.). https://osteopore.com/surgeons (accessed August 9, 2022).
[234] OPM, OsteoFab® Implants | OPM, (n.d.). https://oxfordpm.com/osteofab-medical-devices (accessed August 10, 2022).
[235] OsseoTi® Porous Metal Technology | Zimmer Biomet, ZIMMER BIOMET. (n.d.). https://www.zimmerbiomet.com/en/products-and-solutions/specialties/hip/osseoti-porous-metal-technology.html (accessed August 11, 2022).
[236] Custom Implant Solutions | LRS Implants, LRS IMPLANT. (n.d.). https://www.lrsimplants.com/custom-implant-solutions (accessed August 11, 2022).
[237] M. Ahmadipour, H. Mohammadi, A.L. Pang, M. Arjmand, T. Ayode Otitoju, P.U. Okoye, B. Rajitha, A review: silicate ceramic-polymer composite scaffold for bone tissue engineering, Int. J. Polym. Mater. Polym. Biomater. 71 (2020) 180–195, https://doi.org/10.1080/00914037.2020.1817018.
[238] K. Hayashi, A. Tsuchiya, M. Shimabukuro, K. Ishikawa, Multiscale porous scaffolds constructed of carbonate apatite honeycomb granules for bone regeneration, Mater. Des. 215 (2022), https://doi.org/10.1016/J.MATDES.2022.110468 110468.
[239] E.F. Morgan, G.U. Unnikrisnan, A.I. Hussein, Bone mechanical properties in healthy and diseased states, Annu. Rev. Biomed. Eng. 20 (1) (2018) 119–143.
[240] D. Shekhawat, A. Singh, M.K. Banerjee, T. Singh, A. Patnaik, Bioceramic composites for orthopaedic applications: A comprehensive review of mechanical, biological, and microstructural properties, Ceram. Int. 47 (2021) 3013–3030, https://doi.org/10.1016/j.ceramint.2020.09.214.
[241] M.P. Sekar, H. Budharaju, A. Zennifer, S. Sethuraman, N. Vermeulen, D. Sundaramurthi, D.M. Kalaskar, Current standards and ethical landscape of engineered tissues-3D bioprinting perspective, J. Tissue Eng. 12 (2021) 20417314211027676. https://doi.org/10.1177/20417314211027677.
[242] 3D Printing Ceramics Market by Material type (Oxide based, non-oxide based), Form, End-use Industry (Aerospace & defense, healthcare, automotive, consumer goods and electronics, construction), Application and Region - Global Forecast to 2025, Marketsandmarkets. (2021) 157. https://www.marketsandmarkets.com/Market-Reports/3d-printing-ceramic-market-26085601.html (accessed August 11, 2022).
[243] Bone Implant Market: Information by Biomaterial (Metal and Others), Product (Orthopedic Screws, Orthopedic Plates, and Others), Application (Hip Orthopedic Implants and Others), Device (External and Internal), and End-User– Forecast Till 2027, Market Research Future. (n.d.) 100. https://www.marketresearchfuture.com/reports/bone-implant-market-6291 (accessed August 17, 2022).
[244] Global 4D Printing In Healthcare Market Size By Component (Equipment, Programmable Materials, Software & Services), By Application (Medical Models, Patient-specific Implants, Surgical Guides), By Technology (Polyjet, Fused Deposition Modelling, Selective, Verified market research. (2022) 202. https://www.verifiedmarketresearch.com/product/4D-Printing-in-Healthcare-Market/ (accessed August 17, 2022).
[245] C.R. Alcala-Orozco, I. Mutreja, X. Cui, G.J. Hooper, K.S. Lim, T.B.F. Woodfield, Hybrid biofabrication of 3D osteoconductive constructs comprising Mg-based nanocomposites and cell-laden bioinks for bone repair, Bone 154 (2022), https://doi.org/10.1016/J.BONE.2021.116198 116198.
[246] J. Lee, J. Hong, W.J. Kim, G.H. Kim, Bone-derived dECM/alginate bioink for fabricating a 3D cell-laden mesh structure for bone tissue engineering, Carbohydr. Polym. 250 (2020), https://doi.org/10.1016/j.carbpol.2020.116914 116914.
[247] W. Kim, G. Kim, Collagen/bioceramic-based composite bioink to fabricate a porous 3D hASCs-laden structure for bone tissue regeneration, Biofabrication 12 (2019), https://doi.org/10.1088/1758-5090/ab436d 015007.

[248] H.K. Chang, D.H. Yang, M.Y. Ha, H.J. Kim, C.H. Kim, S.H. Kim, J.W. Choi, H.J. Chun, 3D printing of cell-laden visible light curable glycol chitosan bioink for bone tissue engineering, Carbohydr. Polym. 287 (2022), https://doi.org/10.1016/J.CARBPOL.2022.119328 119328.
[249] M.L. Raffa, V.H. Nguyen, P. Hernigou, C.H. Flouzat-Lachaniette, G. Haiat, Stress shielding at the bone-implant interface: Influence of surface roughness and of the bone-implant contact ratio, J. Orthop. Res®. 39 (2021) 1174–1183, https://doi.org/10.1002/JOR.24840.
[250] M. Ly, S. Spinelli, S. Hays, D. Zhu, 3D printing of ceramic biomaterials, Eng. Regener. 3 (2022) 41–52, https://doi.org/10.1016/J.ENGREG.2022.01.006.
[251] H.J. Jeong, S.J. Gwak, K.D. Seo, S. Lee, J.H. Yun, Y.S. Cho, S.J. Lee, Fabrication of three-dimensional composite scaffold for simultaneous alveolar bone regeneration in dental implant installation, Int. J. Mol. Sci. 21 (2020) 1863. https://doi.org/10.3390/IJMS21051863.
[252] G.A. Fielding, A. Bandyopadhyay, S. Bose, Effects of silica and zinc oxide doping on mechanical and biological properties of 3D printed tricalcium phosphate tissue engineering scaffolds, Dent. Mater. 28 (2012) 113–122, https://doi.org/10.1016/J.DENTAL.2011.09.010.